

國立交通大學

電子工程學系電子研究所

博士論文

應用引導通道協助於寬頻分碼多重進接系統
上行鏈路之干擾消除技術

Pilot-Channel Aided Interference Cancellation for
Uplink WCDMA Systems

研究生：唐之璇

指導教授：魏哲和

中華民國九十六年一月

應用引導通道協助於寬頻分碼多重進接系統 上行鏈路之干擾消除技術

研究生：唐之璇

指導教授：魏哲和博士

國立交通大學

電子工程學系電子研究所

摘要

在分碼多重進接系統中，具有寬頻特性的展頻碼被用來區別不同使用者的窄頻訊號，當這些展頻碼無法正交就會造成多重存取干擾(MAI)。在蜂巢式環境中，如果各使用者訊號無法適切的控制，強接收訊號使用者會嚴重弱化弱接收訊號使用者的接收機效能，也就是發生所謂的近遠效應(near-far effect)，多重使用者檢測(MUD)技術可以用來解使用者之間的相互干擾問題。在各種多重使用者檢測法中，由於具有簡單及在衰變通道環境下錯誤率表現優越的特性，序列式干擾消除法被視為一個可行的技術，在這個論文中，我們首先探討影響序列式干擾消除法效能很大的排序問題，接著提出數項改善序列式干擾消除法缺點的技術，再進一步提出增加系統容量的方法，使序列式干擾消除技術能成為寬頻分碼多工進接存取系統之上傳鏈路中的實用技術。

排序法對於序列式干擾消除法的效能有極大影響，在本論文中，我們提出一適用於寬頻分碼多工進接存取系統的排序法，此法在複雜度及效能上有適中的表現，接著比較三種排序法，包含實作的議題如重排頻率處理延遲時間、潛伏時間及計算複雜度等，還有評比與錯誤率表現有關的參數如引導符碼與使用者資訊符碼增益比、區塊檢測間隔、功率分佈比、及通道與時序估測錯誤等。除了單速率系統，我們也延伸所提架構，使之

同樣適用於多速率系統。

在改善缺失方面，首先，對於通道資訊估測準確度敏感的問題，由於寬頻分碼多工進接存取系統之上傳鏈路具有與傳輸通道正交的引導通道，可以用來達成較準確到通道估測，但也由於非同步接收這些引導符碼會干擾使用者資訊的檢測，因此我們提出引導符碼消除技術來解決這個問題；對於處理延遲時間較長的問題，則提出一包括通道估測及使用者資訊檢測的管線式架構；最後，關於功率控制比較複雜的問題，我們發現，就算在一般性的功率控制法下，適當選擇排序法的序列式干擾消除法仍能優於並列式部分干擾消除法(PPIC)的效能表現。

除了考慮單純的序列式干擾消除法，我們提出一能針對變動環境及不同需求而調整的可調式架構，根據系統負載及效能需求，可調整處理延遲時間及計算複雜度，此法結合序列式干擾消除法、並列式干擾消除法及再精鍊的通道估測法，經過額外增加的計算量，此法的處理延遲時間比純粹序列式干擾消除法少，並可達到更加的效能。

最後，我們延伸序列式干擾消除的概念至有通道編碼的系統，與渦輪碼解碼同時考慮，首先根據排序資訊，提出一提早停止 (early-stopping) 準則以減少渦輪碼解碼時不必要的運算，與其他提早停止準則比較，在幾乎相同的檢測能力下，此準則具有快速及低計算複雜度的特性，接著提出一包含前述準則之遞迴式干擾消除法，將序列式干擾消除運用在符碼及跨級之碼塊干擾上，並且只有被檢定為錯誤的編碼區塊訊號需要再進一級的遞迴檢測，此法不僅在效能表現上更為優越，也節省了大量且不必要的計算量。

Pilot-Channel Aided Interference Cancellation for Uplink WCDMA Systems

Student: Chih-Hsuan Tang

Advisor: Dr. Che-Ho Wei

Department of Electronics Engineering & Institute of Electronics
National Chiao Tung University

Abstract

In CDMA systems, the narrowband message signals of different users are discriminated by multiplying the spreading signals with large bandwidth. The multiple access interference (MAI) is introduced when spreading signals are non-orthogonal. In the cellular environment, if the power of each user within a cell is not controlled appropriately, error performance of the user with small received power can be dramatically decreased by the user with large received power, i.e., the near-far problem occurs. A technique known as multiuser detection (MUD) can be employed to mitigate the MAI. The successive interference cancellation (SIC) is considered a promising technique among the MUDs due to its simplicity and superior error performance in fading environment.

To make SIC a practical technique in uplink WCDMA systems, we first analyze the ordering method which has large influence on the performance of SIC. Then we present techniques to alleviate the drawbacks of SIC. Furthermore, techniques to increase the system capacity are proposed.

It has been shown that the ordering method has a great effect on the performance of SIC. Three ordering methods are discussed and compared in the aspect of the implementation issues (such as reordering frequency, processing delay, latency, and computational

complexity), and error performance related parameters (such as pilot-to-traffic amplitude ratio, cancellation-ordering method, grouping interval, received power distribution ratio and channel estimation as well as timing estimation errors). In addition to considering the single-rate system, a generalized pilot-channel aided SIC scheme is presented to apply to multirate communications.

SIC has several drawbacks: sensitive to channel estimation error due to error propagation from stage to stage, longer processing delay than parallel interference cancellation (PIC), and complicated power control. In the uplink of WCDMA systems, the pilot-channel signals can be employed to reduce channel estimation errors. However, the traffic-channel signals are always interfered by other users' pilot and traffic signals even without any fading. This interference can be alleviated by employing pilot-channel signal removal (PCSR) technique. To shorten processing delay, a pipeline scheme is proposed. It is shown in the thesis that even with the equal power control profile, the SIC with properly chosen ordering method still outperforms multistage partial PIC (PPIC).

In addition to considering pure SIC in uplink WCDMA systems, an adaptable scheme with the ability of adapting its structure according to the environment and channel condition is presented. The processing delay and computational complexity can be adjusted based on system loading and required performance. The proposed scheme combines SIC and PPIC for data detection and performs refined channel estimation. The processing delay is shorter than pure SIC with reasonable hardware, and better error performance on both channel parameter estimation and user data detection are achieved.

To extend the SIC technique to turbo-coded systems, an iterative IC with ordered SIC at front-end is proposed. To avoid unnecessary computation, the ordering information obtained from SIC front-end is utilized in a low-complexity stopping criterion with high efficiency. In addition to bit-wise interference cancellation, the SIC technique is also applied to code-block-wise interference cancellation. And, only the bits in incorrect blocks should be

preceded to the next outer iteration. As a result, huge amount of computational complexity can be saved, and better performance is achieved.



誌 謝

在此，向我的指導教授 魏哲和 教授，獻上最誠摯的感謝與敬意，老師總是適時的指導我正確的研究方法與態度，並讓我充分發揮，不僅如此，老師的風範與待人處世也一直是我所崇敬與學習的目標。

非常感謝在我求學過程中每一位曾經教導過我的老師及學長，林嘉慶教授適時的指導令我感佩在心，還有所有我曾經參與修課及旁聽的教授們，以他們融會後的心得，悉心授課引領，使我能有深入研究的良好基礎。

同時要感謝共同組成通訊電子與訊號處理實驗室的教授們，特別是林大衛教授與杭學鳴教授，使我能從更寬廣的角度思考，看到更多的可能與可為。還有我所認識的歷屆的學長，學姐，同學，學弟，學妹們，每個人的獨一無二，豐富了我的求學生涯。

最要感謝的，是我親愛的父母，以及姊姊之瑋，因為有你們無限的支持與鼓勵，使我得以無後顧之憂，並努力堅持到順利完成學業。

要感謝的人，事，物太多，就感謝天吧！人生的學問，將在永無止盡的學習與探索中，為自己找尋答案。

唐之璇

謹誌於台灣新竹交通大學

西元二〇〇七年一月

Contents

Contents	i
List of Tables	iii
List of Figures	iv
Abbreviations and Acronyms	ix
Chapter 1	2
Introduction	2
1.1 CDMA Technology.....	3
1.2 Multiuser Detection	4
1.3 Outline of the Thesis.....	8
Chapter 2	12
Overview of WCDMA Systems	12
2.1 Physical Layer of WCDMA Technology.....	13
2.2 System Model	25
Chapter 3	41
Pilot-Channel Aided Successive Interference Cancellation	41
3.1 Overview	41
3.2 Channel Estimation	42
3.3 Pilot Channel Signal Removal.....	44
3.4 Ordering Type.....	48
3.5 Performance Analysis	51
3.6 Results and Discussions	56
3.7 Pilot-Channel Aided SIC for Multirate Systems	61
3.8 Summary.....	64

Chapter 4.....	76
Advanced Techniques for Pilot-Channel Aided Interference Cancellation	76
4.1 Overview	76
4.2 Pilot-Channel Aided Pipeline Interference Cancellation Scheme	77
4.3 Pilot-Channel Aided Adaptable Interference Cancellation Scheme	82
4.4 Summary	88
Chapter 5.....	96
Pilot-Channel Aided Iterative Interference Cancellation in Turbo-Coded Systems	96
5.1 Overview	96
5.2 Stopping Criterion for Turbo Decoding with SIC at Front End	98
5.3 A Novel Iterative IC	110
5.4 Summary	113
Chapter 6.....	118
Conclusions	118
Appendix A HSDPA.....	121
Appendix B HSUPA	125
Appendix C Derivation of Equation (2-4)	131
Bibliography.....	134



List of Tables

Table 2-1 Main WCDMA parameters [33].....	33
Table 2-2 Mapping from $z_n(i)$ to $c_{short,1,n}(i)$ and $c_{short,2,n}(i)$, $i = 0, 1, \dots, 255$	33
Table 2-3 UL reference measurement channel (64 kbps).....	33
Table 2-4 Maximum number of simultaneously-configured uplink dedicated channels ...	128
Table 2-5 E-DPDCH Fixed reference channel 5 (FRC5).....	128
Table 3-1 Characteristics of Three SICs per G Bits per K Users.....	66
Table 3-2 Simulation Parameters.....	66
Table 3-3 Propagation Conditions for Multipath Fading Environments [71].	66
Table 3-4 Simulation Parameters for Multirate Systems.....	66
Table 4-1 Implementation issues with the proposed pipelined SIC	89
Table 5-1 Average redundant iteration number of deciding correct CB versus average false alarm probability at SNR = 6.9dB, 8 users.....	114
Table 5-2 Average inner iteration in the proposed method and the generalized iterative method	114

List of Figures

Fig. 1-1 The global access of IMT-2000	11
Fig. 1-2 Block diagram of the generalized communication systems.....	11
Fig. 2-1 TrCH multiplexing structure for uplink.....	33
Fig. 2-2 TrCH multiplexing structure for downlink.....	34
Fig. 2-3 Rate 1/2 and rate 1/3 convolutional coders.....	34
Fig. 2-4 Structure of rate 1/3 Turbo coder (dotted lines apply for trellis termination only)	34
Fig. 2-5 Channel coding for the UL reference measurement channel (64 kbps).....	35
Fig. 2-6 Summarizing the mapping of TrCH s onto PhCHs	35
Fig. 2-7 Configuration of uplink scrambling sequence generator.....	36
Fig. 2-8 Uplink short scrambling sequence generator for 255 chip sequence.....	36
Fig. 2-9 Configuration of downlink scrambling code generator	36
Fig. 2-10 Code-tree for generation of OVVSF codes	37
Fig. 2-11 Frame structure for uplink DPDCH/DPCCH	37
Fig. 2-12 The uplink spreading of DPCCH and DPDCHs.....	37
Fig. 2-13 Spreading for uplink dedicated channels.....	38
Fig. 2-14 Uplink modulation.....	38
Fig. 2-15 Frame structure for downlink DPCH.....	38
Fig. 2-16 Spreading for all downlink PhCHs except SCH.....	38
Fig. 2-17 Combining of downlink PhCHs.....	39
Fig. 2-18 Downlink modulation	39
Fig. 2-19 Transmitter model.....	39
Fig. 2-20 Spreader for the k -th user.....	39

Fig. 2-21 Multipath fading channel model	40
Fig. 2-22 Structure of the MRC RAKE with F finger combining.....	40
Fig. 2-23 The difference between retransmission handling with HSDPA and Release '99 [33]	123
Fig. 2-24 Spreading for uplink HS-DPCCH.....	123
Fig. 2-25 A simple illustration of the general functionality of HSDPA [33]	124
Fig. 2-26 Coding chain for HS-DSCH	124
Fig. 2-27 HS-DSCH HARQ functionality.....	124
Fig. 2-28 E-DPDCH frame structure.....	129
Fig. 2-29 Spreading for E-DPDCH/E-DPCCH	129
Fig. 2-30 E-DPDCH Fixed reference channel 5 (FRC5).....	129
Fig. 2-31 TrCH processing for E-DCH.....	130
Fig. 2-32 E-DCH HARQ functionality.....	130
Fig. 3-1 The received signal timing and data detection group (a) $\tau_{k,p;J,f} \geq 0$ and (b) $\tau_{k,p;J,f} < 0$ where $\tau_{k,p;J,f} = \tau_{k,p} - \tau_{J,f}$	67
Fig. 3-2 Channel estimation of user J with F paths.....	67
Fig. 3-3 Structure of the pilot respread of the k -th user with F paths.....	67
Fig. 3-4 Structure of the data respread of the k -th user with F paths	68
Fig. 3-5 Block diagram of pilot-channel signal regenerator and remover, $1 \leq k \leq K$, $1 \leq f \leq P$	68
Fig. 3-6 Generalized SIC structure at the u -th stage	68
Fig. 3-7 Block diagram of SIC I with PCSR ($1 \leq f \leq F$).....	69
Fig. 3-8 Block diagram of SIC II with PCSR ($1 \leq f \leq F$).....	69
Fig. 3-9 Block diagram of SIC III with PCSR ($1 \leq f \leq F$).....	69

Fig. 3-10 MSE of channel estimates with various SNRs, flat Rayleigh fading channel, $PDR=1.0, G=1$	70
Fig. 3-11 BER versus PDR with different grouping interval G for (a) SIC I, (b) SIC II, (c) SIC III; AWGN, know channel parameters, with PCSR.	70
Fig. 3-12 Simulated and analytical results of SICs with PCSR (a) individual BER in an eight-user system, (b) average BER.	71
Fig. 3-13 BER comparison with different PDRs and SNRs with/without PCSR for (a) SIC I with $G=1$, (b) SIC II with $G=1$, (c) SIC III with $G=1$, (d) SIC I with $G=2400$; AWGN, channel estimation with $W=128$	71
Fig. 3-14 BER versus β_c with/without PCSR when there are (a) 8 users, (b) 16 users in the system; AWGN, channel estimation with $W=128$	72
Fig. 3-15 BER versus PDR for the three SICs in multipath fading channels (a) Case 1, (b) Case 2, (c) Case 3, (d) Case 4; with PCSR, known channel parameters.....	72
Fig. 3-16 BER versus PDR for the three SICs in multipath fading channels (a) Case 1, (b) Case 2, (c) Case 3, (d) Case 4; channel estimation with $W=128$ and timing estimation error with variance 2 samples at 1/32 chips resolution.....	73
Fig. 3-17 BER versus grouping interval G for user in different detection order for (a) SIC I with $PDR=1.3$, (b) SIC II with $PDR=1.0$, (c) SIC III with $PDR=1.0$; channel case 3, known channel parameter, with PCSR.	73
Fig. 3-18 BER versus β_c for multipath fading channels (a) Case 1, (b) Case 2, (c) Case 3, (d) Case 4; channel estimation with $W=128$	74
Fig. 3-19 BER versus grouping interval G for multipath fading channels (a) Case 1, (b) Case 2, (c) Case 3, (d) Case 4; with PCSR	74
Fig. 3-20 BER vs. grouping interval $G_c, f_d=222\text{Hz}$ for (a) multirate systems and (b) single rate systems.	75

Fig. 3-21 Grouping interval G_c for the minimum BER vs. Doppler shift	75
Fig. 4-1 The proposed pipelined scheme for interference cancellation scheme.....	89
Fig. 4-2 PiIC (a) $\#ua$ block and (b) $\#ub$ block in Fig. 4-1, $1 \leq u \leq K$	89
Fig. 4-3 UdIC (a) $\#ua$ block and (b) $\#ub$ block in Fig. 4-1, $1 \leq u \leq K$	90
Fig. 4-4 Average BER versus user number with different schemes	91
Fig. 4-5 Average BER versus SNR with different schemes and user numbers	91
Fig. 4-6 Multistage PIC scheme	92
Fig. 4-7 The s -th stage of PPIC	92
Fig. 4- 8 Detail structure of unit in Block3 in Fig. 4-9	92
Fig. 4-9 The proposed adaptable IC scheme	93
Fig. 4-10 Structure of the RAKE bank with input enables.....	94
Fig. 4-11 Average BER versus iteration of SIC in Block2 in Fig. 4-9, 20 users, 10dB	94
Fig. 4-12 Average BER versus user number, iteration in Block2 equals to user number divide by 2, stage in Block4 is limited to 1	94
Fig. 4-13 Minimum average BER versus user number, PIC stage in Block4 can be up to 3, 10dB	95
Fig. 4-14 Average BER versus different SNR, 20 users.....	95
Fig. 5-1 Block diagram of turbo decoder for one user	115
Fig. 5-2 BER comparison of turbo-coded systems with SIC II and PPIC at front-end.....	115
Fig. 5-3 A novel iterative IC scheme	115
Fig. 5-4 Block diagram of SIC at front-end.....	116
Fig. 5-5 Block diagram of the first outer iteration of the proposed iterative IC.....	116
Fig. 5-6 Block diagram of the 2nd to the I_o -th outer iteration.....	116

Fig. 5-7 Block diagram of variance estimation 117

Fig. 5-8 Generalized iterative IC 117

Fig. 5-9 BER comparison of our proposed iterative IC and the generalized IC without
detection of correct CB..... 117



Abbreviations and Acronyms

2G	Second-generation wireless telephone technology
3G	Third-generation wireless telephone technology
3GPP	Third-Generation Partnership Program
3GPP2	Third-Generation Partnership Program 2
ACK/NACK	Acknowledgement / Non-Acknowledgement
AG	Absolute Grant
AICH	Acquisition Indicator Channel
AMC	Adaptive modulation and coding
AMR	Adaptive multi-rate
APP	A posteriori probability
AWGN	Additive white Gaussian noise
Bps	Bit per second
BCH	Broadcast CHannel
BER	Bit error rate
BoD	Bandwidth on Demand
CB	Code Block
CCTrCH	Coded Composed Transport CHannel
CDMA	Code division multiple access
CPICH	Common Pilot CHannel
CRC	Cyclic redundancy check
DCH	Dedicated CHannel
DCCH	Dedicated Control CHannel
DPCCH	Dedicated Physical Control CHannel
DPCH	Dedicated Physical CHannel
DPDCH	Dedicated Physical Data CHannel
DTCH	Dedicated Transport CHannel
DTX	Discontinues Transmission
E-AGCH	E-DCH Absolute Grant CHannel
E-DCH	Enhanced Dedicated CHannel
E-DPCCH	Enhanced Dedicated Physical Control CHannel
E-DPDCH	Enhanced Dedicated Physical Data CHannel
E-HICH	E-DCH Hybrid ARQ Indicator CHannel
E-RGCH	E-DCH Relative Grant CHannel
ETSI	European Telecommunications Standards Institute

FACH	Forward Access CHannel
FBI	Feedback information
FDD	Frequency Duplex Division
FEC	Forward error control
GSIC	Group successive interference cancellation
HARQ	Hybrid Automatic Repeat Request
HIC	Hybrid interference cancellation
HSDCH	High Speed Data CHannel
HSDPA	High Speed Downlink Packet Access
HS-DSCH	High Speed Downlink Shared CHannel
HS-DPCCH	Dedicated Physical Downlink CHannel (uplink) for HS-DSCH
HS-PDSCH	High Speed Physical Downlink Shared CHannel
HS-SCCH	HS-DSCH-related Shared Control CHannel
HSUPA	High Speed Uplink Packet Access
IC	Interference cancellation
IMT-2000	International Mobile Telecommunication 2000
IR	Incremental redundancy
ITU	International Telecommunications Union
L1	Layer one (physical layer)
LLR	Log-likelihood ratio
MAI	Multiple access interference
MAP	Maximum a posteriori
MBMS	Multimedia Broadcast Multicast Service
MF	Matched filter
MIMO	Multiple input multiple output
ML	Maximum likelihood
MMS	Multimedia Message Services
MMSE	Minimum mean squared error
MRC	Maximum ratio combining
MS	Mobile station
MSE	Mean squared error
MUD	Multiuser detection
NodeB	Base station
OVSF	Orthogonal Variable Spreading Factor
PARR	Peak to average power ratio
PCA	Pilot channel aided
PCCC	Parallel concatenated convolutional codec
PCH	Paging CHannel

PCSR	Pilot-channel signal removal
PDC	Personal Digital Cellular
PDR	Power distribution ratio
PIC	Parallel interference cancellation
PPIC	Partial parallel interference cancellation
PICH	Paging Indicator CHannel
PIL	Prime interleaver
PhCH	Physical CHannel
PN	Pseudorandom noise
PSA	Pilot symbol aided
PSTN	Public switched telephone network
QAM	Quadrature amplitude modulation
QoS	Quality of Service
RACH	Random Access CHannel
RG	Relative Grant
RNC	Radio Network Controller
RSC	Recursive systematic convolutional
RSN	Retransmission Sequence Number
RV	Redundancy version
SCH	Synchronization CHannel
SF	Spreading factor
SIC	Successive interference cancellation
SINR	Signal to interference plus noise power ratio
SISO	Soft-in-soft-out
SNR	Signal to noise power ratio
SRNC	Serving Radio Network Controller
TCSR	Traffic channel signal removal
TD-CDMA	Time division CDMA
TDD	Time Duplex Division
TFCI	Transport Format Combination Indicator
TPC	Transmit Power Control
TrBk	Transport Block
TrCH	Transport CHannel
TTI	Transmission time interval
UE	User equipment
UMTS	Universal Mobile Telecommunications System
UTRA	UMTS Terrestrial Radio Access
VoIP	Voice over Internet Protocol

VSG Variable spreading gain
WCDMA Wideband CDMA
WSSUS Wide sense stationary





Chapter 1

Introduction

A cellular telephone system provides a wireless connection to the public switched telephone network (PSTN) for any user location within the radio range of the system. Within a limited frequency spectrum, the cellular systems accommodate a large number of users in a large geographic area.

Analog cellular systems are commonly referred to as the first generation systems deployed in the mid 1980s. In the early 1990s, the global system for communications (GSM) standard became ubiquitous in Europe. With worldwide acceptance, GSM is the first digital cellular phone standard which can serve at least three times of user as compared to the analog cellular systems over the same bandwidth. It takes the advantage of better voice quality and not easy to be monitored. GSM is a time division multiple access (TDMA) system which supports eight users in 270 kHz channels. In 1993, Qualcomm introduced the first code division multiple access (CDMA) systems which was standardized later named IS-95. These two digital cellular communication systems are so called the second generation (2G) cellular system.

With the increasing demand of supporting a variety of service for a large number of users, the cellular communication systems have to utilize the limited spectrum more efficiently to provide more services such as high quality data, multimedia, streaming audio, streaming video, and broadcast-type services to users.

The 2G standards were evolving to 2.5G communication systems to provide more service such as internet access and higher rate data communications. The 2.5G technologies are

packet-switched and can be overlaid upon existing 2G technologies with modification in base station and subscriber unit. The 2.5G wireless network provides higher radio system capabilities and per user data rate than the 2G system, but does not yet achieve all capabilities provided by the third generation (3G) systems.

3G systems are designed for multimedia communications. In addition to high quality voice services, video telephony, multimedia message services (MMS), location-based services and interactive services such as database retrieval as well as computer games are available due to data rate up to several mega bits per second and techniques to combine mobile communication systems and internet. The global access of International Mobile Telecommunication 2000 (IMT-2000) formulated by International Mobile Telecommunications Union (ITU) is shown in Fig. 1-1. The standard planned to implement a global frequency band in the 2000 MHz range that would support a single, ubiquitous wireless communication for all countries throughout the world. However, the worldwide user community remains split between two parts: Wideband CDMA (WCDMA) standards based on backward compatibility with core network of GSM and IS-136/PDC adopted by 3GPP, and cdma2000 standards based on backward compatibility with core network IS-95 adopted by 3GPP2. Both of these two groups choose CDMA as multiple access technology in 3G systems.

1.1 CDMA Technology

In practical CDMA systems, the narrowband message signal of different users is discriminated by multiplying a very large bandwidth signal called the spreading signal with the message signal. The spreading signal is a pseudo-random code sequence that has a chip rate which is orders of magnitude greater than the data rate of the message. As a consequence, multipath fading may substantially decrease, and a RAKE receiver can be used to collect

information from different delay paths. All user data are transmitted simultaneously in the same frequency band. Theoretically, the cross-correlation of all spreading signals are zero, and the optimal receiver for each user in additive white Gaussian noise (AWGN) is to perform a time correlation operation with user-specified spreading signal at the receiver end. However, because of large number of codes required, non-orthogonal codes such as pseudorandom noise (PN) codes are employed for practical use. The cross-correlation between these codes are no longer zero, and thus interference from other user signals, known as multiple access interference (MAI), is introduced. If there are K users with received power P_k and spreading factor SF_k , the MAI to the desired user J is $\sum_{k=1, k \neq J}^K P_k / SF_J$ after despreading. Thus the signal-to-interference-plus-noise ratio becomes $SINR_J = SF_J P_J / (N_0 + \sum_{k=1, k \neq J}^K P_k)$. If the spreading factor (SF) is moderate and the interfering users is large (>10), the MAI can be modeled as AWGN according to central limit theorem [33]. In the cellular environment, if the power of each user within a cell is not controlled appropriately, SINR of the user with small received power can be dramatically decreased by user with large received power, i.e., the near-far problem occurs. However, since the MAI are not noises, SINR can be increased if the MAI are removed. It has been shown in 1980s that the system capacity can be increased by an optimal detector with high complexity [80], and thus led to a new field known as multiuser detection (MUD).

1.2 Multiuser Detection

1.2.1 Optimum Multiuser Detection

The optimal multiuser detector derived by Verdu [80] can use either maximum a posteriori (MAP) detection or maximum likelihood (ML) sequence detection. For a K -user system, the complexity of the optimal detector is $O(|A|^K)$ where $|A|$ is the alphabet size (two

for binary). In addition to high computational complexity, the detector required the knowledge of the noise variance through the channel, as well as the amplitudes at receiver end, the spreading codes, and timing of all K users. Although the detector is not feasible for practical use, it provides large capacity gain over conventional matched filter (MF). Afterwards, a large number of researches have been triggered to find a sub-optimal receiver with lower complexity and less required information with slight sacrifice in performance [22], [54], [78], [79], [81].

1.2.2 Sub-Optimal Detection

There are many kinds of sub-optimum MUDs announced in the past decade, and these existing detectors can be categorized in many ways. Based on the implementation-oriented categorization, the detectors can be classified to centralized or non-centralized ones. Another way is to classify the detectors to linear or non-linear ones.

■ Centralized vs. Decentralized

The centralized detectors jointly detect each user's data, while the decentralized detectors detect data of the user or users of interest according to the received signal composed of multiple users' data. The decentralized detectors (single-user reception) require no spreading codes or received signal information of other users. The orthogonal filter is well known, which executes updating using the Minimum Mean-Squared Error (MMSE) algorithm so that the spreading code replica used for despreading would be orthogonal to the spreading code of signals of other users (including multipath signals). Although the orthogonal filter has an easier configuration than centralized detectors, it cannot be applied to scrambling codes that have much longer iteration period than the symbol length (long codes). In contrast, centralized detectors uses the reception signals and decoding data sequence of users to reduce the interference of other users in a mutually dependent manner. Generally speaking, the

centralized detectors are used in base stations, and the decentralized detectors can be used either in base stations or mobile receivers.

■ Linear vs. Nonlinear

The linear detectors perform linear filtering according to a specific criterion to suppress the MAI. There are two main kinds of linear MUD, named decorrelator and minimum mean square error (MMSE) detector [48], [49]. These suboptimum MUDs are similar to the zero-forcing and the MMSE equalizers used to combat inter-symbol interference in a single-user channel [1].

Although the linear detectors are easily to analyze, they restrict the system performance. The non-linear detectors are known to achieve better performance in an iterative manner. The first kind of generalized non-linear detectors adopt linear detector as the pre-processing unit to suppress interference, and they suffer the same problems as linear detectors, i.e., matrix inversion must be performed. The second kind of generalized non-linear detectors, often referred to as interference cancellation (IC) [18], perform data decision using the output of matched filter without matrix inversion. The IC scheme tends to partially or fully remove the MAI terms at MF or RAKE outputs. A number of interference cancellation detectors have been proposed [22], [53], [54], [78], [90]. These detectors use soft or hard decisions to reconstruct interfering signal from part or all of the interfering users and subtracted the interfering signal from the received signal. The user of interest can then expect detection without or with only part of MAI if all decisions of interfering users are correct. Otherwise, error decisions of these interferers contribute double interfering signal. IC can be classified into three categories: parallel IC (PIC), successive IC (SIC), and hybrid IC (HIC). These ICs have tradeoff on computational complexity, processing delay and error performance.

The SIC detects user data and cancels multiple access interference in a serial manner. The performance of SIC is influenced by the cancellation order. The PIC simultaneously

processes all K users, canceling their interference after they have all been decoded independently [22], [78], [90], [92]. To alleviate performance saturation due to poor estimated interference in early stages, the partial PIC [22] is often used to partially cancel the estimated MAI from early stages. SIC also tends to remove partial interference from the decision statistics. The difference between SIC and PPIC is that PPIC removes partial interference from all users while SIC removes interference from users that are more reliable than the desired one. The PIC takes the advantage of having lower latency than the SIC at the sacrifice of adding more computational complexity. If there are K users in the system, the computational complexity of PIC are proportional to SK where S is the stage of PIC and that of SIC is proportional to K . As for latency, it is proportional to S for PIC and K for SIC. In addition to simplicity, the SIC performs better and is more robust than PIC [23], [53].

However, there are several drawbacks that prevent SIC becoming a widely used technique [6]: (1) the total decoding time of SIC increases linearly with the number of users; (2) it is thought that the optimum power control for SIC are far more complicated than the equal power control for conventional receiver or PIC: although SIC with controlled user power distribution [6], [16], [42] can reduce the other-cell interference [5], [31] and increase system capacity [19], [87]; (3) the SIC is sensitive to estimation error due to error propagation.

Several techniques have been proposed to solve these drawbacks [2], [7], [17], [35], [68]. Pipelined [35], [68] and hybrid [40], [89] techniques are utilized to combat the problem of long latency of SIC when K is large. The HIC attempts to compromise the characteristics of SIC and PIC, i.e., all users in the system are separated into several parts, a part of users are detected in parallel, removed from the received signal, and then another part of users is detected in parallel. In [89], the so-called groupwise serial interference cancellation (GSIC) is the hybrid version of PIC and SIC which perform interference

cancellation in systems with variable SF. Recently, a frame-error-rate based outer-loop power control is shown to be applicable to SIC [17]. In [7], a simple iterative algorithm to achieve the optimal power control distribution is given. In [2], the authors show that power control can be done in commercial CDMA without modification. Recent work shows that SIC is a practical IC where its simplified version is employed as part of a commercial device to increase the cdma2000 EV-DO Rev A reverse link voice over IP (VoIP) capacity by about 15 percent [37].

1.3 Outline of the Thesis

Due to the simplicity and superior error performance over other MUDs in fading environment, in this thesis, we analyze the characteristics of SIC. Then we propose practical techniques and architectures of pilot-channel-aided SIC over uplink WCDMA systems in the hope of making this technique widely used.

It has been shown that the ordering method has a great effect on the performance of SIC [15], [52], [58], [69]. Our proposed method is presented in Chapter 3, and three ordering methods for SIC in the uplink of WCDMA systems over multipath fading channels are discussed and compared in the aspect of the implementation issues and error performance related parameters. In addition to consider the single-rate system, a generalized pilot-channel aided SIC scheme is presented to apply to multirate communications.

To overcome drawbacks of the well-known SIC, several techniques have been proposed. First, sophisticated detection schemes are sensitive to channel estimation accuracy, so are ICs due to error propagation from stage to stage. When the pilot-channel signals in Q-channel and the traffic-channel signals in I-channel are scrambled by complex scrambling codes and transmitted simultaneously such as that in the uplink of WCDMA systems [75], pilot channel can be employed to reduce channel estimation errors. However,

the traffic-channel signals are always interfered by other users' pilot and traffic signal even without any fading. This interference between I-channel and Q-channel can also be alleviated with interference cancellation techniques. Pilot-channel signal removal (PCSR) technique combining with RAKE receiver [27] and PIC [36] is used to alleviate the interference from other users' pilot signals. In Chapter 3, we propose that the pilot-channel signal of all users are removed from the received signal followed by the SIC for data detection at the cost of slight increase in processing delay. Second, a pipeline scheme is proposed in Chapter 4 to shorten processing delay [68]. Third, it is shown in Chapter 4 that even with the equal power control profile, the SIC with properly chosen ordering method still outperforms multistage PPIC [67].

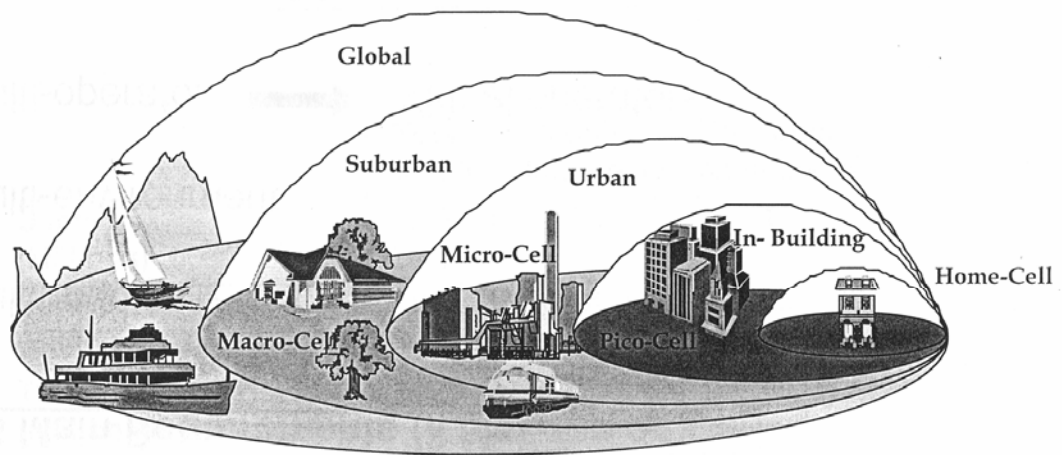
In addition to considering pure SIC in uplink WCDMA systems, we further propose an adaptable scheme with the ability to adjust its structure according to the environment and channel condition. The scheme combines serial (SIC) and parallel (PIC) interference cancellation, and the processing delay and computational complexity can be adjusted based on system loading and required performance. Compared with SIC and PIC, the proposed pilot-channel aided adaptable scheme shows better performance over both ICs with reasonable hardware while it needs shorter processing delay than SIC. The interference between data channel signals and pilot channel signals under multipath fading channel are also taken into consideration. This results in better quality both on channel parameter estimation and user data detection.

To extend the SIC for application in turbo-coded systems, an iterative IC with ordered SIC at front-end is proposed in Chapter 5. Except for the timing information, all parameters used in the proposed scheme are estimated from the received signal. To avoid unnecessary computations, we utilize the ordering information obtained from SIC front-end to propose a stopping criterion with high efficiency and low complexity. After finding the correct CBs,

bits in correct blocks are hard-decisioned, re-encoded and removed from the correlated input signal. Only the bits in incorrect blocks should proceed to the next outer iteration. Also, information of the CB correctness is utilized to decide if the next outer iteration should be done. As a result, huge amount of computational complexity can be saved with BER improvement.

The thesis is organized as follows. The WCDMA system especially the physical layer and the system model is described in Chapter 2. In Chapter 3, the scheme of pilot-channel aided SIC employing three cancellation-ordering methods are presented and compared in the aspect of implementation complexity and error performance. This scheme can be applied to multirate systems. To make the SIC a practical scheme, in Chapter 4 we develop two advanced techniques including pipeline SIC and adaptable IC. Iterative IC receiver with SIC at front-end in turbo-coded systems as well as low-complexity stopping criterion are presented in Chapter 5. Finally, conclusions are given in Chapter 6.

In Fig. 1-2, a block diagram of the generalized communication systems is shown. The block where our thesis is concerned is filled with gray color.



Different Environments for UMTS

Fig. 1-1 The global access of IMT-2000

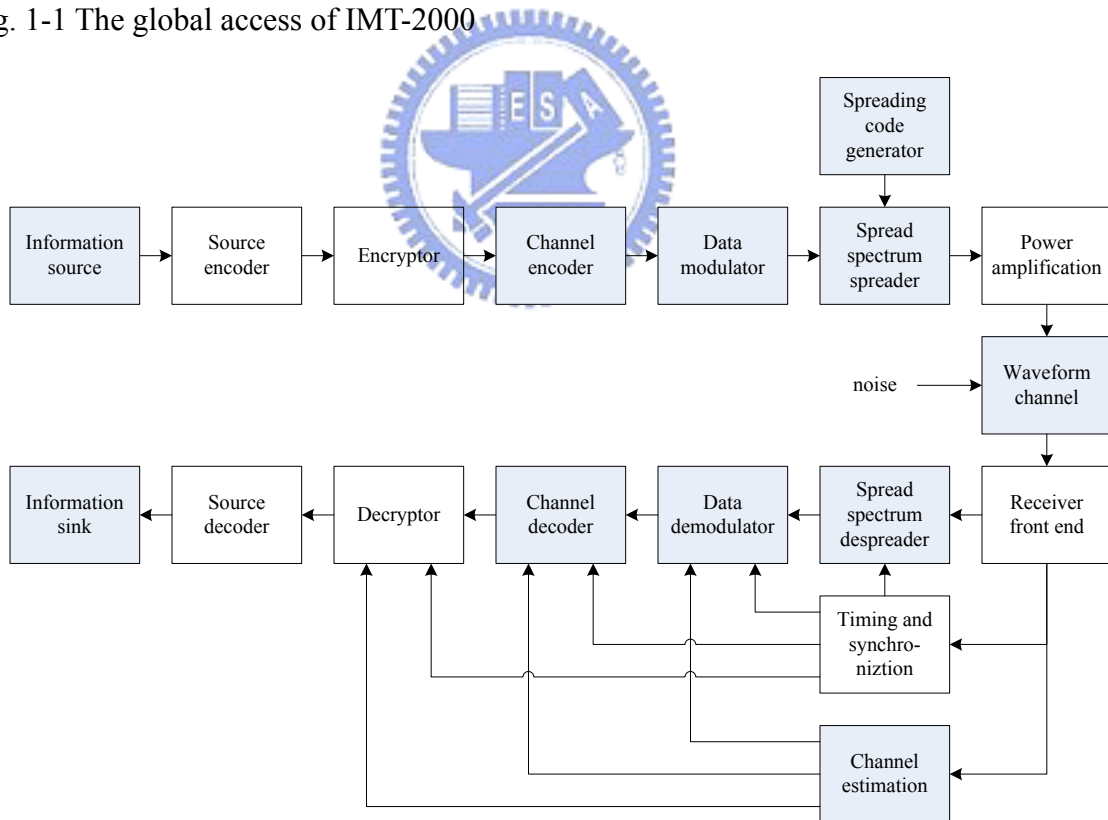


Fig. 1-2 Block diagram of the generalized communication systems

Chapter 2

Overview of WCDMA Systems

WCDMA technology was created in the 3GPP group. In Europe, the 3G mobile communication system is called the Universal Mobile Telecommunications System (UMTS), whereas the terrestrial radio access system is referred to as the UMTS Terrestrial Radio Access (UTRA), which is why WCDMA is called UTRA FDD (Frequency Duplex Division) and TD-CDMA (Time Duplex Division) is called UTRA TDD in Europe. After the completion of the Release '99 specifications, minor adjustments are made, and so called Release 4 was completed in March 2001. The high speed downlink packet access (HSDPA) and IP-based transport layer to achieve high throughput, reduce delay and achieve high peak rates were included in Release 5 which was completed in Mar 2002 for the WCDMA radio aspect. For Release 6 completed in Mar 2005, the high speed uplink packet access (HSUPA) and multimedia broadcast multicast service (MBMS) were introduced. The HSUPA aims at providing significant enhancements in terms of user experience (throughput and delay) and/or capacity, and coverage, while MBMS enables the ability to deliver audio and video data to multiple users simultaneously. The HSDPA and the HSUPA are briefly described in Appendix A and Appendix B, respectively. Readers can refer to [34] for more details. The next step in the evolution is Release 7 which is currently under development. The techniques including MIMO, and 3.84 Mcps and 7.68 Mcps TDD enhanced uplink where the first 1.28 Mbps TDD mode originally from CWTS (China) was included in 3GPP Release 4.

In this chapter, we describe system model used in this thesis. First, the physical layer of WCDMA technology is briefly introduced. Then the transmitter in the uplink and multipath

fading channel followed by the RAKE receiver used in the overall thesis are presented.

2.1 Physical Layer of WCDMA Technology

In the radio interference protocols, which are used to set up, reconfigure and release the Radio Bearer services, the physical layer defines the fundamental capacity limits. The physical layer of the radio interface has been typically the main discussion topic when different cellular systems have been compared against each other.

In WCDMA, the concept of obtaining Bandwidth on Demand (BoD) is well supported, and it is easy to support an asymmetric uplink and downlink configuration by means of independently setting the SF between uplink and downlink for each user. The carrier bandwidth is 5 MHz for the chip rate of 3.84 MHz. Therefore, the transmission power of Mobile Stations (MSs) can be reduced by technologies like RAKE reception with more paths combining. The operation of asynchronous base stations is supported to make deployment of indoor and micro base station easier when no GPS signal needs to be received. WCDMA support two duplex modes: FDD with separate 5MHz carrier frequencies for uplink and downlink and TDD with only one time-shared 5MHz spectrum for both uplink and downlink. Coherent detection is employed based on the used of pilot symbols or common pilot to increase the coverage and capacity on both uplink and downlink. In addition, advanced CDMA receiver techniques, such as multiuser detection, can be employed to increase capacity and coverage of the overall system. Main WCDMA parameters are listed in Table 2-1.

The physical layer of WCDMA FDD is described in [72], [73], [74], [75], [76]. Main body of WCDMA physical layer is established in Release '99. In UTRA, the physical layer is required to support variable bit rate transport channels (TrCHs) to offer BoD services, and to be able to multiplex several services to one connection. User data and control signal in

TrCHs from Media Access Control (MAC) layer are multiplexed and mapped to different physical channels (PhCHs) to be transmitted in air interface in physical layer. Multiplexing is a combination of error detection, error correcting, rate matching, interleaving and TrCHs mapping onto or splitting from PhCHs [73]. Data in PhCH is then spread and modulated and transmitted over the air. The use of a variable SF and multi-code connections is supported for practically achievable bit rate transmission up to 384 kbps. There are many procedures essential for system operation, such as the fast power control and handover measurements [75]. We focus our introduction on data transmission in dedicated channel of physical layer in WCDMA Release '99.

2.1.1 Transport Channels

There are two types of TrCHs defined: dedicated channel and common channels. A Dedicated channel is reserved for a single user only and using inherent addressing of UE while a Common channel is a resource divided between all or a group of users in a cell, and using explicit addressing of UE if addressing is needed.

The dedicated TrCH, Dedicated CHannel (DCH), is a downlink or uplink TrCH that carries user data or control information from layers above the physical layer. The DCH is characterized by features such as fast power control, fast data rate change on a frame-by-frame basis, and possibility of transmission to a certain part of the cell or sector with varying antenna weights in adaptive antenna systems. The DCH supports soft handover.

The common TrCHs needed for the basic network operation are three downlink TrCHs (Broadcast CHannel (BCH) is used to broadcast system- and cell-specific information in downlink. Forward Access CHannel (FACH) is used to carry control information to terminals known to locate in the given cell. Paging CHannel (PCH) is used to carry data relevant to the paging procedure to support efficient sleep-mode procedure) and one uplink

TrCH (Random Access CHannel (RACH) is used to carry control information from the terminal, such as requests to set up a connection). Common channels do not have soft handover but some of them can have fast power control.

In addition to the above TrCHs, there are High Speed Downlink Shared Channel (HS-DSCH) in Release 5 for HSDPA and Enhanced Dedicated Channel (E-DCH) introduced in Release 6 for HAUPA. There are significant differences in physical layer operations between these two channels and other channels earlier than Release 5. HS-DSCH and E-DCH are briefly described in Appendix A and Appendix B, respectively.

2.1.2 Multiplexing

At the transmitter side, data arrives at the coding/multiplexing unit in form of transport block sets once every transmission time interval (TTI). The TrCHs are multiplexed to different PhCHs. The TTI is transport-channel specific and it can be 10 ms, 20 ms, 40 ms, or 80 ms. The coding/multiplexing steps for the uplink and downlink are shown in Fig. 2-1 and Fig. 2-2, respectively. Each function block is briefly described in the following and the details are in [73]. In the uplink, the symbols on the DPDCH (PhCH of TrCH DCH) are sent with equal power level for all services, i.e. in order to balance the power level requirements for the channel symbols, the relative symbol rates for different services should be adjusted by coding and channel multiplexing.

■ CRC Attachment

After receiving a transport block from higher layers, the first operation is Cyclic Redundancy Check (CRC) attachment for error checking on transport blocks at the receiver end. The physical layer provides the transport block to higher layers together with the error indication from the CRC check. The CRC length can be 0, 8, 12, 16 and 24 bits. Large CRC bit number can lead to low probability of an undetected error of the transport block.

■ Channel Coding

Two types of coding schemes, namely, convolutional encoding and turbo encoding, have been defined in UTRA. The turbo encoding/decoding method is an 8-state parallel concatenated convolutional codec (PCCC). In convolutional encoding, a coding rate of either 1/2 or 1/3 (constraint length = 9 in both cases) with the use of tail bits is applied depending on QoS.

Fig. 2-3 illustrates the configuration of a *convolutional coder*. Eight tail bits with binary value 0 shall be added to the end of the CB before encoding. The initial value of the shift register of the coder shall be "all 0" when starting to encode the input bits.

Fig. 2-4 illustrates the configuration of a *Turbo coder*. The transfer function of the 8-state constituent code for PCCC is:

$$G(D) = \begin{bmatrix} 1, \frac{g_1(D)}{g_0(D)} \end{bmatrix},$$

where

$$g_0(D) = 1 + D^2 + D^3,$$

$$g_1(D) = 1 + D + D^3.$$



The initial value of the shift registers of the 8-state constituent encoders shall be all zeros when starting to encode the input bits. Output from the Turbo coder is $u[1], u^{p1}[1], u^{p2}[1], u[2], u^{p1}[2], u^{p2}[2], \dots, u[M], u^{p1}[M], u^{p2}[M]$, where $u[1], u[2], \dots, u[M]$ are the bits input to the Turbo coder i.e. both first 8-state constituent encoder and Turbo code internal interleaver, and K is the number of bits, and $u^{p1}[1], u^{p1}[2], \dots, u^{p1}[M]$ and $u^{p2}[1], u^{p2}[2], \dots, u^{p2}[M]$ are the bits output from first and second 8-state constituent encoders, respectively. The bits output from Turbo code internal interleaver are denoted by $u'[1], u'[2], \dots, u'[M]$, and these bits are to be input to the second 8-state constituent encoder.

The Turbo code internal interleaver is prime interleaver (PIL) based on block interleaving

[63]. Bits-input are first written in a rectangular matrix with padding. Then the Intra-row and inter-row permutations of the rectangular matrix is performed. After that, bits-output from the rectangular matrix with pruning are sent. The output of the Turbo code internal interleaver is the bit sequence read out column by column where the output is pruned by deleting dummy bits that were padded to the input of the rectangular matrix.

Trellis termination is performed by taking the tail bits from the shift register feedback after all information bits are encoded. Tail bits are padded after the encoding of information bits. The first three tail bits shall be used to terminate the first constituent encoder (upper switch of Fig. 2-4 in lower position) while the second constituent encoder is disabled. The last three tail bits shall be used to terminate the second constituent encoder (lower switch of Fig. 2-4 in lower position) while the first constituent encoder is disabled. The transmitted bits for trellis termination shall then be: $u[M+1], u^{p1}[M+1], u[M+2], u^{p1}[M+2], u[M+3], u^{p1}[M+3], u'[M+1], u^{p2}[M+1], u'[M+2], u^{p2}[M+2], u'[M+3], u^{p2}[M+3]$.

Because of the characteristics of the coding schemes, turbo encoding is effective for video and other high-speed, high-quality data (coding rate = $1/3$, constraint length = 4), whereas convolutional encoding is effective for speech and other low-speed data.

■ First Interleaving

Interleaving is a practical technique to enhance the error correcting capability of coding, especially for the channel with burst errors. It plays an important role in achieving good performance [82]. Interleaving rearranges the ordering of a data sequence in a one-to-one deterministic format. The first interleaving is a block interleaver with inter-column permutations, i.e. write the input sequence into the interleaving matrix row by row. Perform the inter-column permutation for the matrix. Finally, read the output bits of the block interleaver column by column.

■ Second Interleaving

The second interleaving is a block interleaver and consists of bits input to a matrix with padding, inter-column permutation for the matrix and bits output from the matrix with pruning. The number of columns in the matrix is 30, and then the number of rows is obtained. Second interleaving is similar to first interleaving except for the inter-column permutation pattern.

In addition to the above procedures to protect data through wireless channel, there are several procedures used for mapping TrCHs to PhCHs with proper length and format. The **transport block concatenation/segmentation** procedure is used to make the transport block size fit the available CB size defined in the channel coding method. **Radio frame size equalization** is only performed in the uplink, and it is the padding of the input bit sequence in order to ensure that the output can be segmented into data segments of the same size. In **radio frame segmentation**, when the TTI is longer than 10 ms, the input bit sequence is segmented and mapped onto consecutive radio frames of 10 ms each. **Rate matching** means that bits on a TrCH are “repeated” or “punctured” to make the radio frame in PhCH to meet the correct number of bits in one of the predefined formats. In the downlink the transmission is interrupted if the number of bits is lower than maximum. However, when the number of bits between different TTIs in uplink is changed, bits are repeated or punctured to ensure that the total bit rate after TrCH multiplexing is identical to the total channel bit rate of the allocated dedicated PhCHs. Every 10 ms, one radio frame from each TrCH is delivered to the **TrCH multiplexing**. These radio frames are serially multiplexed into a coded composite transport channel (CCTrCH). When more than one PhCHs is used, **physical channel segmentation** divides the bits among the different PhCHs. After the above procedures, in **physical channel mapping**, the original TrCHs can be mapped to PhCHs now. In the uplink, the PhCHs used during a radio frame are either completely filled with bits that are transmitted over the air or not used at all.

2.1.3 Mapping and Association of Physical Channels and Transport Channels

After multiplexing and coding, the TrCHs are mapped to PhCHs. Fig. 2-6 summarizes the mapping of TrCHs onto PhCHs. The different TrCHs are mapped to different PhCHs, though some of the TrCHs are carried by identical PhCHs. The multiplexed DCHs are mapped sequentially (first-in-first-mapped) directly to the PhCH(s). In addition to TrCH-mapped PhCHs, some PhCHs carry only information relevant to physical layer procedures without mapping to TrCHs. SCH, CPICH, AICH, PICH are not visible to higher layers.

An example of channel coding, multiplexing and PhCH mapping is given in Fig. 2-5 and Table 2-3 [71]. This is an example of transmitting 4.1 kbps data and 12.2 kbps AMR speech data in the uplink. The 4.1 kbps data is in one TrCH with 40 ms and AMR speech data is in three TrCH with 20 ms each. These four TrCHs have their own channel coding schemes and different rate-matching attributes. The change of bits for each TrCH and the combination of different length TrCHs are performed. Dedicated control channel (DCCH) and Dedicated traffic channel (DTCH) in Fig. 2-5 are two types of logical channel from which the TrCHs are mapping.

2.1.4 Physical Channels

PhCHs are defined by a specific carrier frequency, scrambling code, channelization code, time start and stop (giving duration). Time durations are defined by start and stop instants, measured in integer multiples of chips.

- Radio frame: A radio frame is a minimum processing duration which consists of 15 slots. The length of a radio frame corresponds to 38400 chips and the time duration is 10 ms.

- Slot: The minimum unit in the Layer 1 bit sequence. The length of a slot corresponds to 2560 chips. The number of bits per slot may be different for different PhCHs and may, in some cases, vary in time.

In FDD mode, PhCHs are identified by code and frequency. After the TrCHs are mapped to PhCHs, they are spread and modulated and sent out to the air interface. Spreading consists of two operations: channelization and scrambling. The channelization operation transforms every data symbol into a number of chips, thus increasing the bandwidth of the signal. The number of chips per data symbol is called SF. Channelization codes are short spreading codes with chip length 4~512, and 4 to 512 types of codes can be used depending on the length. Scrambling codes are relatively long codes with chip length 38,400 (long scrambling codes) or 256 (short scrambling codes), and an extremely large number of scrambling codes can be used. The channelization codes and scrambling codes are used in a different manner between uplink and downlink. In uplink, each UE uses a channelization code to identify PhCH s. Multiple UEs can share the same channelization code, and the BS identifies the UEs according to their scrambling codes. In downlink, channelization codes are used for identifying UEs. Sectors can share the same channelization code, as a different scrambling code is assigned to each sector. Each UE identifies the sector by executing despreading with the use of the scrambling code used in the visited sector. The downlink set of the primary scrambling codes is limited to 512 codes.

The Dedicated uplink Physical CHannels (DPCHs) which is associated with TrCHs Dedicated CHannel (DCH) are described in the following. Other PhCHs of uplink and downlink can be found in [72]. DPCHs are bidirectional uplink/downlink channels and assigned individually to each UE. They are consists of the Dedicated Physical Data CHannel (DPDCH) and the Dedicated Physical Control CHannel (DPCCH), and mapped to I phase and Q phase, respectively.

■ Dedicated Uplink Physical Channels

The Uplink Dedicated Physical Data CHannel (uplink DPDCH) is used for transmitting data from DCH. At least one DPDCH is assigned to each UE. The Uplink Dedicated Physical Control CHannel (uplink DPCCH) is used for carrying control information generated at Layer 1. Only one DPCCH is assigned to each UE using DPCH. The Layer 1 control information consists of known pilot bits to support channel estimation for coherent detection, transmit power-control (TPC) commands, feedback information (FBI), and an optional transport-format combination indicator (TFCI) used to inform the receiver which TrCH is active for the current frame.

Fig. 2-11 shows the frame structure of the uplink DPDCH and the uplink DPCCH. Each radio frame of length 10 ms is split into 15 slots, each of length $T_{\text{slot}} = 2560$ chips, corresponding to one power-control period. The DPDCH and DPCCH are always frame aligned with each other. The parameter k in Fig. 2-11 determines the number of bits per uplink DPDCH slot. It is related to the SF of the DPDCH as $\text{SF} = 256/2^k$. The DPDCH SF may range from 256 down to 4. The SF of the uplink DPCCH is always equal to 256, i.e. there are 10 bits per uplink DPCCH slot.

For the DPCCH and DPDCHs, the uplink spreading of DPCCH and DPDCHs is shown in Fig. 2-12. The binary DPCCH and DPDCHs to be spread are represented by real-valued sequences. The DPCCH is spread to the chip rate by the channelization code $c_c = C_{\text{ch},256,0}$ and $C_{\text{ch},256,0}$ is described in 2.1.5. The n -th DPDCH called DPDCH_n is spread to the chip rate by the channelization code $c_{d,n}$. When only one DPDCH is to be transmitted, DPDCH_1 shall be spread by code $c_{d,1} = C_{\text{ch},\text{SF},k}$, $k = \text{SF} / 4$ and $C_{\text{ch},256,0}$ is described in 2.1.5. When more than one DPDCH is to be transmitted, all DPDCHs have SF equal to 4. DPDCH_n shall be spread by the code $c_{d,n} = C_{\text{ch},4,k}$, where $k = 1$ if $n \in \{1, 2\}$, $k = 3$ if $n \in \{3, 4\}$, and $k = 2$ if $n \in \{5, 6\}$.

After channelization, the real-valued spread signals are weighted by gain factors, β_p for

DPCCH, β_d for all DPDCHs. The β_p and β_d values are signaled by higher layers or derived [75]. At every instant in time, at least one of the values β_p and β_d has the amplitude 1.0. The β_p and β_d values are quantized into 4 bit words.

After the weighting, the stream of real-valued chips on the I- and Q-branches are then summed and treated as a complex-valued stream of chips. This complex-valued signal of uplink dedicated PhCHs (DPCCH, DPDCHs, HS-DPCCH, E-DPCCH, E-DPDCHs) are then summed and scrambled by the complex-valued scrambling code $S_{\text{dpch},n}$ as shown in Fig. 2-13. The code used for scrambling of the uplink dedicated PhCHs may be of either long or short type. The n -th uplink scrambling code, denoted $S_{\text{dpch},n}$, is defined as $S_{\text{dpch},n}(i) = C_{\text{long},n}(i)$, $i = 0, 1, \dots, 38399$, when using long scrambling codes, and $S_{\text{dpch},n}(i) = C_{\text{short},n}(i)$, $i = 0, 1, \dots, 38399$, when using short scrambling codes. $C_{\text{long},n}$ and $C_{\text{short},n}$ are described in 2.1.5.

The scrambling code is applied aligned with the radio frames, i.e. the first scrambling chip corresponds to the beginning of a radio frame. The modulating chip rate is 3.84 Mcps, and the complex-valued chip sequence generated by the spreading process is QPSK modulated as shown in Fig. 2-14.

■ Dedicated Downlink Physical Channels

Dedicated downlink PhCH is different from the uplink one. The DPDCH and DPCCH are time-multiplexed in the time slot. Within one downlink DPCH, dedicated data generated at DCH are transmitted in time-multiplex with control information generated at physical layer. Fig. 2-15 shows the frame structure of the downlink DPCH. Each frame of length 10 ms is split into 15 slots, each of length $T_{\text{slot}} = 2560$ chips corresponding to one power-control period. The parameter k in Fig. 2-15 determines the total number of bits per downlink DPCH slot. It is related to the SF of the PhCH as $\text{SF} = 512/2^k$. The SF may thus range from 512 down to 4. $C_{\text{ch},\text{SF},n}$ is the channelization code used for non-compressed frames.

Fig. 2-16 illustrates the spreading operation for all PhCHs except SCH in the downlink.

The spreading operation includes a modulation mapper stage successively followed by a channelization stage, an IQ combining stage and a scrambling stage. The PhCH using QPSK where each pair of two consecutive symbols is first serial-to-parallel converted and mapped to I and Q branch. Fig. 2-17 illustrates how different downlink channels are combined. Each complex-valued spread channel, corresponding to point S in Fig. 2-16, may be separately weighted by a weight factor G_i . The complex-valued P-SCH and S-SCH may be separately weighted by weight factors G_p and G_s . All downlink PhCHs shall then be combined using complex addition. Modulation of the complex-valued chip sequence generated by the spreading process is shown in Fig. 2-18.

2.1.5 Spreading Codes

■ Channelization Codes

The channelization codes for both uplink and downlink are Orthogonal Variable Spreading Factor (OVSF) codes that preserve the orthogonality between a user's different PhCHs. The OVSF codes can be defined using the code tree as shown in Fig. 2-10. The generation method for the channelization code is defined as

$$C_{ch,1,0} = 1,$$

$$\begin{bmatrix} C_{ch,2,0} \\ C_{ch,2,1} \end{bmatrix} = \begin{bmatrix} C_{ch,1,0} & C_{ch,1,0} \\ C_{ch,1,0} & -C_{ch,1,0} \end{bmatrix} = \begin{bmatrix} 1 & 1 \\ 1 & -1 \end{bmatrix}$$

$$\begin{bmatrix} C_{ch,2^{(n+1)},0} \\ C_{ch,2^{(n+1)},1} \\ C_{ch,2^{(n+1)},2} \\ C_{ch,2^{(n+1)},3} \\ \vdots \\ C_{ch,2^{(n+1)},2^{(n+1)}-2} \\ C_{ch,2^{(n+1)},2^{(n+1)}-1} \end{bmatrix} = \begin{bmatrix} C_{ch,2^n,0} & C_{ch,2^n,0} \\ C_{ch,2^n,0} & -C_{ch,2^n,0} \\ C_{ch,2^n,1} & C_{ch,2^n,1} \\ C_{ch,2^n,1} & -C_{ch,2^n,1} \\ \vdots & \vdots \\ C_{ch,2^n,2^{n-1}} & C_{ch,2^n,2^{n-1}} \\ C_{ch,2^n,2^{n-1}} & -C_{ch,2^n,2^{n-1}} \end{bmatrix}$$

The leftmost value in each channelization code word corresponds to the chip transmitted first in time. The channelization codes are uniquely described as $C_{ch,SF,k}$, where k is the code number, $0 \leq k \leq SF-1$.

■ Scrambling Codes

The long scrambling codes are used in both uplink and downlink while the short scrambling codes are used in the uplink only.

● Uplink Long Scrambling Sequences

The long scrambling sequences are constructed from position wise modulo 2 sum of 38400 chip segments of two binary m-sequences with 25 degree generator polynomials. The resulting sequences thus constitute segments of a set of Gold sequences are shown in Fig. 2-7.

Let $n_{23} \dots n_0$ be the 24 bit binary representation of the scrambling sequence number n with n_0 being the least significant bit. The x sequence depends on the chosen scrambling sequence number n and is denoted x_n , in the sequel. Furthermore, let $x_n(i)$ and $y(i)$ denote the i -th symbol of the sequence x_n and y , respectively. The m -sequences x_n and y are constructed as:

Initial conditions:

$$- x_n(0)=n_0, x_n(1)= n_1, \dots =x_n(22)= n_{22}, x_n(23)= n_{23}, x_n(24)=1.$$

$$- y(0)=y(1)= \dots =y(23)= y(24)=1.$$

The complex-valued long scrambling sequence $C_{long,n}$, is defined as:

$$C_{long,n}(i) = c_{long,1,n}(i) \left(1 + j(-1)^i c_{long,2,n}(2 \lfloor i/2 \rfloor) \right)$$

where $i = 0, 1, \dots, 38399$ and $\lfloor \cdot \rfloor$ denotes rounding to nearest lower integer. The scrambling codes are repeated for every 10 ms radio frame.

● Uplink Short Scrambling Sequences

The configuration of short scrambling sequences is shown in Fig. 2-8. Let $n_{23}n_{22} \dots n_0$ be the 24 bit binary representation of the code number n . The sequence $z_n(i)$ of length 255 is generated according to the following relation:

$$-z_n(i) = a(i) + 2b(i) + 2d(i) \text{ modulo } 4, i = 0, 1, \dots, 254;$$

where the quaternary sequence $a(i)$ is generated recursively by the polynomial $g_0(x) = x^8 + 3x^5 + x^3 + 3x^2 + 2x + 3$ with $a(0) = 2n_0 + 1$ modulo 4; $a(i) = 2n_i$ modulo 4, $i = 1, 2, \dots, 7$; $a(i) = 3a(i-3) + a(i-5) + 3a(i-6) + 2a(i-7) + 3a(i-8)$ modulo 4, $i = 8, 9, \dots, 254$; and the binary sequence $b(i)$ is generated recursively by the polynomial $g_1(x) = x^8 + x^7 + x^5 + x + 1$ with $b(i) = n_{8+i}$ modulo 2, $i = 0, 1, \dots, 7$, $b(i) = b(i-1) + b(i-3) + b(i-7) + b(i-8)$ modulo 2, $i = 8, 9, \dots, 254$, and the binary sequence $d(i)$ is generated recursively by the polynomial $g_2(x) = x^8 + x^7 + x^5 + x^4 + 1$ with $d(i) = n_{16+i}$ modulo 2, $i = 0, 1, \dots, 7$; $d(i) = d(i-1) + d(i-3) + d(i-4) + d(i-8)$ modulo 2, $i = 8, 9, \dots, 254$.

The sequence $z_n(i)$ is extended to length 256 chips by setting $z_n(255) = z_n(0)$. The mapping from $z_n(i)$ to the real-valued binary sequences $c_{\text{short},1,n}(i)$ and $c_{\text{short},2,n}(i)$, $i = 0, 1, \dots, 255$ is defined in Table 2-2. Finally, the complex-valued short scrambling sequence $C_{\text{short},n}$ is defined as $C_{\text{short},n}(i) = c_{\text{short},1,n}(i \bmod 256)(1 + j(-1)^i c_{\text{short},2,n}(2\lfloor (i \bmod 256)/2 \rfloor))$ where $i = 0, 1, 2, \dots$ and $\lfloor \cdot \rfloor$ denotes rounding to nearest lower integer.

● Downlink Long Scrambling Sequences

The scrambling codes of downlink are shown in Fig. 2-9. It use the same Gold codes as uplink except with an 18-degree code generator. For downlink modulation, the chip rate is the same as uplink, i.e., 3.84 Mcps.

2.2 System Model

The system model used in this thesis is described as follows, and it is simplified from the transmitter for uplink physical layer described in 2.1.

2.2.1 Transmitter Model

A K -user asynchronous turbo-coded CDMA system with QPSK modulation is considered.

The transmitter model used in this thesis is shown in Fig. 2-19 where the spreader for the k -th user is shown in Fig. 2-20. Fig. 2-19 is the simplified version of Fig. 2-1 while Fig. 2-20 is simplified from uplink DPDCH/DPCCH in WCDMA systems shown in Fig. 2-12. The turbo encoder used is described in Fig. 2-4. The information bit stream $\mathbf{u}_k = \{u_k[i]\}$, $u_k[i] \in \{0,1\}$, $0 < i \leq M_k + 3$, is encoded with the rate- $R=1/3$ turbo encoder where M_k is the CB size. The internal interleaved version of information bit stream is $\mathbf{u}'_k = \{u'_k[i]\}$, $u'_k[i] \in \{0,1\}$, $0 < i \leq M_k + 3$. The parity bits can be generated from encoder E1 or encoder E2 and are defined as $\mathbf{u}^{px}_k = \{u^{px}_k[i]\}$, $u^{px}_k[i] \in \{0,1\}$, $0 < i \leq M_k + 3$. The resultant coded bit stream $\mathbf{b}'_k = \{b'_k[n']\}$ at the output of P/S block is as described in 2.1.2. The Mapper maps $\{0,1\} \rightarrow \{-1,1\}$ and the interleaver Π is the second interleaver described in 2.1.2 which reorders the coded bits and obtains $\mathbf{b}_k = \{b_k[n]\}$ where $\{b_k[n]\} = \Pi(\{b'_k[n']\})$, $0 < n \leq N_{b,k}$ where $N_{b,k} = 3M_k + n_{tail}$. $n_{tail} = 12$ is the number of tail bits generated from the encoder. The equivalent complex baseband representation of the transmitted signal of the k -th user at the mobile station is given by

$$s_k(t) = \sqrt{P_k} \{ \beta_d C_{O,d}(t) B_k(t) + j \beta_p C_{O,p}(t) A_{pilot}(t) \} C_k(t) \quad (2-1)$$

- P_k is the signal power, and power distribution of all users in the system follows a power distribution ratio (PDR) where $PDR = P_k/P_{k+1} \geq 1$ for $1 \leq k \leq K - 1$ when there are K users in the system. For the sake of justice, total transmit power of all users is K with any given PDR , and $P_K = K(PDR - 1) / (PDR)^{K-1}$.
- β_d and β_p are the traffic-channel gain and pilot-channel gain, respectively. $\beta_d + \beta_p = 1$, and $\beta_c = \beta_p / \beta_d$ denotes the pilot-to-traffic amplitude ratio.

- $B_k(t) = \sum b_k[n]p_b(t-nT_b)$ are the traffic-channel signals, where b_k is the binary data signal taking the values ± 1 from the Interleaver output.
- $A_{pilot}(t) = \sum a_{pilot}[n_{pi}]p_{pi}(t-n_{pi}T_{pi})$ are the uncoded pilot signals modulated at Q -channel and has the same characteristic as $B_k(t)$ but with a symbol period equal to T_{pi} .
- $C_k(t) = \sum c_k[n_c]p_c(t-n_cT_c) = \sum (c_{k,I}[n_c] + jc_{k,Q}[n_c])p_c(t-n_cT_c)$ are the complex scramble sequences S_{dpch} in Fig. 2-12, where $\{c_{k,I}[n_c]\}$ and $\{c_{k,Q}[n_c]\}$ are the Gold sequences with period equal to the length of one frame and composed of $N(SF)$ chips described in 2.1.5, where N is the bit number in a frame.
- $C_{O,x}(t) = \sum c_{O,x}[n_c]p_c(t-n_cT_c)$, where $c_{O,x}$ are the OVFSF codes as shown in 2.1.5 with period equal to SF , where $SF = T_b/T_c$, and $\sum c_{O,x1}[n_c]c_{O,x2}[n_c] = 0$ when $x_1 \neq x_2$. In the following, $c_O = c_{O,d}$, $C_O = C_{O,d}$, and $c_{O,p}$ is neglected since it is an all one sequence.
- p_c, p_b and p_{pi} are unit power pulses with duration T_c, T_b and T_{pi} , respectively. $SF_{pilot} = T_{pi}/T_c$ is the SF for pilot signal, and $F_{sf} = T_{pi}/T_c$.

2.2.2 Fading Channel Model

In the wireless environments, the information-bearing signals encounter fading when they are transmitting through the channel. Small scale fading, or simply fading, is used to describe the rapid fluctuation of the amplitude of a radio signal over a short period of time or distance. The multipath propagation, mobile and surrounding objects movement, and bandwidth of transmitted signal influence the fading. Based on the Doppler spread, the fading channel can be classified as either fast fading or slow fading. When mobile station and other object are moving, the channel characteristics are changing according to the moving speed. If the channel changes so fast that the symbol period is no longer less than the coherence time, this channel is a time selective (fast) fading channel. Based on the multipath

time delay spread, the fading channel can be classified as either flat fading or frequency-selective fading. When the transmission bandwidth is broader than the channel bandwidth, the multipath can be resolved and the channel is called frequency-selective channel. In CDMA systems, the transmission bandwidth is usually wider than the coherence bandwidth. Consequently, the information-bearing signals encounter multipath fading channels. According to the wide-sense stationary uncorrelated scattering (WSSUS) model [56], each delay path p of user k has independent attenuation and phase shift expressed by $\alpha_{k,p}(t)$ in multipath fading channel. The envelope of the output is Rayleigh distributed while the phase of the output is uniformly distributed. Fig. 2-21 shows the multipath fading channel model with four paths. In this thesis, the fading profile of each path is modeled as Jakes model in which a U-shaped Doppler spectrum with given maximum Doppler frequency f_d defines the characteristics of fading. The U-shaped spectrum is defined as

$$S_f(f) = \begin{cases} \frac{\sigma_f^2}{\pi\sqrt{f_d^2 - f^2}} & |f| \leq f_d \\ 0 & \text{elsewhere} \end{cases}$$

where σ_f^2 is the average power of the faded carrier, and f_d is the maximum Doppler frequency caused by the mobile motion where $f_d = v/\lambda$, v is the vehicular speed and λ is the wavelength of the carrier. To generate fading channel coefficients, in the Jakes' model [38], the narrowband time-dispersive multipath fading is basically a combination of oscillators with different frequency. The outputs of the oscillators for real part and imaginary part can be described as $x_c(t)$ and $x_s(t)$, respectively, and are defined as follows.

$$x_c(t) = 2 \sum_{n=1}^{N_n} \cos \beta_n \cos \omega_n t + \sqrt{2} \cos \alpha \cos \omega_D t$$

$$x_s(t) = 2 \sum_{n=1}^{N_n} \sin \beta_n \cos \omega_n t + \sqrt{2} \sin \alpha \cos \omega_D t$$

where $\omega_D = 2\pi/f_d$ is the maximum Doppler frequency in radian, N_n is the number of other lower frequency oscillators, Generally speaking, N_0 equal to or larger than 8 gives good approximation and $\omega_n = \omega_D \cos(2\pi n/N)$ while $n=1, 2, \dots, N_n$ and $N=(2N_n+1)/2$. In order to normalize average power to unity, we should set $\alpha=0, \beta_n = \pi/(N_n+1)$ that let $\langle x_c(t)x_s(t) \rangle = 0$ and $\langle x_c(t)^2 \rangle = N_n, \langle x_s(t)^2 \rangle = N_n+1$. Thus we have $x_c(t)$ and $x_s(t)$ as follows.

$$x_c(t) = \sqrt{\frac{2}{N_n}} \sum_{n=1}^{N_n} \cos \beta_n \cos \omega_n t + \frac{1}{\sqrt{2}} \cos \alpha \cos \omega_D t$$

$$x_s(t) = \sqrt{\frac{2}{N_n+1}} \sum_{n=1}^{N_n} \sin \beta_n \cos \omega_n t$$

The complex baseband output of the Jakes model is then given by

$$y_f(t) = x_c(t) + jx_s(t)$$

where the output $y_f(t)$ is a baseband signal with Rayleigh fading characteristics.

After the transmitted signal $s_k(t)$ of the k -th user in (2-1) passing through a P -ray Rayleigh fading channel, assuming that the channel variation in a symbol interval is constant, the asynchronous received signal is represented as

$$r(t) = \sum_{k=1}^K \sum_{p=1}^P \alpha_{k,p}(t) s_k(t - \tau_{k,p}) + n(t) \quad (2-2)$$

where $n(t)$ is the complex AWGN with zero mean and one-sided power spectral density N_0 . $\tau_{k,p}$ and $\alpha_{k,p}(t)$ are the delay and the complex channel gain of the k -th user at the p -th path, respectively. $\tau_{k,p}$ are uniformly distributed random variables in $[0, T_b)$ for asynchronous systems. $\alpha_{k,p}(t)$ is still a zero-mean complex-valued Gaussian random variable without loss of generality when the carrier phase shift part is absorbed in it [88]. For simplicity, we assume

that the $\tau_{k,p}$ are perfectly estimated for all users. $\alpha_{J,p}(t)$ are constant in a symbol interval, i.e.

$\alpha_{J,p}^{(n)} = \alpha_{J,p}(t)|_{t=\tau_{J,p}+nT_b}$ where we assume that $\sum_{p=1}^P E[|\alpha_{J,p}^{(n)}|^2] = 1$ if the n -th bit of user J in the

first CB of the first frame is the bit and the user of interest.

2.2.3 RAKE Receiver

The matched filter (MF) is the optimal receiver when all interferences are viewed as background noise with Gaussian distributed characteristics. The RAKE receiver is considered as the optimal receiver in frequency-selective fading channel and combines multiple resolvable paths at receiver end to improve the performance [1]. Among combination criteria, the maximal ratio combining (MRC) maximizes the instantaneous signal-to-noise power ratio (SNR). The MRC RAKE for uplink dedicated channel is shown in Fig. 2-22. The received signal $r(t)$ is directly sent into the correlator followed by a summation of all fingers' outputs. The real part of the RAKE output is given by

$$\begin{aligned} \hat{Y}_J^{(n)} &= \sum_{f=1}^F \text{Re} \left\{ \frac{1}{2\beta_d T_b} \int_{nT_b+\tau_{J,f}}^{(n+1)T_b+\tau_{J,f}} (\hat{\alpha}_{J,f}^{(n)})^* r(t) C_o(t-\tau_{J,f}) C_J^*(t-\tau_{J,f}) dt \right\} \\ &= \sum_{f=1}^F \text{Re} \{ (\hat{\alpha}_{av;J,f}^{(n)})^* (\sqrt{P_J} \alpha_{J,f}^{(n)} b_J[n] + MAI_{\hat{b}_{J,f}}^{(n)} + I_{\hat{b}_{J,f}}^{(n)}) \} \end{aligned} \quad (2-3)$$

where $\hat{\alpha}_{av;J,f}^{(n)}$ are the channel estimates of $\alpha_{J,f}^{(n)}$ while the channel estimation method will

be addressed in 3.2. $(x)^*$ denotes the complex conjugate of x , F is the number of RAKE

fingers, and in this thesis we assume that $F=P$. Thus, the denominator $\sum_{f=1}^F E[|\alpha_{J,f}^{(n)}|^2] = 1$ can

be neglected. $MAI_{\hat{b}_{J,f}}^{(n)}$ and $I_{\hat{b}_{J,f}}^{(n)}$ in (2-3) are defined as

$$MAI_{\hat{b}_{J,f}}^{(n)} = \sqrt{P_J} \sum_{p=1, p \neq f}^P \alpha_{J,p}^{(n)} \{ \lambda_{J,p;J,f}^{(n)}(\tau_1) + j\beta_c \mu_{J,p;J,f}^{(n)}(\tau_1) \} + \sum_{k=1, k \neq J}^K \sqrt{P_k} \sum_{p=1}^P \alpha_{k,p}^{(n)} \{ \lambda_{k,p;J,f}^{(n)}(\tau) + j\beta_c \mu_{k,p;J,f}^{(n)}(\tau) \} \quad (2-4)$$

where

$$\lambda_{k,p;J,f}^{(n)}(\tau) = \begin{cases} b_k[n]\rho_{k,p;J,f}^{\prime(n)}(\tau) + b_k[n-1]\dot{\rho}_{k,p;J,f}^{\prime(n)}(\tau), & \tau \geq 0 \\ b_k[n]\rho_{k,p;J,f}^{\prime(n)}(\tau) + b_k[n+1]\dot{\rho}_{k,p;J,f}^{\prime(n)}(\tau), & \tau < 0 \end{cases} \quad (2-5)$$

and

$$\mu_{k,p;J,f}^{(n)}(\tau) = \begin{cases} a_{pilot}[\lfloor nl \rfloor]\gamma_{k,p;J,f}^{\prime(n)}(\tau) + a_{pilot}[\lfloor (n-1)l \rfloor]\dot{\gamma}_{k,p;J,f}^{\prime(n)}(\tau), & \tau \geq 0 \\ a_{pilot}[\lfloor nl \rfloor]\gamma_{k,p;J,f}^{\prime(n)}(\tau) + a_{pilot}[\lfloor (n+1)l \rfloor]\dot{\gamma}_{k,p;J,f}^{\prime(n)}(\tau), & \tau < 0 \end{cases} \quad (2-6)$$

where $\rho_{k,p;J,f}^{\prime(n)}(\tau)$, $\dot{\rho}_{k,p;J,f}^{\prime(n)}(\tau)$, $\gamma_{k,p;J,f}^{\prime(n)}(\tau)$ and $\dot{\gamma}_{k,p;J,f}^{\prime(n)}(\tau)$ are defined in (C8) ~ (C11) in Appendix

C. Also, we have

$$I_{b;J,f}^{(n)} = \frac{1}{2\beta_d T_b} \int_{nT_b + \tau_{J,f}}^{(n+1)T_b + \tau_{J,f}} n(t)C_o(t - \tau_{J,f})C_J^*(t - \tau_{J,f})dt.$$

In (2-4), it is shown that the second and the fourth interference terms come from the pilot-channel signal of multipath and other users, respectively. The data decision is made by taking sign bit of RAKE output $\hat{Y}_J^{(n)}$, i.e. $\text{sgn}\{\hat{Y}_J^{(n)}\}$, where $\text{sgn}\{\cdot\}$ is the sign function.

The conventional (RAKE) receiver is easy to implement. However, MAI from both pilot signal and data signal of other users due to non-orthogonality are viewed as background noise. This results in dramatically reduction in system capacity. Additionally, in (2-4) it is also shown that users with large channel gain result in larger MAI than those with small channel gain. In mobile environments, large channel gain usually comes from users who are located close to the base station. Users with weaker received signal are overwhelmed by users with stronger received signal. This is the so called near-far effect. The system capacity is expected to be larger if the MAI in RAKE output $\hat{Y}_J^{(n)}$ in (2-3) can be eliminated.



Table 2-1 Main WCDMA parameters [33]

Multiple access method	DS-CDMA
Duplexing method	Frequency division duplex/time division duplex
Base station synchronisation	Asynchronous operation
Chip rate	3.84 Mcps
Frame length	10 ms
Service multiplexing	Multiple services with different quality of service requirements multiplexed on one connection
Multirate concept	Variable spreading factor and multicode
Detection	Coherent using pilot symbols or common pilot
Multiuser detection, smart antennas	Supported by the standard, optional in the implementation

Table 2-2 Mapping from $z_n(i)$ to $c_{short,1,n}(i)$ and $c_{short,2,n}(i)$, $i = 0, 1, \dots, 255$

$z_n(i)$	$c_{short,1,n}(i)$	$c_{short,2,n}(i)$
0	+1	+1
1	-1	+1
2	-1	-1
3	+1	-1

Table 2-3 UL reference measurement channel (64 kbps)

Parameter	Level	Unit
Information bit rate	64	Kbps
DPCCH	240	Kbps
Power control	Off	
TFCI	On	
Repetition	19	%

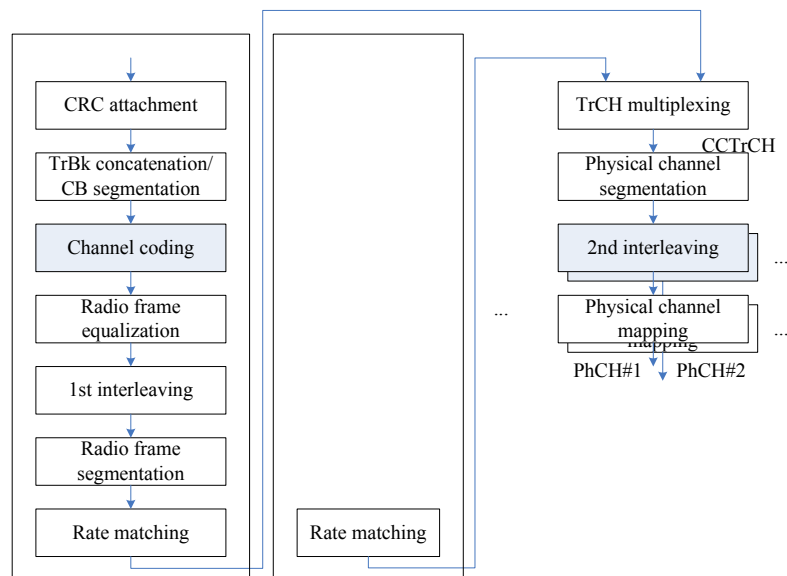


Fig. 2-1 TrCH multiplexing structure for uplink

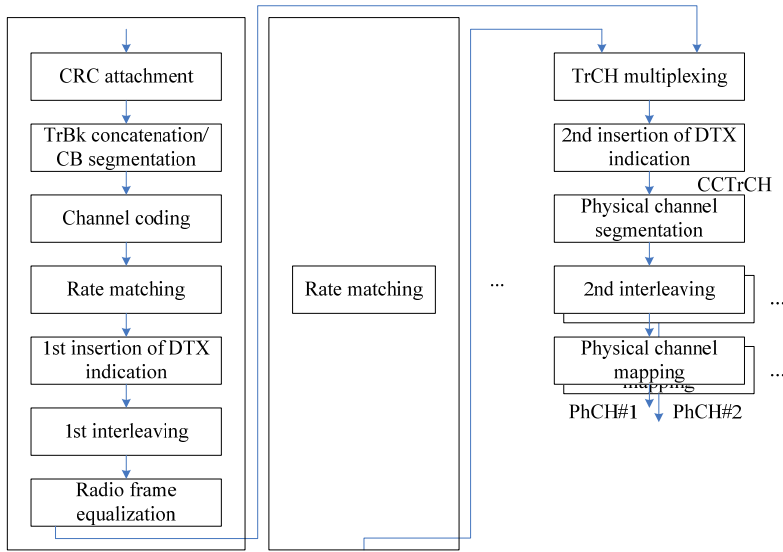


Fig. 2-2 TrCH multiplexing structure for downlink

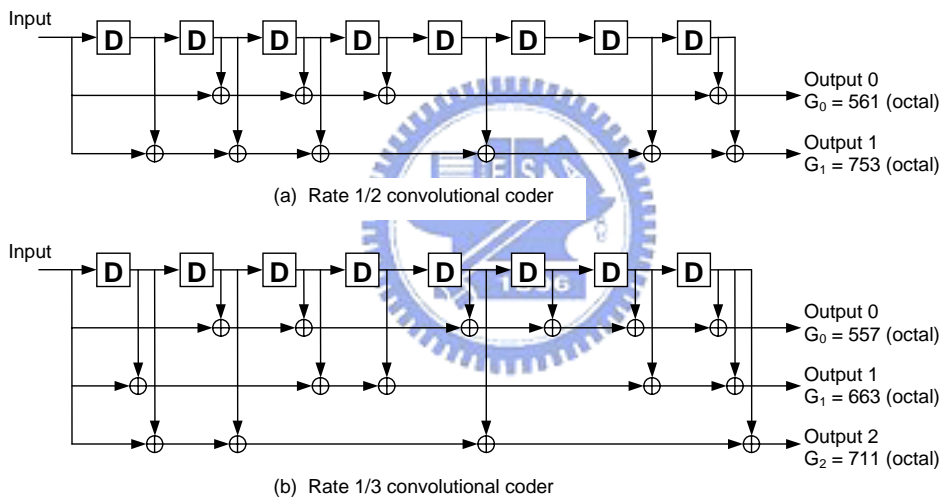


Fig. 2-3 Rate 1/2 and rate 1/3 convolutional coders

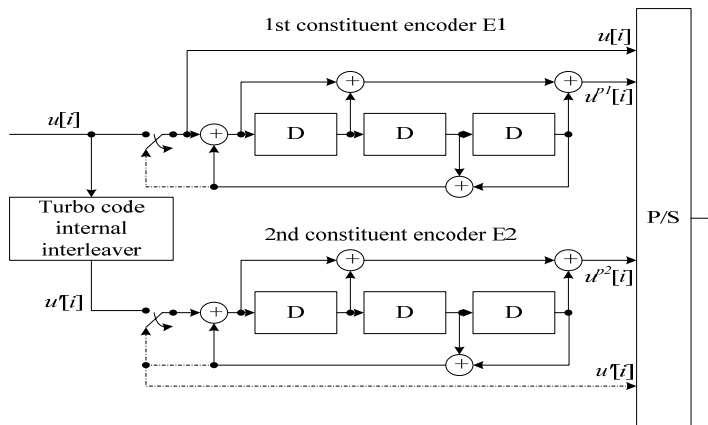


Fig. 2-4 Structure of rate 1/3 Turbo coder (dotted lines apply for trellis termination only)

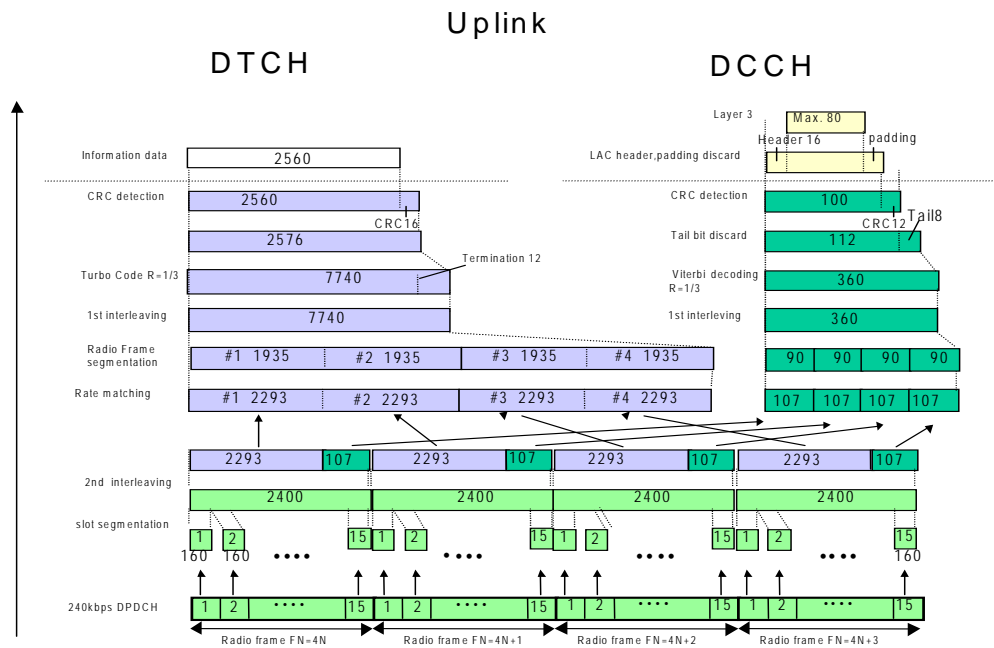


Fig. 2-5 Channel coding for the UL reference measurement channel (64 kbps)

Transport Channels	Physical Channels
DCH	Dedicated Physical Data Channel (DPDCH)
	Dedicated Physical Control Channel (DPCCH)
	Fractional Dedicated Physical Channel (F-DPCH)
E-DCH	E-DCH Dedicated Physical Data Channel (E-DPDCH)
	E-DCH Dedicated Physical Control Channel (E-DPCCH)
	E-DCH Absolute Grant Channel (E-AGCH)
	E-DCH Relative Grant Channel (E-RGCH)
	E-DCH Hybrid ARQ Indicator Channel (E-HICH)
RACH	Physical Random Access Channel (PRACH)
	Common Pilot Channel (CPICH)
BCH	Primary Common Control Physical Channel (P-CCPCH)
FACH	Secondary Common Control Physical Channel (S-CCPCH)
PCH	Synchronisation Channel (SCH)
	Acquisition Indicator Channel (AICH)
	Paging Indicator Channel (PICH)
	MBMS Notification Indicator Channel (MICH)
HS-DSCH	High Speed Physical Downlink Shared Channel (HS-PDSCH)
	HS-DSCH-related Shared Control Channel (HS-SCCH)
	Dedicated Physical Control Channel (uplink) for HS-DSCH (HS-DPCCH)

Fig. 2-6 Summarizing the mapping of TrCH s onto PhCHs

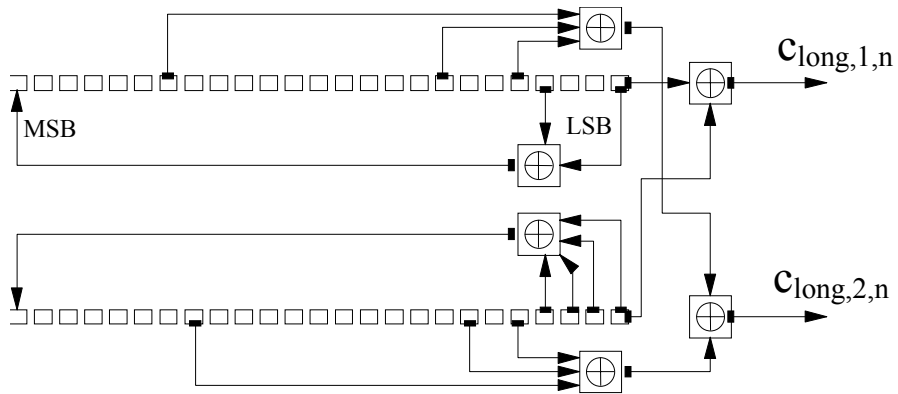


Fig. 2-7 Configuration of uplink scrambling sequence generator

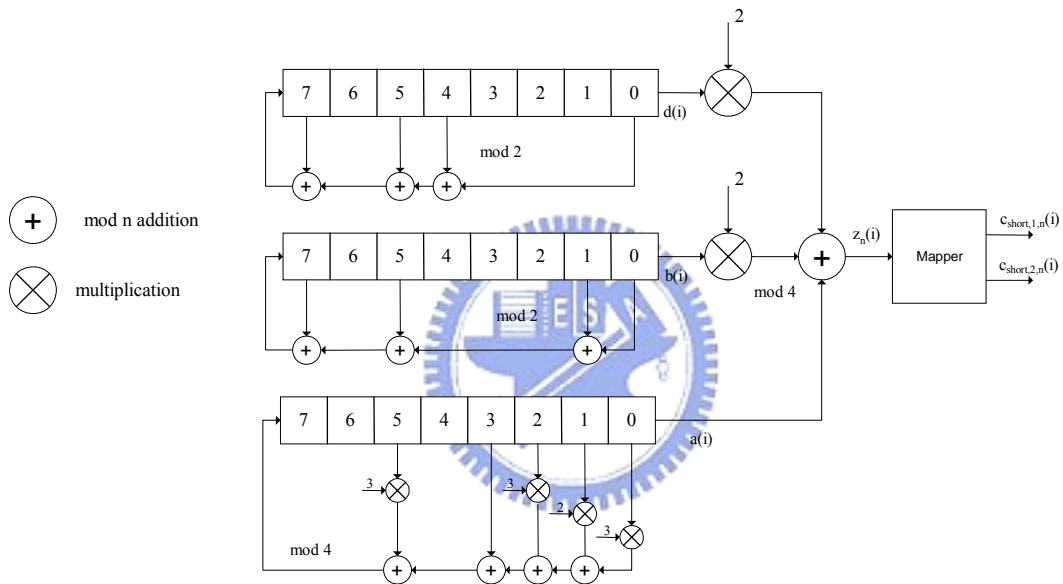


Fig. 2-8 Uplink short scrambling sequence generator for 255 chip sequence

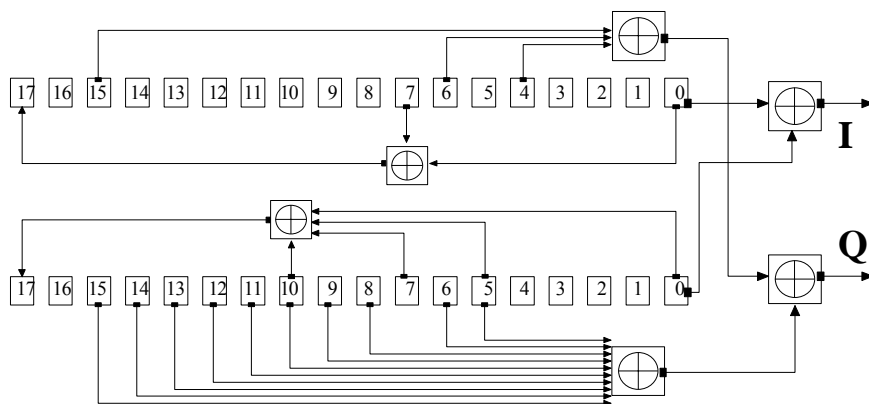


Fig. 2-9 Configuration of downlink scrambling code generator

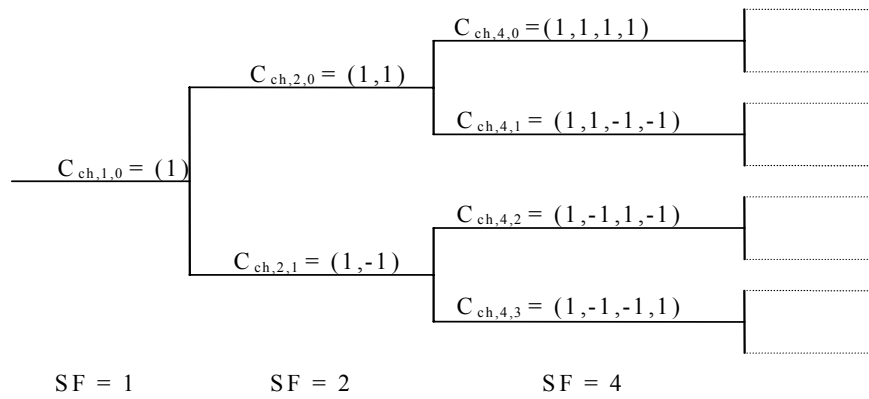


Fig. 2-10 Code-tree for generation of OVSF codes

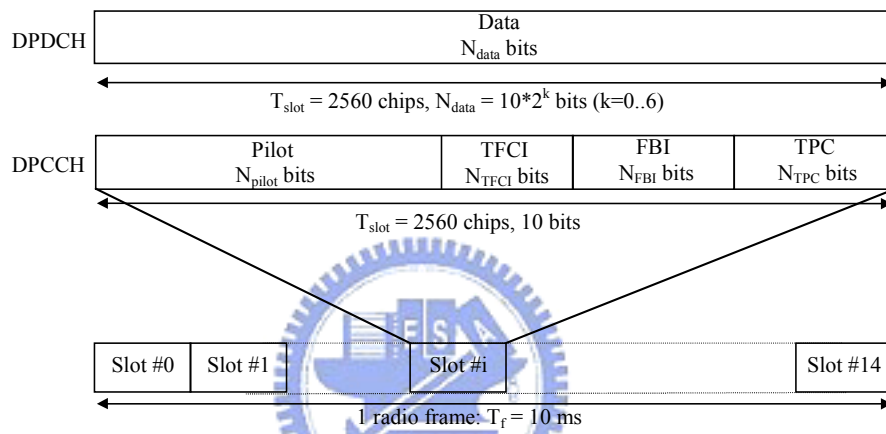


Fig. 2-11 Frame structure for uplink DPDCH/DPCCH

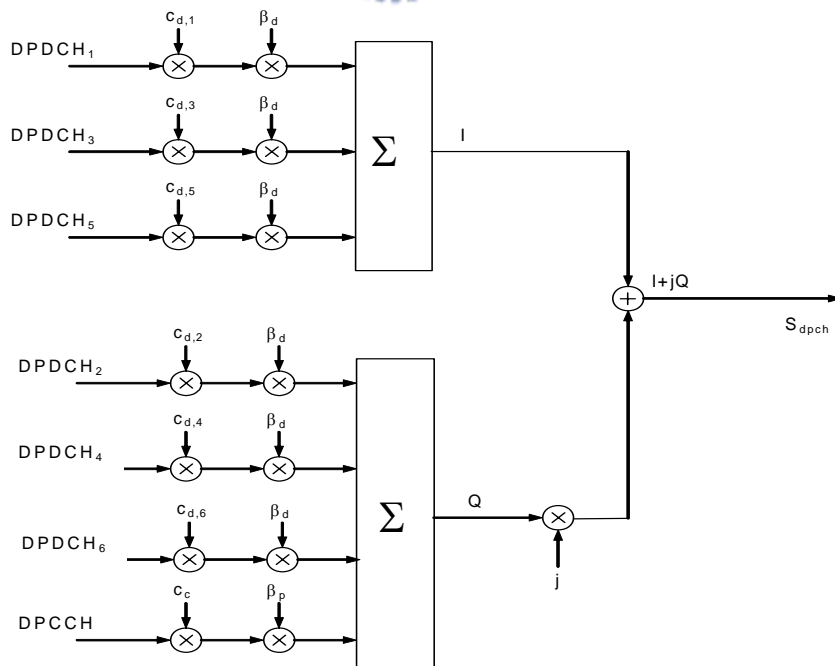


Fig. 2-12 The uplink spreading of DPCCH and DPDCHs

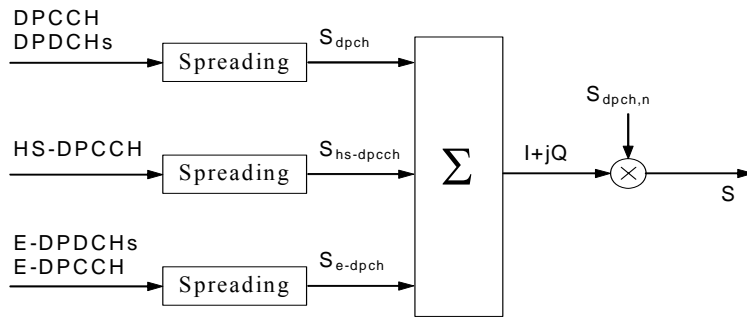


Fig. 2-13 Spreading for uplink dedicated channels

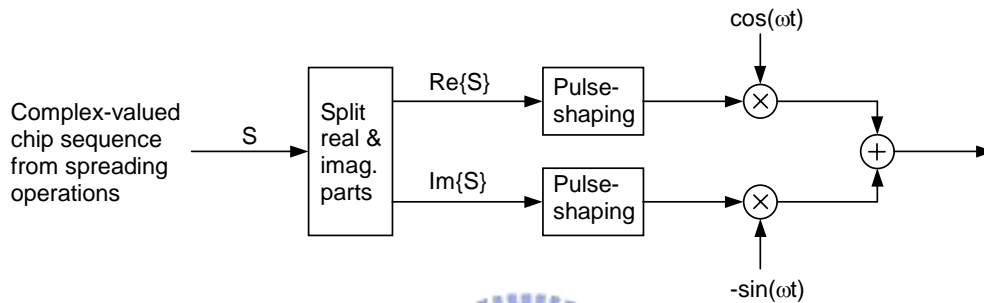


Fig. 2-14 Uplink modulation

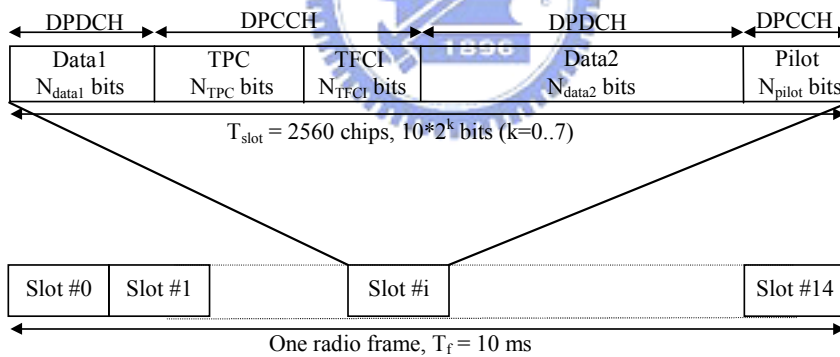


Fig. 2-15 Frame structure for downlink DPCH

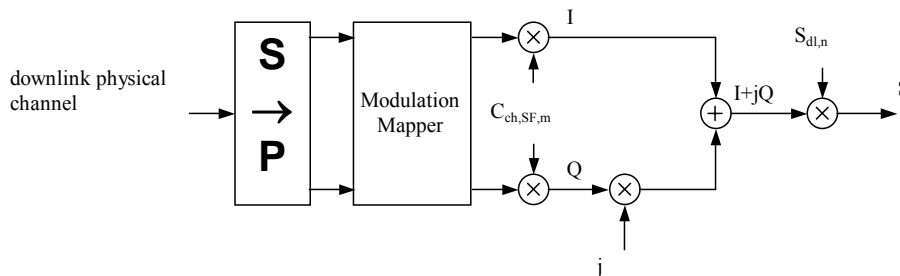


Fig. 2-16 Spreading for all downlink PhCHs except SCH

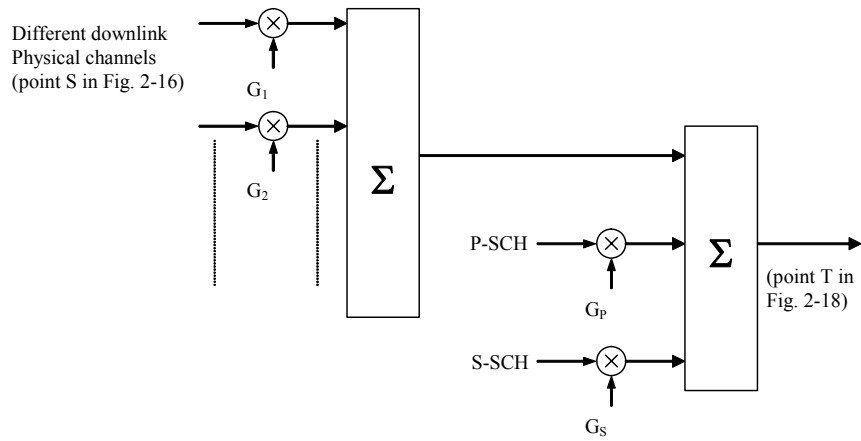


Fig. 2-17 Combining of downlink PhCHs

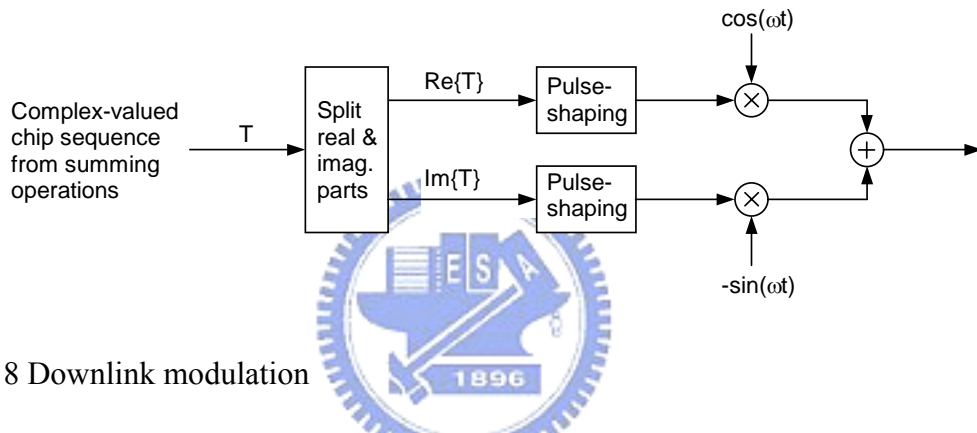


Fig. 2-18 Downlink modulation

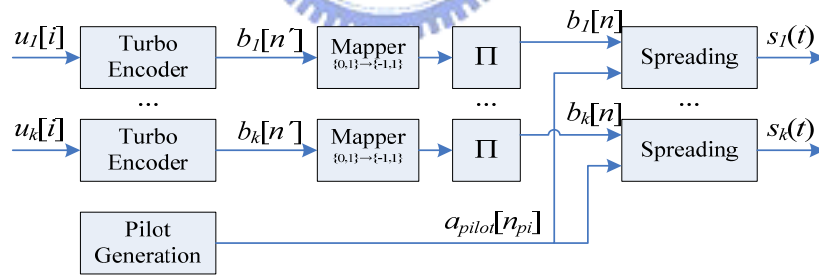


Fig. 2-19 Transmitter model

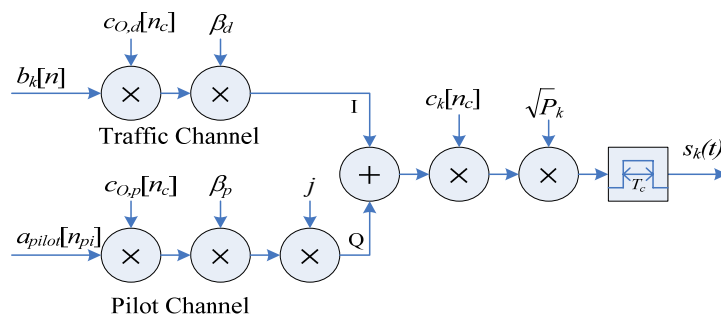


Fig. 2-20 Spreader for the k -th user

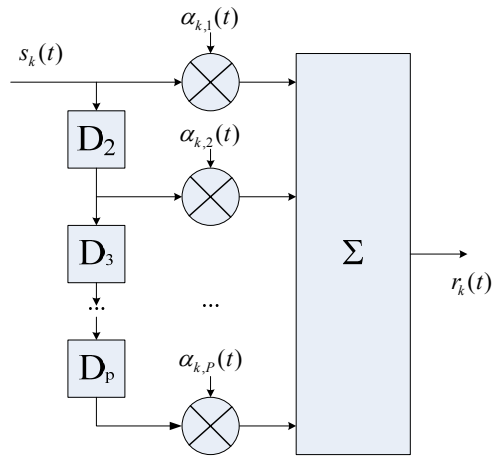


Fig. 2-21 Multipath fading channel model

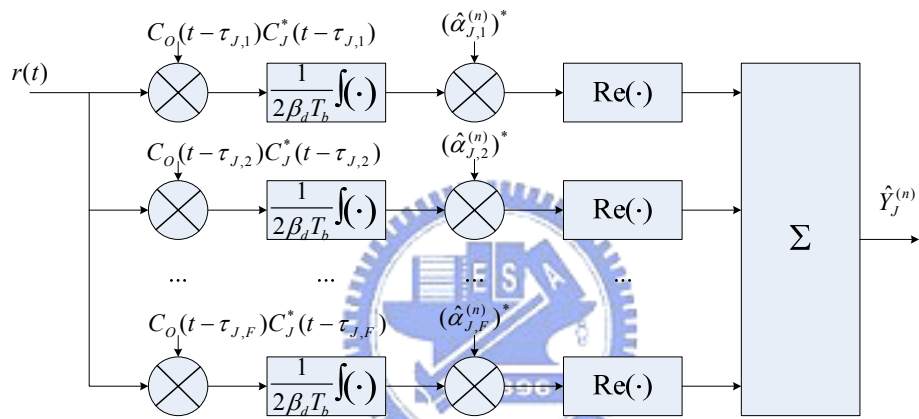


Fig. 2-22 Structure of the MRC RAKE with F finger combining

Chapter 3

Pilot-Channel Aided Successive Interference Cancellation

3.1 Overview

The SIC technique intends to detect and removes the user signal with decreasing signal strength to acquire better error performance. Due to the variety of ordering method and the superiority over PIC, in this chapter we present the pilot-channel signal removed SIC with three ordering methods.

In Chapter 2, we find that in the uplink WCDMA systems, the traffic-channel signals are always interfered by other users' pilot and traffic signal even without any fading. The interference from pilot signal in Q-channel before scrambling is removed first before data detection is performed. Also, channel estimation performed independently with the pilot-channel of each user is taken into consideration in the analyses. For practical use, the MRC RAKE receiver with hard decision for data detection and windowed moving average technique for channel estimation are adopted.

It has been shown that the ordering method has a great effect on the performance of SIC [15], [52], [58], [69]. To determine the cancellation order, reference [26] uses the gain-ranking list obtained from channel estimates for successive cancellation. In reference [89], the correlator outputs pass on to a selector to select the user with the strongest correlation values for decoding and cancellation in each stage. For asynchronous systems, G bits of each user are grouped into the cancellation frame, and the ranking of the users is

obtained from the averages of correlations over G bits. In [90], the average power is used to decide the cancellation order. Our proposed method is to use the signal strength obtained at the outputs of the first stage's RAKE bank as the basis for ranking detection order [67]. In a recent work [87], the effects of ordering method on hard-decision based SIC with equal received power over AWGN and flat Rayleigh fading channels for an asynchronous system are examined. In this chapter, three ordering methods for SIC in the uplink of WCDMA systems over multipath fading channels are discussed and compared in the aspect of the implementation issues (such as reordering frequency, processing delay, latency, and computational complexity), and error performance related parameters (such as pilot-to-traffic amplitude ratio, ordering method, grouping interval, received power distribution ratio and channel estimation as well as timing estimation errors). We also apply our proposed scheme to the multirate environment.

3.2 Channel Estimation

In a time-varying mobile communication system, channel estimation is essential for coherent demodulation. Two types of the conventional channel sounding schemes, pilot-channel aided (PCA) scheme and pilot-symbol aided (PSA) scheme, are utilized to estimate the channel conditions in the uplink and downlink DPCH channels in WCDMA systems, respectively. The PCA scheme uses an extra channel to carry the pilot signal while in the PSA scheme, the pilot symbols are arranged to put between data symbols in the same channel. The PCA scheme results in an increased peak-to-average-ratio (PAPR) with more precise channel estimation. In other words, part of the transmitted power is used for pilot transmission all the time. In the PSA scheme, the channel estimates between the positions of pilot symbols can be interpolated by a filter where the maximum Doppler frequency has an upper limit for a precise estimation.

In the uplink of WCDMA systems, for ease of implementation, instead of using the optimal Wiener filter [66], a straightforward method as shown in Fig. 3-2 to obtain the channel estimate is to correlate the received signal with known pilot signal modulated at Q -channel of user J at the f -th path followed by a moving average filter to reduce the variance of the noisy channel estimate. The channel estimate thus becomes

$$\hat{\alpha}_{av;J,f}^{(n)} = \frac{1}{j2W\beta_p T_b} \int_{nT_b+\tau_{J,f}}^{(n+1)T_b+\tau_{J,f}} A_{pilot}(t-\tau_{J,f})r(t)C_J^*(t-\tau_{J,f})dt = \frac{1}{W} \left(\sqrt{P_J} \sum_{n_b=n-W/2}^{n+W/2-1} \alpha_{J,f}^{(n_b)} + MAI_{\hat{\alpha}_{J,f}}^{(n)} + I_{\hat{\alpha}_{J,f}}^{(n)} \right) \quad (3-1)$$

where $(x)^*$ denotes the complex conjugate of x , and W is an even integer denoting the length of the moving average filter and n is assumed to be equal to or larger than $W/2$. Here we neglect the situation of $n < W/2$, since the effect of initial channel estimation is negligible for the long-term system performance measurement in a real system. Besides, as $n+W/2 > N$, the scramble sequence will be reused again. When the transmitted signal is subject to fading channel, $\alpha_{J,f}^{(n)} \neq \frac{1}{W} \sum_{n_b=n-W/2}^{n+W/2-1} \alpha_{J,f}^{(n_b)}$, since it is assumed that the channel parameters vary with bit index n . However, when the channel variation is not very fast compared to WT_b , $\frac{1}{W} \sum_{n_b=n-W/2}^{n+W/2-1} \alpha_{J,f}^{(n_b)}$ can be used to approximate $\alpha_{J,f}^{(n)}$. The multiple access interference (MAI) coming from other paths and other users is expressed as

$$MAI_{\hat{\alpha}_{J,f}}^{(n)} = a_{pilot}[\lfloor nT \rfloor] \left[\sqrt{P_J} \sum_{p=1, p \neq f}^P \alpha_{J,p}^{(n)} \left\{ \frac{1}{j\beta_c} \lambda_{J,p;J,f}^{(n)}(\tau_1) + \mu_{J,p;J,f}^{(n)}(\tau_1) \right\} + \sum_{k=1, k \neq J}^K \sqrt{P_k} \sum_{p=1}^P \alpha_{k,p}^{(n)} \left\{ \frac{1}{j\beta_c} \lambda_{k,p;J,f}^{(n)}(\tau) + \mu_{k,p;J,f}^{(n)}(\tau) \right\} \right] \quad (3-2)$$

where $l=1/F_{sf}$, and $\lfloor x \rfloor$ indicates the largest integer smaller than or equal to x . τ and τ_1 denotes $\tau_{k,p;J,f}$ and $\tau_{J,p;J,f}$, respectively, for notational simplicity. The AWGN induced interference is expressed as

$$I_{\hat{\alpha}_{J,f}}^{(n)} = \frac{1}{j2\beta_p T_b} \int_{nT_b + \tau_{J,f}}^{(n+1)T_b + \tau_{J,f}} A_{pilot}(t - \tau_{J,f}) n(t) C_J^*(t - \tau_{J,f}) dt. \quad (3-3)$$

$\lambda_{k,p;J,f}^{(n)}(\tau)$ and $\mu_{k,p;J,f}^{(n)}(\tau)$ in (3-2) denote the interferences from other users' traffic-channel signal and pilot-channel signal, respectively, and are defined as follows.

$$\lambda_{k,p;J,f}^{(n)}(\tau) = \begin{cases} b_k[n]\rho_{k,p;J,f}^{(n)}(\tau) + b_k[n-1]\dot{\rho}_{k,p;J,f}^{(n)}(\tau), & \tau \geq 0 \\ b_k[n]\rho_{k,p;J,f}^{(n)}(\tau) + b_k[n+1]\dot{\rho}_{k,p;J,f}^{(n)}(\tau), & \tau < 0 \end{cases} \quad (3-4)$$

and

$$\mu_{k,p;J,f}^{(n)}(\tau) = \begin{cases} a_{pilot}[\lfloor nl \rfloor]\gamma_{k,p;J,f}^{(n)}(\tau) + a_{pilot}[\lfloor (n-1)l \rfloor]\dot{\gamma}_{k,p;J,f}^{(n)}(\tau), & \tau \geq 0 \\ a_{pilot}[\lfloor nl \rfloor]\gamma_{k,p;J,f}^{(n)}(\tau) + a_{pilot}[\lfloor (n+1)l \rfloor]\dot{\gamma}_{k,p;J,f}^{(n)}(\tau), & \tau < 0 \end{cases} \quad (3-5)$$

where $\rho_{k,p;J,f}^{(n)}(\tau)$, $\dot{\rho}_{k,p;J,f}^{(n)}(\tau)$, $\gamma_{k,p;J,f}^{(n)}(\tau)$ and $\dot{\gamma}_{k,p;J,f}^{(n)}(\tau)$ are defined in (C4) ~ (C7) in Appendix C.



3.3 Pilot Channel Signal Removal

From (2-4), it is shown that the second and the fourth interference terms come from the pilot-channel signal of multipath and other users, respectively. Two methods can be used to alleviate the MAI due to pilot-channel signals. One method is to reduce the power ratio. Although reducing the power ratio will alleviate the MAI due to pilot signals, it also reduces the accuracy of channel estimation. Another way is using the proposed method as shown in Fig. 3-5. The scheme reduces MAI due to pilot channel signal, which is regenerated by a pilot signal regenerator and then subtracted at the regenerator output. Therefore, if the pilot-channel signals of all users are removed from $r(t)$ before $r(t)$ is fed into the correlators, the variance of $\hat{Y}_J^{(n)}$ in (2-3) can be reduced, especially when β_c is large.

According to this, $r(t)$ in (2-3) is replaced by

$$\hat{r}(t) = r(t) - \sum_{k=1}^K \hat{C}_{pilot;k}(t) \quad (3-6)$$

where

$$\hat{C}_{pilot;k}(t) = \sum_{p=1}^F j\beta_p \hat{\alpha}_{av;k,p}^{(l(t-\tau_{k,p})/T_b)} a_{pilot} [\lfloor l(t-\tau_{k,p})/T_b \rfloor] C_k(t-\tau_{k,p}). \quad (3-7)$$

Then, $\hat{Y}_J^{(n)}$, $MAI_{\hat{b}_{J,f}}^{(n)}$, and $I_{\hat{b}_{J,f}}^{(n)}$ in (2-3) become $\hat{Y}_J^{(n)}$, $MAI_{\hat{b}_{J,f}}^{(n)}$, and $I_{\hat{b}_{J,f}}^{(n)}$, respectively, where

$$\begin{aligned} MAI_{\hat{b}_{J,f}}^{(n)} = & \sqrt{P_J} \sum_{p=1, p \neq f}^P \alpha_{J,p}^{(n)} \lambda_{J,p;J,f}^{(n)}(\tau_1) + \sum_{k=1, k \neq J}^K \sqrt{P_k} \sum_{p=1}^P \alpha_{k,p}^{(n)} \lambda_{k,p;J,f}^{(n)}(\tau) \\ & + j\beta_c \left\{ \sqrt{P_J} \sum_{p=F+1}^P \alpha_{J,p}^{(n)} \mu_{J,p;J,f}^{(n)}(\tau_1) + \sum_{k=1, k \neq J}^K \sqrt{P_k} \sum_{p=F+1}^P \alpha_{k,p}^{(n)} \mu_{k,p;J,f}^{(n)}(\tau) \right\} - j\beta_c \left\{ \sum_{p=1, p \neq f}^F \hat{\sigma}_{J,p;J,f}^{(n)}(\tau_1) + \sum_{k=1, k \neq J}^K \sum_{p=1}^F \hat{\sigma}_{k,p;J,f}^{(n)}(\tau) \right\} \end{aligned} \quad (3-8)$$

with

$$\hat{\sigma}_{k,p;J,f}^{(n)}(\tau) = \begin{cases} a_{pilot} [\lfloor nl \rfloor] MAI_{\hat{\alpha}_{av;k,p}}^{(n)} \gamma'_{k,p;J,f}^{(n)}(\tau) + a_{pilot} [\lfloor (n-1)l \rfloor] MAI_{\hat{\alpha}_{av;k,p}}^{(n-1)} \gamma'_{k,p;J,f}^{(n)}(\tau), & \tau \geq 0 \\ a_{pilot} [\lfloor nl \rfloor] MAI_{\hat{\alpha}_{av;k,p}}^{(n)} \gamma'_{k,p;J,f}^{(n)}(\tau) + a_{pilot} [\lfloor (n+1)l \rfloor] MAI_{\hat{\alpha}_{av;k,p}}^{(n+1)} \gamma'_{k,p;J,f}^{(n)}(\tau), & \tau < 0 \end{cases} \quad (3-9)$$

The AWGN induced interference $I_{\hat{b}_{J,f}}^{(n)}$ is expressed as

$$I_{\hat{b}_{J,f}}^{(n)} = I_{\hat{b}_{J,f}}^{(n)} - j\beta_c \left(\sum_{k=1, k \neq J}^K \sum_{p=1}^F \hat{\zeta}_{k,p;J,f}^{(n)}(\tau) + \sum_{p=1, p \neq f}^F \hat{\zeta}_{J,p;J,f}^{(n)}(\tau_1) \right) \quad (3-10)$$

with

$$\hat{\zeta}_{k,p;J,f}^{(n)}(\tau) = \begin{cases} I_{\hat{\alpha}_{av;k,p}}^{(n)} a_{pilot}[[nl]] \gamma'_{k,p;J,f}^{(n)}(\tau) + I_{\hat{\alpha}_{av;k,p}}^{(n-1)} a_{pilot}[(n-1)l] \gamma'_{k,p;J,f}^{(n)}(\tau), & \tau \geq 0 \\ I_{\hat{\alpha}_{av;k,p}}^{(n)} a_{pilot}[[nl]] \gamma'_{k,p;J,f}^{(n)}(\tau) + I_{\hat{\alpha}_{av;k,p}}^{(n+1)} a_{pilot}[(n+1)l] \gamma'_{k,p;J,f}^{(n)}(\tau), & \tau < 0 \end{cases} \quad (3-11)$$

where both $\hat{\sigma}'_{k,p;J,f}^{(n)}(\tau)$ and $\hat{\zeta}'_{k,p;J,f}^{(n)}(\tau)$ in (3-10) and (3-11) come from the channel estimation errors. After obtaining $\hat{Y}_J^{(n)}$, the initial decision of the coded bit $b_J[n]$ is given by $\hat{b}_J[n] = \text{sgn}\{\hat{Y}_J^{(n)}\}$, where $\text{sgn}\{\cdot\}$ is the sign function. Thus, for the u -th canceled user of all SICs, the real part of RAKE output is

$$\begin{aligned} \hat{Y}_{SIC<u>}^{(n)} &= P_{<u>} \sum_{f=1}^F |\alpha_{<u>}^{(n)}|^2 b_{<u>}[n] \\ &+ \sum_{f=1}^F \text{Re}\{\sqrt{P_{<u>}} (\alpha_{<u>}^{(n)})^* (MAI_{\hat{b}_{SIC<u>,f}}^{(n)} + I_{\hat{b}_{SIC<u>,f}}^{(n)}) + (MAI_{\hat{\alpha}_{av;<u>,f}}^{(n)} + I_{\hat{\alpha}_{av;<u>,f}}^{(n)})^* (\sqrt{P_{<u>}} \alpha_{<u>}^{(n)} b_{<u>}[n] + MAI_{\hat{b}_{SIC<u>,f}}^{(n)} + I_{\hat{b}_{SIC<u>,f}}^{(n)})\} \end{aligned} \quad (3-12)$$

where

$$\hat{r}_{SIC;u}(t) = \hat{r}(t) - \sum_{k=\langle 1 \rangle}^{\langle u-1 \rangle} \check{C}_{data,k}(t)$$

$$(3-13)$$

and

$$\check{C}_{data,k}(t) = \sum_{p=1}^F \beta_d \hat{\alpha}_{av;k,p}^{(t-\tau_{k,p}/T_b)} \hat{b}_{SIC;k}[[t-\tau_{k,p}/T_b]] C_o(t-\tau_{k,p}) C_k(t-\tau_{k,p}), \quad (3-14)$$

where $mGT_b \leq t-\tau_{k,p} < (m+1)GT_b$. $\hat{b}_{SIC;k}[n]$ is the data decision of the coded bit $b_{SIC;k}[n]$

where $\hat{b}_{SIC;k}[n] = \text{sgn}\{\hat{Y}_{SIC;k}^{(n)}\}$ for $\langle 1 \rangle \leq k \leq \langle u-1 \rangle$. According to the graphical illustration shown in Fig. 3-1, it is shown that

$$\begin{aligned}
MAI_{\hat{b}_{SIC <u>,f}}^{(n)} &= j\beta_c \left\{ \underbrace{\sqrt{P_J} \sum_{p=F+1}^P \alpha_{<u>,p}^{(n)} \mu'_{<u>,p;<u>,f}(\tau_1) + \sum_{k=1,k \neq J}^K \sqrt{P_k} \sum_{p=F+1}^P \alpha_{k,p}^{(n)} \mu'_{k,p;<u>,f}(\tau)}_{\text{from un-cancelled pilot}} \right\} \\
&+ \underbrace{\sqrt{P_{<u>}} \sum_{p=1,p \neq f}^P \alpha_{<u>,p}^{(n)} \lambda'_{<u>,p;<u>,f}(\tau_1)}_{\text{from un-cancelled multipath}} + \underbrace{\sum_{k=<u>+1}^{<K>} \sqrt{P_k} \sum_{p=1}^P \alpha_{k,p}^{(n)} \lambda'_{k,p;<u>,f}(\tau)}_{\text{from un-cancelled user}} + \underbrace{\sum_{k=<1>}^{<u-1>} \sqrt{P_k} \sum_{p=F+1}^P \alpha_{k,p}^{(n)} \lambda'_{k,p;<u>,f}(\tau)}_{\text{from un-cancelled multipath of cancelled users}} \\
&- j\beta_c \left\{ \underbrace{\sum_{p=1,p \neq f}^F \hat{\sigma}'_{<u>,p;<u>,f}(\tau_1) + \sum_{k=1,k \neq J}^K \sum_{p=1}^F \hat{\sigma}'_{k,p;<u>,f}(\tau)}_{\text{from imperfect pilot removal}} - \underbrace{\left\{ \sum_{p=1,p \neq f}^F \hat{\varphi}'_{SIC;<u>,p;<u>,f}(\tau_1) + \sum_{k=<1>}^{<u-1>} \sum_{p=1}^F \hat{\varphi}'_{SIC;k,p;<u>,f}(\tau) \right\}}_{\text{from imperfect channel estimation \& incorrect data decision}} \right\}
\end{aligned} \tag{3-15}$$

where τ and τ_1 denote $\tau_{k,p;<u>,f}$ and $\tau_{<u>,p;<u>,f}$, respectively, for notational simplicity.

The 3-*rd* and 4-*th* terms in (3-15) are MAI from un-cancelled multipath and users where

$$\lambda'_{k,p;<u>,f}(\tau) = \begin{cases} b_k[n] \rho'_{k,p;<u>,f}(\tau) & , n = mG \\ b_k[n] \rho'_{k,p;<u>,f}(\tau) + b_k[n-1] \rho'_{k,p;<u>,f}(\tau), & \text{otherwise} \end{cases}, \tau \geq 0, \\
b_k[n] \rho'_{k,p;<u>,f}(\tau) + b_k[n+1] \rho'_{k,p;<u>,f}(\tau) & , \tau < 0
\end{cases} \tag{3-16}$$

and the last two terms in (3-15) come from incorrect data decision, imperfect channel estimation and un-cancelled MAI due to asynchronous channels where

$$\hat{\varphi}'_{SIC;k;<u>}(\tau) = \begin{cases} \left. \begin{aligned} &\left\{ \begin{aligned} &\{MAI_{\hat{\alpha}_{av;k,p}}^{(n)} - 2(\sqrt{p_k} \alpha_{k,p}^{(n)} + MAI_{\hat{\alpha}_{av;k,p}}^{(n)}) \Delta_k^{(n)}\} b_k[n] \rho'_{k,p;<u>,f}(\tau) \\ &+ \{MAI_{\hat{\alpha}_{av;k,p}}^{(n-1)} - 2(\sqrt{p_k} \alpha_{k,p}^{(n-1)} + MAI_{\hat{\alpha}_{av;k,p}}^{(n-1)}) \Delta_k^{(n-1)}\} b_k[n-1] \rho'_{k,p;<u>,f}(\tau) \end{aligned} \right\}, \tau \geq 0 \\ &\left\{ \begin{aligned} &\{MAI_{\hat{\alpha}_{av;k,p}}^{(n)} - 2(\sqrt{p_k} \alpha_{k,p}^{(n)} + MAI_{\hat{\alpha}_{av;k,p}}^{(n)}) \Delta_k^{(n)}\} b_k[n] \rho'_{k,p;<u>,f}(\tau) \\ &+ b_k[n+1] \rho'_{k,p;<u>,f}(\tau) \end{aligned} \right\}, n = (m+1)G - 1 \\ &\left\{ \begin{aligned} &\{MAI_{\hat{\alpha}_{av;k,p}}^{(n)} - 2(\sqrt{p_k} \alpha_{k,p}^{(n)} + MAI_{\hat{\alpha}_{av;k,p}}^{(n)}) \Delta_k^{(n)}\} b_k[n] \rho'_{k,p;<u>,f}(\tau) \\ &+ \{MAI_{\hat{\alpha}_{av;k,p}}^{(n+1)} + 2(\sqrt{p_k} \alpha_{k,p}^{(n+1)} + MAI_{\hat{\alpha}_{av;k,p}}^{(n+1)}) \Delta_k^{(n+1)}\} b_k[n+1] \rho'_{k,p;<u>,f}(\tau) \end{aligned} \right\}, \text{otherwise} \end{aligned} \right\}, \tau < 0
\end{cases} \tag{3-17}$$

with $\Delta_k^{(n)} = 1$ when $b_k[n] \neq \hat{b}_{SIC;k}[n]$, and $\Delta_k^{(n)} = 0$ when $b_k[n] = \hat{b}_{SIC;k}[n]$. And

$$I_{\hat{b}_{SIC <u>,f}}^{(n)} = I_{\hat{b}_{<u>,f}}^{(n)} - \left\{ \sum_{p=1,p \neq f}^F \hat{\psi}'_{<u>,p;<u>,f}(\tau_1) + \sum_{k=<1>}^{<u-1>} \sum_{p=1}^F \hat{\psi}'_{SIC;k,p;<u>,f}(\tau) \right\} \tag{3-18}$$

where

$$\hat{\psi}_{SIC;k,p;<u>,f}^{(n)}(\tau) = \begin{cases} I_{\hat{\alpha}_{av;k,p}}^{(n)} \Omega_k^{(n)} b_k[n] \rho'_{k,p;<u>,f}(\tau) + I_{\hat{\alpha}_{av;k,p}}^{(n-1)} \Omega_k^{(n-1)} b_k[n-1] \rho'_{k,p;<u>,f}(\tau) & , \tau \geq 0 \\ I_{\hat{\alpha}_{av;k,p}}^{(n+1)} \Omega_k^{(n+1)} b_k[n+1] \rho'_{k,p;<u>,f}(\tau) & , n = (m+1)G-1 \\ I_{\hat{\alpha}_{av;k,p}}^{(n)} \Omega_k^{(n)} b_k[n] \rho'_{k,p;<u>,f}(\tau) + I_{\hat{\alpha}_{av;k,p}}^{(n+1)} \Omega_k^{(n+1)} b_k[n+1] \rho'_{k,p;<u>,f}(\tau), & otherwise \end{cases}, \tau < 0 \quad (3-19)$$

Here, we have $\Omega_k^{(n)} = 1$ when $b_k[n] \neq \hat{b}_{SIC;k}[n]$, and $\Omega_k^{(n)} = -1$ when $b_k[n] = \hat{b}_{SIC;k}[n]$. After hard decision, the data decision becomes $\hat{b}_{SIC;<u>}[n] = \text{sgn}\{\hat{Y}_{SIC;<u>}^{(n)}\}$, and the detection error is denoted as $\varepsilon_{r\hat{b}_{SIC;<u>}}^{(n)} = 2\Delta_{<u>}^{(n)} b_{<u>}[n]$

3.4 Ordering Type

In the following, SIC is performed to alleviate the MAI from other users to achieve better error performance. The general SIC receiver is shown in Fig. 3-6. At every processing instant, the chosen user is made decision, respread (shown in Fig. 3-4) and then removed from the received signal. The process continues until all users are detected. To decrease MAI due to asynchronous reception, a group of G -bit data named Grouping interval is detected in the sequel, i.e. the n -th bit of user J is detected before or after another user's data is detected where $mG \leq n < (m+1)G$, and m is a nonnegative integer. The graphical illustration is shown in Fig. 3-1 where $1 \leq f \leq F$ and F is the number of RAKE fingers.

Generally speaking, signals are detected and canceled in order of their strength since the user with large received signal power is more reliable but leads to serious interference to other users. However, as shown in (3-8), the transmitted signal power P , channel gain α and correlation terms such as λ' and μ' , all affect the received signal strength and MAI to other users. Three ordering methods based on different consideration are described as follows

3.4.1 SIC I: Ordering Based on Average Power

In SIC I, the cancellation order is decided by the average power measured over a period much longer than $1/f_d$ where f_d is the Doppler shift. According to computer simulations, $f_d/12$ is large enough to be used as the reordering frequency. When the stationary channel is assumed, the reordering frequency can be much less than $f_d/12$. To detect a group of G -bit data of all users, the architecture for SIC I is shown in Fig. 3-7 where the index in $\{.\}$ at the output of each block denotes the processing step, and $\langle u \rangle_n = J$ denotes that the user with index J at bit index n is detected in the u -th order/stage. For notational simplicity, n is omitted in the following. After performing channel estimation {1} and pilot-channel signal removing {2}, all information in Buffer A are sent to Buffer B in each G -bit interval {3}, and Buffer A can continue to collect the next G -bit information without delay. At this moment, through the bus-like connection (bold line in part II), the user index and the corresponding channel estimates of the first detected user are sent to RAKE {4} followed by Decision {5}. Then data resampling {6} and traffic-channel signal removing {7} are performed, and the remaining signal is sent back to Buffer B {8}. $\hat{r}_{SIC;u}(t) = \hat{r}(t)$ when $u=1$. After that, according to the cancellation order decided in Part I, steps $5u-1$ to $5u+3$ are repeated for all the other users, where $2 \leq u \leq K$.

3.4.2 SIC II: Ordering Based on RAKE Outputs after G-bit

Cancellation of One User

In SIC II, the G -bit summation of the RAKE output strengths in each stage are used to find the next detected user. The architecture of SIC II is shown in Fig. 3-8. At first, we find the user with the maximum $\sum_{n=mG}^{(m+1)G-1} |\hat{Y}_{SICk}^{(n)}|$ at the output of RAKE Bank {5} with the Finding

Max block, and sent the user index to Buffer B {6}, where $\hat{Y}'_{SIC_k} = \hat{Y}_k^{(n)}$ and $\hat{Y}'_{SIC_{<u>}} = \hat{Y}_J^{(n)}$ with $u=1$. With this index, decision making {7}, data respreading {8} and removing from $\hat{r}(t)$ {9} are performed followed by storing the remaining signal $\hat{r}_{SIC;u+1}(t)$ in Buffer B. Then u is increased by one, and steps $6u-2$ to $6u+3$ are repeated where $2 \leq u \leq K$. Note that the Finding Max block must suspend and wait until $\hat{Y}'_{SIC_k} = \hat{Y}_k^{(n)}$ are shown at the outputs of RAKE Bank where k denotes all the undetected users..

3.4.3 SIC III: Ordering Based on RAKE Outputs at First Stage in Each G-bit Interval

In SIC III, the cancellation order is decided according to the signal strength of $\sum_{n=mG}^{(m+1)G-1} |\hat{Y}_k^{(n)}|$ obtained in RAKE Bank in Part I {3} as shown in Fig. 3-9. In each G -bit interval, information of all users are sent to Buffer B {4}. Then, in Finding Max block, the index of the user with maximum $\sum_{n=mG}^{(m+1)G-1} |\hat{Y}_k^{(n)}|$ is found {6} and then sent back to Buffer B. When the first user ($u=1$) is detected {8}, respreaded {9} and canceled from $\hat{r}(t)$ {10}, the Finding Max block finds the user with second largest signal strength according to the same $\sum_{n=mG}^{(m+1)G-1} |\hat{Y}_k^{(n)}|$ at the same time {10}. Thus, the RAKE output of the second detected user can be obtained right after $\hat{r}_{SIC2}(t)$ is sent out of Buffer B. For $2 \leq u \leq K$, steps $5u+1$ to $5u+5$ are repeated.

For all SICs in Fig. 3-7 to Fig. 3-9, in order to remove all interferences from the pilot-channel signals of all users in the n -th bit interval where $mG \leq n < (m+1)G$, $\hat{r}(t)$ with $t > [(m+1)G+1]T_b$ in Buffer A are sent to Buffer B. After G -bit data of all users are detected, the remaining signal $\hat{r}_{SIC;K+1}(t)$ with $t \geq (m+1)GT_b$ are cascaded with the incoming $\hat{r}(t)$

for the next G -bit data detection. Ordering in SIC I only takes the transmitted power and long-term channel gain into consideration. This ordering method is often used in literature when SIC is compared with other ICs. SIC II and SIC III take advantages of instant received signal strength, i.e. ordering is based on the compromise between reliability and channel estimates (weighting of MAI to others) where SIC III is the simplified version of SIC II. Increasing grouping interval G can decrease un-cancelled MAI to late detected users due to asynchronous reception. However, there is tradeoff between alleviating extra MAI and sensitivity to instant signal strength in SIC II and SIC III. For these two SICs, The early detected users may have small instantaneous SNR within a bit interval, as G increases.

3.5 Performance Analysis

3.5.1 Numerical Analysis

In this section, a closed-form expression for the average bit error rate (BER) over AWGN channel is presented. Channel estimation accompanying with the pilot-channel aided SIC employing three types of cancellation-ordering method in asynchronous systems (but assumed chip synchronous, i.e., $\tau \neq 0$ and $\tau' = 0$ where τ and τ' are defined in Appendix C is analyzed.

■ Channel Estimation

For sake of simplicity, the long scramble sequences are viewed as random sequences where $\{c_s\}$ are modeled as i.i.d. random variables. Thus, code correlations are assumed to be zero-mean complex-valued Gaussian random variables where $Var(\text{Re}[\lambda_{k,j}^{(n)}(\tau_{k,j})]) = Var(\text{Re}[\mu_{k,j}^{(n)}(\tau_{k,j})]) = 1/(2SF)$ when chip synchronous assumption is made, and $Var(\text{Re}[\lambda_{k,j}^{(n)}(\tau_{k,j})]) = Var(\text{Re}[\mu_{k,j}^{(n)}(\tau_{k,j})]) = 1/(3SF)$ when chip asynchronous assumption is

made [90]. $I_{\hat{\alpha}_J}^{(n)}$ is also a zero-mean complex-valued Gaussian random variable. It can be shown that the mean-squared error (MSE) of the channel estimation is given by

$$MSE(\hat{\alpha}_{av;J}^{(n)}) = \frac{1}{W} E[|\hat{\alpha}_J^{(n)} - \sqrt{P_J} \alpha_J^{(n)}|^2] = E[|MAI_{av;J}^{(n)}|^2] + E[|I_{av;J}^{(n)}|^2] = \frac{1}{W} \left(\frac{\beta_c^2 + 1}{\beta_c^2} \right) \left(\sum_{k=1, k \neq J}^K \frac{P_k}{(SF)} + \frac{N_0}{2T_b} \right) \quad (3-20)$$

■ Data Detection

Without loss of generality, the time dependency is negligible in the following discussions.

Thus, from (3-12), the decision statistics at the u -th stage are given as follows.

$$\begin{aligned} \hat{Y}_{SIC<u>} &= P_{<u>} b_{<u>}[n] + \sqrt{P_{<u>}} \operatorname{Re}[MAI_{av;<u>} + I_{av;<u>}] b_{<u>}[n] \\ &+ \{ \sqrt{P_{<u>}} + \operatorname{Re}[MAI_{av;<u>} + I_{av;<u>}] \} \operatorname{Re}[MAI_{bSIC<u>} + I_{bSIC<u>}] + \operatorname{Im}[MAI_{av;<u>} + I_{av;<u>}] \operatorname{Im}[MAI_{bSIC<u>} + I_{bSIC<u>}] \end{aligned} \quad (3-21)$$

● SIC I: Ordering Based on Average Power

In this type of SIC, user data is detected and removed according to the descending average power. According to the central limit theorem, $\hat{Y}_{SIC<u>} | b_{<u>}$ are assumed as Gaussian-distributed random variables with mean $P_{<u>} b_{<u>}$ and variance

$$\operatorname{Var}(\hat{Y}_{SIC<u>} | b_{<u>}) \approx [P_{<u>} + MSE(\hat{\alpha}_{av;<u>})] \left\{ \operatorname{Var}(\operatorname{Re}[MAI_{bSIC<u>}]) + \operatorname{Var}(\operatorname{Re}[I_{bSIC<u>}]) \right\} \quad (3-22)$$

since the decision statistics are the sum of many variables. This assumption is commonly made in the case of successive cancellation [54]. As shown in the next section, it provides good approximation to the AWGN-dominant systems. The variation of signal power is neglected for simplicity, and the interference components are assumed to be uncorrelated with $b_{<u>}$. According to $\hat{\varphi}_{SIC;k;<u>}^*(\tau)$, $\lambda_{k;<u>}(\tau)$ and $\hat{\psi}_{SIC;k;<u>}^*(\tau)$ in (3-17), (3-19) and (3-16),

respectively, it is shown that

$$Var\left(\text{Re}[MAI_{\hat{b}_{SIC <u>}}]\right) = \frac{1}{2SF} \left(\begin{aligned} & 1/G \left[\frac{3}{4} \left(\sum_{k=<u+1>}^{<K>} P_k + \sum_{k=<1>}^{<u-1>} E[|MAI_{\hat{\alpha}_{av};k}|^2] + \sum_{k=<1>}^{<u-1>} P_k E[(\hat{b}_{SIC;k})^2] \right) + \left(\frac{1}{4} \sum_{k=<1>}^{<u-1>} P_k \right) \right] \\ & + (1-1/G) \left[\sum_{k=<u+1>}^{<K>} P_k + \sum_{k=<1>}^{<u-1>} E[|MAI_{\hat{\alpha}_{av};k}|^2] + \sum_{k=<1>}^{<u-1>} P_k E[(\hat{b}_{SIC;k})^2] \right] \\ & + \beta_c^2 \sum_{k=1, k \neq <u>}^K E[|MAI_{\hat{\alpha}_{av};k}|^2] \end{aligned} \right) \quad (3-23)$$

where $E[(\hat{b}_{SIC;k})^2] = 4p_{r, TI, k}^{(K)}$ and $p_{r, TI, k}^{(K)}$ denotes the BER of user k [92]. The probability of $\tau \geq 0$ or $\tau < 0$ is equal to 1/2. In addition, only the expected values of the variance of partial code correlations are considered in (3-23). Also,

$$Var\left(\text{Re}[I_{\hat{b}_{SIC <u>}}]\right) = \frac{(\beta_c^2 + 1)N_0}{4T_b} \left(1/G \left[\frac{3}{4} \cdot \frac{u-1}{\beta_c^2 W(SF)} \right] + (1-1/G) \left[\frac{u-1}{\beta_c^2 W(SF)} \right] + 1 + \frac{K-1}{W(SF)} \right) \quad (3-24)$$

where the first and the third terms come from channel estimation errors. Strictly speaking, the BER analysis must be analyzed with the method of robust statistics as far as error detection is concerned [66]. Nevertheless, for simplicity, the error probability for the u -th canceled can be approximated as

$$p_{r, TI, <u>}^{(K)} \approx Q\left(\sqrt{P_{<u>}^2 / Var(\hat{Y}_{SIC <u>} | b_{<u>})}\right) \quad (3-25)$$

where $Q(x) = (1/2\pi) \int_x^\infty \exp(-t^2/2) dt$. The average BER with K users in the system thus is $\bar{p}_{r, TI}^{(K)}$

$$= \sum_{k=1}^K p_{r, TI, <k>}^{(K)} / K .$$

- **SIC II: Ordering Based on RAKE Outputs after G-bit Cancellation of One User**

This SIC finds the next detected user after each cancellation of the currently detected user,

i.e., decision statistics of undetected users at each stage are used as ordering bases. For SIC II and SIC III, the BER analysis of the cases with $G > I$ is very complicated, and thus only the case of $G = I$ is performed. Fortunately, as shown in the next section, when G increases, the BER of the three types of SIC are comparable in the AWGN channel. The error probability for the u -th canceled user is given as follows.

$$P_{r,III,<u>}^{(K)} = \frac{(K-1)!}{(K-u)!} \sum_{\substack{\langle u \rangle = 1 \\ \langle 1 \rangle \neq \langle u \rangle}}^K \sum_{\substack{\langle 1 \rangle \neq \langle u \rangle \\ \langle u-1 \rangle = 1 \\ \langle u-1 \rangle \neq \langle u \rangle \& \langle 1 \rangle \dots \langle u-2 \rangle \\ \langle u+1 \rangle \neq \langle 1 \rangle \dots \langle u \rangle}}^K \dots \sum_{\substack{\langle u+1 \rangle = u \\ \langle u+1 \rangle \neq \langle 1 \rangle \dots \langle u \rangle}}^K \sum_{\substack{\langle K \rangle = K-1 \\ \langle K \rangle \neq \langle 1 \rangle \dots \langle K-1 \rangle}}^K \int_0^\infty \int_{-\infty}^\infty \dots \int_{-\infty}^\infty d_{\langle u \rangle}(x_u) \cdot \prod_{k=1}^{k=u-1} g_{\langle u \rangle, \langle k \rangle}(x_{k+1} - x_k) \left(1 - \left| \frac{Q\left(\frac{P_{\langle k \rangle} - x_k}{c(\langle k \rangle, k)}\right) - Q\left(\frac{P_{\langle k \rangle} + x_k}{c(\langle k \rangle, k)}\right)}{1} \right| \right) \prod_{k=u+1}^K \left(\left| \frac{Q\left(\frac{P_{\langle k \rangle} - x_u}{c(\langle k \rangle, u)}\right) - Q\left(\frac{P_{\langle k \rangle} + x_u}{c(\langle k \rangle, u)}\right)}{1} \right| \right) dx_1 dx_2 \dots dx_u \quad (3-26)$$

where

$$c(v_1, v_2) = \left\{ \left[P_{v_1} + MSE(\hat{\alpha}_{av,v_1}) \right] \left[\frac{1}{2SF} \left(\frac{3}{4} \sum_{k'=1, k' \neq v_1, \& \sum_{\langle 1 \rangle \dots \langle v_2-1 \rangle}^K P_{k'} + \frac{1}{4} \sum_{k'=1}^K P_{k'} + \frac{3}{4} \sum_{k'=1}^{\langle v_2-1 \rangle} E[|MAI_{\hat{\alpha}_{av,k'}}|^2] \right) \right] \right\}^{1/2} \cdot \left[\frac{1}{2SF} \beta_c^2 \sum_{k'=1, k' \neq v_1}^K E[|MAI_{\hat{\alpha}_{av,k'}}|^2] + \frac{(\beta_c^2 + 1)N_0}{4T_b} \left(1 + \frac{K-1}{W(SF)} + \frac{3}{4} \frac{v_2-1}{\beta_c^2 W(SF)} \right) \right] \quad (3-27)$$

$d_{\langle u \rangle}(x) = 1/\sqrt{2\pi Var(\hat{Y}_{SIC\langle u \rangle} | b_{\langle u \rangle})} \exp(-(x - \sqrt{P_{\langle u \rangle}})^2 / 2Var(\hat{Y}_{SIC\langle u \rangle} | b_{\langle u \rangle}))$ is the probability distribution function (pdf) of Gaussian random variables $\hat{Y}_{SIC\langle u \rangle} | b_{\langle u \rangle}$ with mean $\sqrt{P_{\langle u \rangle}}$ and variance $Var(\hat{Y}_{SIC\langle u \rangle} | b_{\langle u \rangle}) = c(\langle u \rangle, u)$ when it is conditioned on $b_{\langle u \rangle} = -1$. It is easy to show that the error probability of the case $b_{\langle u \rangle} = 1$ is the same. $g_{v_1, v_2}(x)$ are assumed to be the pdf of Gaussian random variables with zero mean and variance equal to

$$\frac{1}{2SF} \left[P_{v_1} + MSE(\hat{\alpha}_{av,v_1}) \right] \frac{3}{4} \left[P_{v_2} + MSE(\hat{\alpha}_{av,v_2}) + \frac{(\beta_c^2 + 1)N_0}{2\beta_c^2 WT_b} \right] \quad (3-28)$$

Equation (31) denotes that the decision variables of the u -th detected user falling on x_1 , x_2 , ..., and x_{u-1} at the first, second, ..., and the $(u-1)$ -th stage, respectively, are smaller than

those of users $\langle 1 \rangle, \langle 2 \rangle, \dots, \langle u-1 \rangle$ which are decided to be detected at the first, second, \dots , and $(u-1)$ -th stage, respectively. When it comes to the u -th stage, the decision variables fall on x_u since interferences from previously detected $u-1$ users are canceled, and there are $K-u$ users whose decision variables are smaller than that of user $\langle u \rangle$ where decision error occurs when $x_u \geq 0$. To simplify the calculation, we assume that $x_{k+1} \approx x_k$ since $g_{\langle u \rangle, \langle k \rangle}(x_{k+1} - x_k)$ is small when it is compared to other random variables in (31). Then the error probability is approximated as

$$P_{r,III,u}^{(K)} = \frac{(K-1)!}{(K-u)!} \sum_{\substack{\langle u \rangle=1 \\ \langle l \rangle \neq \langle u \rangle}}^K \sum_{\substack{\langle l \rangle=1 \\ \langle l \rangle \neq \langle u \rangle}}^K \cdots \sum_{\substack{\langle u-1 \rangle=1 \\ \langle u-1 \rangle \neq \langle u \rangle \& \langle l \rangle \dots \langle u-2 \rangle \\ \langle u+1 \rangle \neq \langle u \rangle \& \langle l \rangle \dots \langle u \rangle}}^K \sum_{\substack{\langle u+1 \rangle=u \\ \langle u+1 \rangle \neq \langle u \rangle \& \langle l \rangle \dots \langle u-2 \rangle \\ \langle K \rangle \neq \langle u \rangle \& \langle l \rangle \dots \langle K-1 \rangle}}^K \cdots \sum_{\substack{\langle K \rangle=K-1 \\ \langle K \rangle \neq \langle u \rangle \& \langle l \rangle \dots \langle K-1 \rangle}}^K \int_0^\infty d_{\langle u \rangle}(x) \\ \cdot \prod_{k=1}^{k=u-1} \left(1 - \left| \mathcal{Q}\left(\frac{P_{\langle k \rangle} - x}{c(\langle k \rangle, k)}\right) - \mathcal{Q}\left(\frac{P_{\langle k \rangle} + x}{c(\langle k \rangle, k)}\right) \right| \right) \prod_{k=u+1}^K \left(\left| \mathcal{Q}\left(\frac{P_{\langle k \rangle} - x}{c(\langle u \rangle, k)}\right) - \mathcal{Q}\left(\frac{P_{\langle k \rangle} + x}{c(\langle u \rangle, k)}\right) \right| \right) dx \quad (3-29)$$

Then the average BER of SIC II thus is given by $\bar{p}_{r,III}^{(K)} = \sum_{k=1}^K P_{r,III,\langle k \rangle}^{(K)} / K$.

- **SIC III: Ordering Based on RAKE Outputs at First Stage in Each G-bit Interval**

In this type of SIC, user data is detected and canceled according to descending signal strength at the correlator outputs of the first stage, i.e., decision statistics of all users at the first stage are used as the ordering basis. Thus, the error probability for the u -th canceled user is modified to

$$P_{r,III,\langle u \rangle}^{(K)} = \frac{(K-1)!}{(u-1)!(K-u)!} \sum_{\substack{\langle u \rangle=1 \\ \langle l \rangle \neq \langle u \rangle}}^K \sum_{\substack{\langle l \rangle=1 \\ \langle l \rangle \neq \langle u \rangle \& \langle l \rangle}}^K \sum_{\substack{\langle l \rangle=1 \\ \langle l \rangle \neq \langle u \rangle \& \langle l \rangle}}^K \cdots \sum_{\substack{\langle u-1 \rangle=1 \\ \langle u-1 \rangle \neq \langle u \rangle \& \langle l \rangle \dots \langle u-2 \rangle \\ \langle u+1 \rangle \neq \langle u \rangle \& \langle l \rangle \dots \langle u \rangle}}^K \sum_{\substack{\langle u+1 \rangle=u \\ \langle u+1 \rangle \neq \langle u \rangle \& \langle l \rangle \dots \langle u-2 \rangle \\ \langle K \rangle \neq \langle u \rangle \& \langle l \rangle \dots \langle K-1 \rangle}}^K \cdots \sum_{\substack{\langle K \rangle=K-1 \\ \langle K \rangle \neq \langle u \rangle \& \langle l \rangle \dots \langle K-1 \rangle}}^K \int_0^\infty \int_{-\infty}^\infty d_{\langle u \rangle}(x_2) \sum_{k=1}^{u-1} g_{\langle u \rangle, \langle k \rangle}(x_2 - x_1) \\ \cdot \prod_{k=1}^{k=u-1} \left(1 - \left| \mathcal{Q}\left(\frac{P_{\langle k \rangle} - x_1}{c(\langle k \rangle, 1)}\right) - \mathcal{Q}\left(\frac{P_{\langle k \rangle} + x_1}{c(\langle k \rangle, 1)}\right) \right| \right) \prod_{k=u+1}^K \left(\left| \mathcal{Q}\left(\frac{P_{\langle k \rangle} - x_1}{c(\langle k \rangle, 1)}\right) - \mathcal{Q}\left(\frac{P_{\langle k \rangle} + x_1}{c(\langle k \rangle, 1)}\right) \right| \right) dx_1 dx_2 \quad (3-30)$$

Equation (3-30) indicates that a user with decision variables $\hat{Y}_{\langle u \rangle} = c(\langle u \rangle, 1)$ fallen on x_1 at

the first stage was decided to be canceled in the u -th stage since there are $u-1$ users having larger value of decision variables and there are $K-u$ users with smaller value of decision variables than user $\langle u \rangle$. When it comes to the u -th stage, the value of decision variables becomes x_2 since interferences from previously detected $u-1$ users are canceled, and the decision error occurs when $x_2 \geq 0$ in the case $b_{\langle u \rangle} = -1$. The decision errors of previously detected users are ignored for simplicity in both SIC II and SIC III. Then, the average BER for a system with K users is $\bar{p}_{r,III}^{(K)} = \sum_{k=1}^K p_{r,III,\langle k \rangle}^{(K)} / K$.

From the above analyses, channel estimation errors are shown to lead to nonlinear influence on the decision statistics as well as system performance. Analytical methods used in SIC II and SIC III can be viewed as the modification of the order statistics [21] where the ordering basis of SIC II changes after each cancellation.

3.5.2 Computational Complexity

Ordering in SIC I only takes the transmitted power and long-term channel gain into consideration. In SIC II and SIC III, they fully take advantages of instant received signal strength, i.e., ordering is based on the compromise between reliability and channel estimates (weighting of MAI to others) where SIC III is the simplified version of SIC II. In Table 3-1, the reordering frequency, throughput, latency, and computational complexity of all SICs are summarized. The processes in Part I of all SICs can be pipelined since they do not need feedback information from Part II.

3.6 Results and Discussions

The general simulation parameters are summarized in Table 3-2 and Table 3-3 according to 3GPP standard if they are not explicitly specified in the text. β_c is chosen for the optimal

BER according to the simulation results. The average SNR denotes the average of energy per bit of each user divided by noise variance. The chip resolution in AWGN is chosen to be 1 chip since chip synchronous is assumed, while the general chip resolution in multipath fading environment is 0.25 chips where chip asynchronous is assumed.

3.6.1 Channel Estimation

Fig. 3-10 shows the analytical and simulated results of mean square error (MSE) with $W=64$ and $W=128$ over flat Rayleigh fading channels where Doppler shift $f_d = 222\text{Hz}$, corresponding to a vehicle speed of 120 km/hr. We can see that the analytical MSE provides good approximation to the simulated MSE. Besides, large β_c results in better channel estimates since λ in (3-9) is alleviated in proportion to the reciprocal of β_c .

3.6.2 Data Detection

■ AWGN Channel



In Fig. 3-11, we examine the influence of various grouping intervals and power distribution ratios in AWGN channel. The analytical results of $G=1$ and $G=2400$ are shown in dotted line where SIC I with $G=2400$ is used to approximate SIC II and SIC III with $G=2400$, and it shows good approximation to the simulated results. The BER difference of the three SICs is explicit when G is small and PDR is close to unity, and SIC II outperforms the other two SICs in this situation. As G or PDR increases, all SICs have almost the same performance. This is because that the difference in the cancellation order of the three SICs is less and less as PDR or G increases.

Fig. 3-12 (a) shows the individual BER of the u -th detected user with eight active users in the system. When $G=1$, we find that the late-detected users of SIC I outperform those of SIC II and SIC III. Nevertheless, the early-detected users of SIC II and SIC III perform much

better than those of SIC I, thus, SIC II and SIC III still outperform SIC I after averaging as shown in Fig. 3-12(b). Fig. 3-12(b) shows the average BER versus user number for the three SICs when $G=1$ and 2400. Only SIC I with $G=2400$ is presented since it is shown in Fig. 3-11 that the three SICs have almost the same BER. All users in SIC II in Fig. 3-12(a), except the last one, outperform those in SIC III, and thus the average BER of SIC II in Fig. 3-12(b) is lower than that of SIC III.

In Fig. 3-13, the BER with different PDR s and SNR s are examined when $G=1$ and $G=2400$. β_c is chosen for optimal BER of the corresponding SNR. In this chapter, SIC without PCSR denotes that the pilot-channel signals are not removed first from the received signal, but they are removed accompanying with the data-channel signal of the corresponding user. Thus, SIC with PCSR outperforms SIC without PCSR only at the cost of demanding slightly more latency. As SNR increases, the benefit of SIC with PCSR becomes obvious, and all SICs with $G=2400$ outperform SIC II with $G=1$. For $G=2400$ as shown in Fig. 3-13(d), increasing SNR also results in the increasing in PDR for the optimum BER. The reason is that MAI dominates the BER at high SNR , and increasing PDR can alleviate MAI from early detected users.

In Fig. 3-14, we examine the influence of pilot-to-traffic amplitude ratio (β_c). For the last two lines in Fig. 3-14 (a) and Fig. 3-14 (b), the PDR s are chosen for the minimum BER for the SIC with PCSR when $G=2400$, i.e. $PDR=1.3$ ($K=8$) and $PDR=1.1$ ($K=16$) for all SICs. In Fig. 3-10, it is shown that large β_c brings better channel estimates. However, large β_c also leads to poor data detection since the percentage of transmitted power for data signal decreases, and MAI from pilot signal increases. It is shown that SIC with PCSR can dramatically alleviate MAI from pilot signal, especially when β_c increases. Also, SIC with PCSR is less sensitive to the variation of β_c in both moderately loaded case in Fig. 3-14(a) and heavily loaded case in Fig. 3-14(b).

■ Multipath Fading Channels

Four cases of propagation conditions for multipath fading environments used in the following are presented in Table 3-3. It is assumed that all paths are tracked and combined in the RAKE, i.e., $F=P$.

In Fig. 3-15, we can find that three SICs in all considered channels perform much better than the RAKE receiver. The best BER occurs at $PDR=1.3$ for SIC I in all cases, while it occurs at $PDR=1.0$ for SIC II and SIC III in channel Case 1 and channel Case 2, and at $PDR \neq 1.0$ in channel Case 3 and channel Case 4. SIC II performs slightly better than SIC III when PDR is close to unity and G is small, and they both achieve better BER than SIC I. This is because SIC II and SIC III have the ability to track channel variation but SIC I does not.

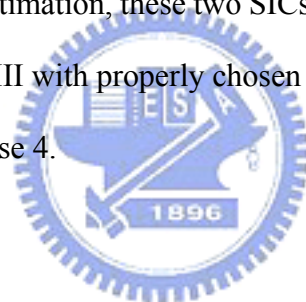
In Fig. 3-16, the BER is investigated with channel estimation where $W=128$. The timing estimation errors are modeled as Gaussian distributed random variables with zero mean and variance 0.0625 (2 samples) at 1/32 chips resolution where 95% of the probability mass is concentrated within ± 4 samples [59]. The simulated results are similar to those in Fig. 3-15 except that the best BER occurs at $PDR=1.0$ for SIC II and SIC III in all channel cases.

Fig. 3-17 indicates the BER of individual user in different cancellation order with the PDR for the optimum BER in each SIC in channel Case 3. For SIC I in Fig. 3-17(a), influences of G are obvious only when G is small. For SIC II in Fig. 3-17(b) and SIC III in Fig. 3-17(c), the early canceled users have smaller BER than that of the late canceled users for small G . As $G > 1000$, their BER becomes worse than SIC I where the early canceled users have larger BER than that of the late canceled users. Also, SIC II slightly outperforms SIC III when G is small.

The BER versus β_c over all channel cases are given in Fig. 3-18 where G and PDR are selected for the best BER, i.e., $G=2400$ in channel Case 1 and channel Case 2, $G=32$ in channel Case 3, and $G=16$ in channel Case 4 for all SICs. Similar to the results shown in Fig.

3-14 for AWGN channel, the PCSR helps to improve BER and increase β_c for the optimum BER. Better timing synchronization can be achieved since pilot-channel signal power is increased. SIC II and SIC III still perform much better than SIC I. Moreover, SIC II and SIC III have similar performance.

In Fig. 3-19, the BER for various channel cases are examined. According to the results in Fig. 3-15, the *PDRs* for the minimum BER of each SIC are chosen. In channel Case 1 and channel Case 2, the one-frame long grouping interval, i.e., $G=2400$, results in the best BER for all SICs. However, in channel Case 3 and channel Case 4, the optimum BER for SIC II and SIC III occur at about $G=100$ and $G=50$, respectively. Among all channel cases, SIC II and SIC III outperform SIC I, and except in channel Case 3 and channel Case 4 when G is small than about 20 with channel estimation, these two SICs almost have the same BER. It is worthy to note that SIC II and SIC III with properly chosen G as *PDR*=1 are suitable for fast fading channels such as channel Case 4.



3.6.3 Discussion

From the above simulations and analyses, we find that:

The SIC with PCSR can achieve better BER than that without PCSR when β_c is large in both AWGN and selective fading channels. The optimal β_c for SIC with PCSR is larger than that without PCSR. Larger β_c implies less timing estimation error which is critical in most communication systems.

The benefit of detecting and canceling a group of G -bit in AWGN channel becomes obvious when noise and MAI decrease. The reason has been mentioned in 3.4. The relationship between f_d and the optimal G of SIC III-like SIC in multirate systems in multipath fading channels is examined in the later section [70] where the optimal G is shown inversely proportional to f_d in fading environment. In addition, larger G results in better BER

in SIC I in all fading channel cases since the detection order is not affected by G .

There is also tradeoff between decreasing MAI and propagation error to later detected users (increasing PDR) and increasing SNR of the later detected users (decreasing PDR). When the noise (including estimation errors) and MAI increase, the PDR for the optimum BER in AWGN channel becomes closer to one, and the reason has been explained in Fig. 3-13. For SIC I over fading channels, it is shown that the optimum BER always occurs at $PDR \neq 1$. And as for SIC II and SIC III, whether the PDR of optimum BER is equal to unity depends on the channel condition.

The BER of SIC I is inferior to the other two SICs when G is small. For SIC II and SIC III, they perform almost the same in both AWGN channel and fading channel when G or PDR is larger than one. Since in these cases, SIC II and SIC III has similar detection. In the view of BER, SIC II would be a good choice when it is applied to a heavily loaded system over AWGN channel with $G=1$ or when G for the optimum BER is smaller than 16 over multipath fading channels. (With the simulation parameters used in chapter, $G=16$ when the vehicle speed is at about 250km/hr.)

3.7 Pilot-Channel Aided SIC for Multirate Systems

The WCDMA systems in the uplink support multiple services. Since the MAI primarily limits the system capacity, especially high-power users can seriously corrupt users with low receiving power. A multiuser receiver that can accommodate multi-rate communications is inevitable. When variable-spreading-gain (VSG) communication systems are concerned, deciding the cancellation order of SIC becomes complicated since the desired SINRs of different users are not the same. In [65], it is proven that ranking users in descending order of channel gain minimizes the total transmission power for arbitrary SINR setting, while in [39] the authors show that the optimal decoding order of users with imperfect interference

cancellation is a function of their required SINR as well as path gain. A generalized pilot-channel aided SIC scheme is presented to apply to multirate communications in uplink WCDMA systems over multipath Rayleigh fading channels. In the previous section, we find a group-detected pilot-channel aided SIC scheme with cancellation ordering based on the average RAKE output strength over a properly chosen grouping interval at the 1st stage of SIC is a proper ordering method, since it outperforms the average power ordering method in bit error rate (BER) and reordering after each cancellation method in computational complexity and processing delay. The pilot-channel aided SIC scheme is slightly modified to adapt to either single rate or multirate systems. Although a similar grouping method has been proposed for the asynchronous systems [54] or VSG multirate communications [10], for users with relatively large spreading gain, it is shown in the following that the choice of the optimal grouping interval (G_c) for the minimum BER depends on the Doppler shift of Rayleigh fading channels.

The scheme performs data detection in a group manner for each user, and the cancellation order is decided based on the average RAKE output strength over the grouping interval at the first stage of SIC. The grouping detection method helps the users with relatively large spreading gain to perform much better at the expense of slight performance loss of the user with the lowest spreading gain. In addition to showing that the optimal grouping interval for high rate users depends on the Doppler shift of Rayleigh fading channel, the BERs of individual spreading gain are compared with those in the single rate system.

3.7.1 Pilot-Channel Aided SIC for Multirate Systems

In the pilot-channel aided SIC scheme, a group of $G_{b,J}$ -bit of each user is detected in the sequel where $G_{b,J} = G_c / (SF)_J$, i.e., the n_J -th bit of user J is detected before or after another user's data is detected where $mG_{b,J} \leq n_J < (m+1)G_{b,J}$. m is a nonnegative integer which

denotes grouping index. To minimize the influence of error propagation, the cancellation order of the adopted SIC is decided according to the signal strength of $\sum_{n_k=mG_{b,k}}^{(m+1)G_{b,k}-1} |\hat{Y}_k^{(n_k)}| / G_{b,k}$ where $|\hat{Y}_k^{(n_k)}|$ is obtained from (2-3). After ranking the cancellation order, $J = \langle u \rangle$ denotes that the user with index J is to be detected in the u -th order. Thus, for the u -th canceled user, the real part of RAKE output becomes

$$\hat{Y}_{SIC \langle u \rangle}^{(n_J)} = \sum_{j=1}^F \operatorname{Re} \left\{ \frac{1}{2\beta_d T_{b,J}} \int_{n_j T_{b,J} + \tau_{J,f}}^{(n_J+1)T_{b,J} + \tau_{J,f}} (\hat{\alpha}_{J,f}^{(n_J)})^* \hat{r}_{SIC,u}(t) C_{O,J}(t - \tau_{J,f}) C_J^*(t - \tau_{J,f}) dt \right\} \quad (3-31)$$

where

$$\hat{r}_{SIC,u}(t) = \hat{r}(t) - \sum_{k=\langle 1 \rangle}^{\langle u-1 \rangle} \tilde{C}_{data,k}(t)$$

and

$$\tilde{C}_{data,k}(t) = \sum_{p=1}^F \beta_d \hat{\alpha}_{av}^{(\lfloor (t - \tau_{k,p}) / T_{b,k} \rfloor)} \hat{b}_{SIC,k}[\lfloor (t - \tau_{k,p}) / T_{b,k} \rfloor] C_{O,k}(t - \tau_{k,p}) C_k(t - \tau_{k,p}) \quad (3-32)$$

where $mG_c T_c \leq t - \tau_{k,p} < (m+1)G_c T_c$ and $\lfloor x \rfloor$ indicates the largest integer smaller than or equal to x . And the data decision thus is

$$\hat{b}_{SIC;k}[n_k] = \operatorname{sgn} \{ \hat{Y}_{SIC;k}^{(n_k)} \}.$$

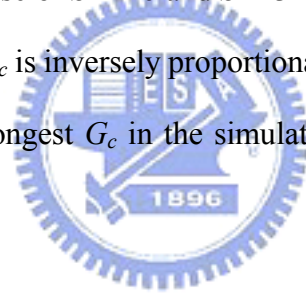
3.7.2 Simulation Results

In the following, the BER of the pilot-channel aided SIC is examined through computer simulations. The general simulation parameters are summarized in Table 3-4 if they are not explicitly specified in the text. Although it is shown that the SIC with average power ordering

method has optimal BER in non-equal power profile [54], it is found in Fig. 3-16 that the optimal BER occurs in equal power profile with non-perfect parameters estimation over multipath fading channels. Thus, only equal power profile is considered in the following.

In Fig. 3-20, BER versus varying G_c is shown in (a) multirate systems and (b) single rate systems where the BER of users with the same rate are averaged. We can observe that the relationship between BER and G_c of these two systems are similar though the exact value of BERs are slightly different. The benefit of properly chosen G_c is obvious when $SF=32$. G_c for the minimum BER in the cases of $SF=16$ and $SF=32$ are almost the same. As SF increases, the BER difference between SIC and the pure RAKE receiver becomes larger.

Fig. 3-21 shows the grouping interval in chips (G_c) for the minimum BER versus different Doppler shift (f_d) in the case of $SF=16$ and $SF=32$. It is shown that no matter what the data rate of individual user is, G_c is inversely proportional to f_d . Note that there are 38400 chips in one frame, which is the longest G_c in the simulation. Thus G_c saturates at 38400 when $f_d < 10$.



3.7.3 Discussion

In this section, we present a pilot-channel aided SIC scheme for multirate WCDMA systems in the uplink. The cancellation order is decided by ranking the average of RAKE output strength at the 1st stage of SIC over the grouping interval, and properly chosen grouping interval help to reduce the BER of users with relatively large spreading gain. The characteristics of grouping interval shown in the single-rate systems can be also found in multirate systems.

3.8 Summary

In this chapter, we investigate a pilot-channel aided SIC scheme for uplink WCDMA

systems. The scheme alleviates the interference from traffic-channel as well as pilot-channel signals of other users. Also, we discuss three SICs with different ordering method, and compare their corresponding architectures as well as processing delays and computational complexities. In addition to showing the superiority over the conventional RAKE receiver, the influence of ordering method, pilot-to-traffic amplitude ratio, grouping interval, power distribution ratio, channel and timing estimation errors on the BER are jointly examined and discussed. It is found that ordering based on average power (SIC I) requires the least computational complexity at the expense of BER when grouping interval is small, and it seems to be suitable for AWGN channels with moderate loading. Ordering based on RAKE outputs after each cancellation of grouping-interval bits of one user (SIC II) outperforms ordering based on RAKE outputs at initial stage in each grouping interval (SIC III) when grouping interval is small. But SIC II has the highest computational complexity and the largest processing delay among all SICs. SIC III is proposed to be a better choice over multipath fading channels when BER and computational complexity are jointly concerned.

The pilot-channel aided SIC scheme for multirate WCDMA systems in the uplink is also presented. The scheme alleviates interference resulting from data-channel signals as well as pilot-channel signals of other users in the received signals. The cancellation order is decided by ranking the average of RAKE output strength at the 1st stage of SIC over the grouping interval, and properly chosen grouping interval help to reduce the BER of users with relatively large spreading gain depends on the Doppler shift of channel.

Table 3-1 Characteristics of Three SICs per G Bits per K Users

SIC	Reordering Frequency (denoted as RF)	Throughput (Bits/Step)	Latency (Steps)	Hardware Required for Minimum Delay	Computational Complexity $C(.)$ BASE=PCSR+CE +DS+RAKE+DR+AD
I	$\ll f_d$	$G/5$	$5K+3$	As shown in block diagrams in Fig. 3-7 ~ Fig. 3-9	$K*C(BASE)+K*C(OR)*Gf_dT_b/RF$
II	$K/(GT_b)$	$G/6$	$6K+3$		$K*C(BASE)+K*C(FM)+K(K-1)/2*C(RAKE)$
III	$1/(GT_b)$	$G/5$	$5K+5$		$K*C(BASE)+K*C(FM)+(K-1)*C(RAKE)$
PCSR: Pilot Channel Signal Removal; CE: Channel Estimation; DS: Decision; DR: Data Respread; AD: Adder; FM: Find Max; OR: Average Power					

Table 3-2 Simulation Parameters

Symbol	Quantity		
$1/T_c$	Chip Rate	3.84Mhz	
f_c	Carrier Frequency	2 GHz	
SF	Spreading Factor	16	
$1/T_b$	Bit Rate	240 Kbps	
N	Scramble Sequence Length	38400 Chips	
NT_c	Frame Period	10 ms	
β_c	Pilot-to-Traffic Amplitude Ratio	AWGN	7/15
		Fading Channels	10/15
K	User Number	8	
SNR	Average E_b/N_0	AWGN	15 dB
		Fading Channels	20 dB
	Multipath Fading Channel Conditions	See Table 3-3	

Table 3-3 Propagation Conditions for Multipath Fading Environments [71].

Case 1, speed 3km/h		Case 2, speed 3 km/h		Case 3, 120 km/h		Case 4, 250 km/h	
Relative Delay [ns]	Average Power [dB]	Relative Delay [ns]	Average Power [dB]	Relative Delay [ns]	Average Power [dB]	Relative Delay [ns]	Average Power [dB]
0	0	0	0	0	0	0	0
976	-10	976	0	260	-3	260	-3
		20000	0	521	-6	521	-6
				781	-9	781	-9

Table 3-4 Simulation Parameters for Multirate Systems

Chip Rate ($1/T_c$)	3.84Mhz
Carrier Frequency	2GHz
Scramble Sequence Length (N_c)	38400Chips
Pilot-to-Traffic Gain Ratio (β_c)	2/3
User Number (K)	6
Spreading Factor (SF_k)	Randomly Chosen from {8,16,32}
Chip Energy to Noise Ratio (E_c/N_0)	-3 dB
Moving Average Window for Channel Estimation(W_c)	2048Chips
Multipath Fading Channel Conditions	Case 3 in Table 3-3

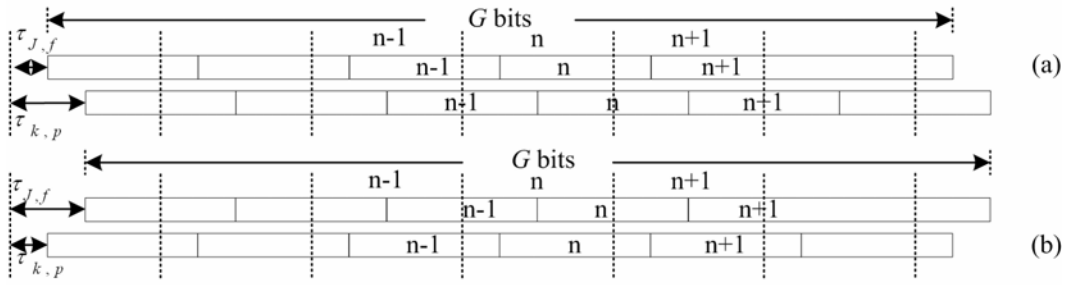


Fig. 3-1 The received signal timing and data detection group (a) $\tau_{k,p;J,f} \geq 0$ and (b) $\tau_{k,p;J,f} < 0$ where $\tau_{k,p;J,f} = \tau_{k,p} - \tau_{J,f}$.

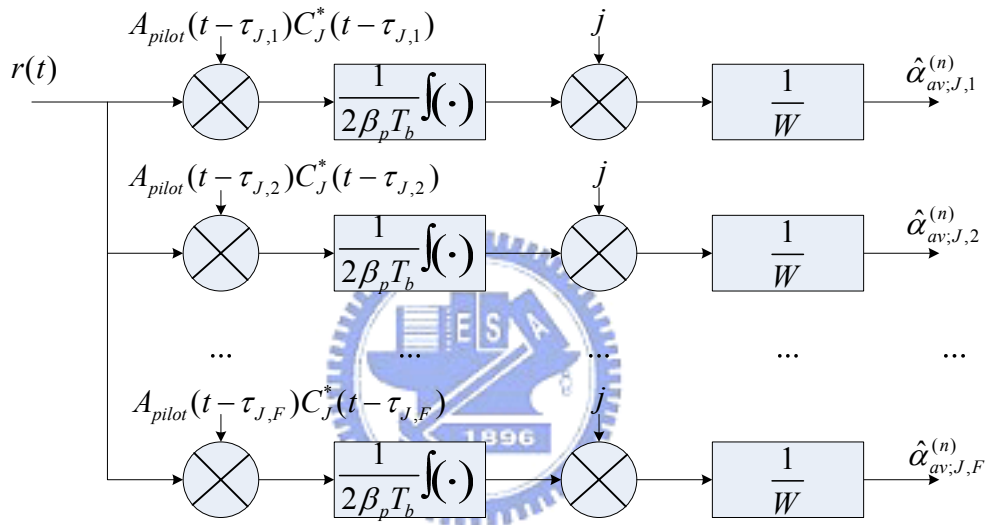


Fig. 3-2 Channel estimation of user J with F paths

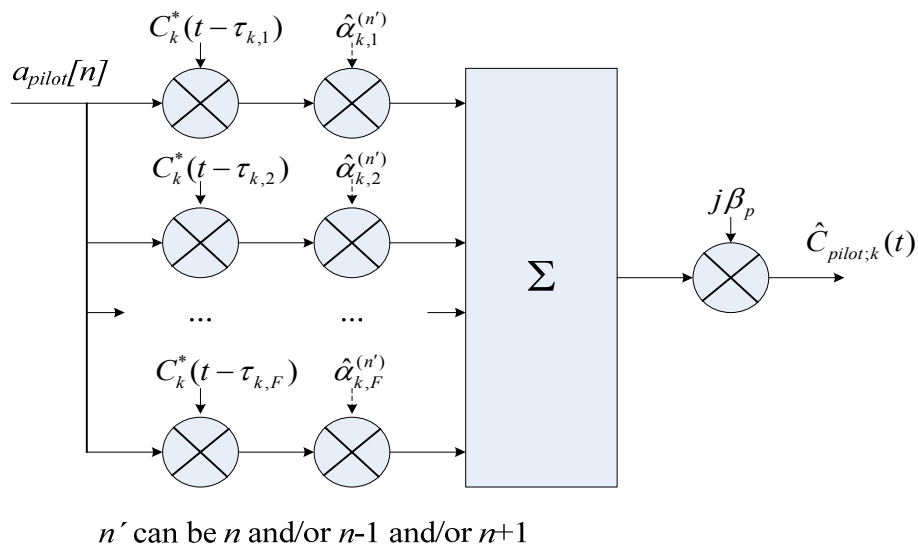


Fig. 3-3 Structure of the pilot respread of the k -th user with F paths

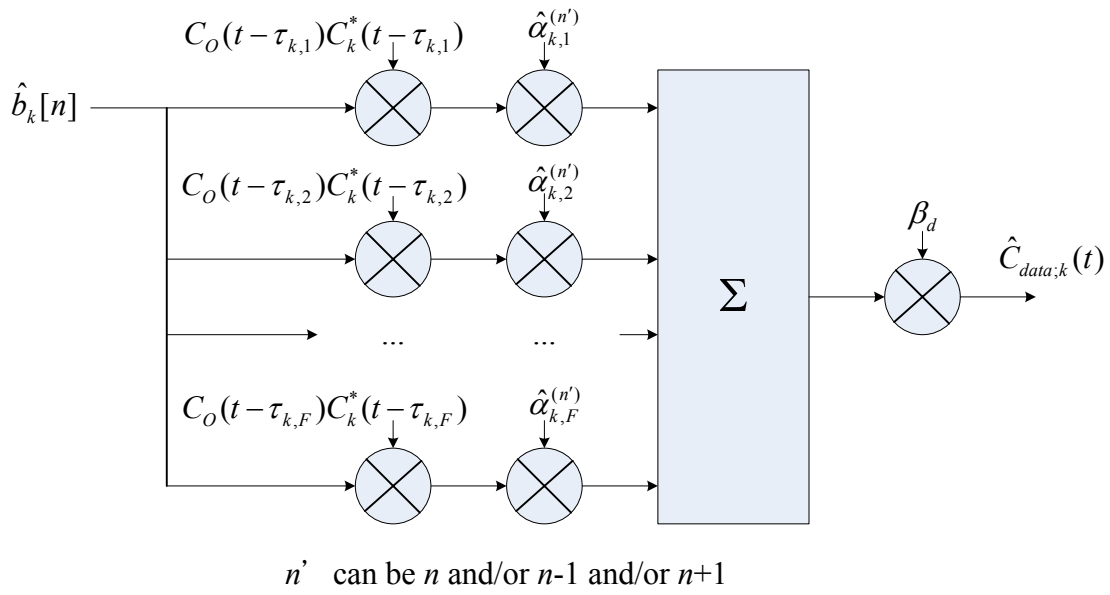


Fig. 3-4 Structure of the data despreading of the k -th user with F paths

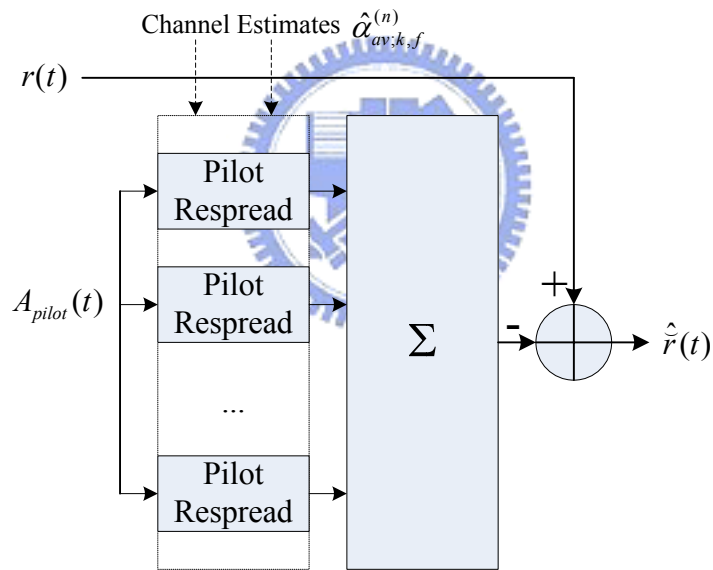


Fig. 3-5 Block diagram of pilot-channel signal regenerator and remover, $1 \leq k \leq K$, $1 \leq f \leq P$

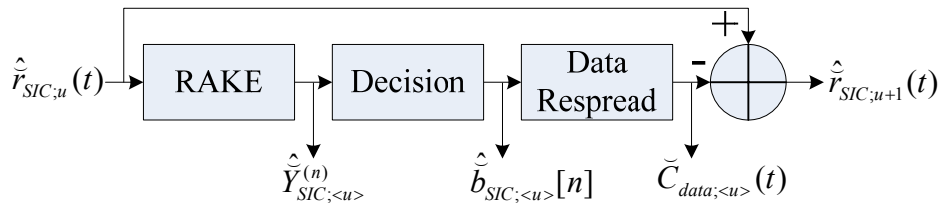


Fig. 3-6 Generalized SIC structure at the u -th stage

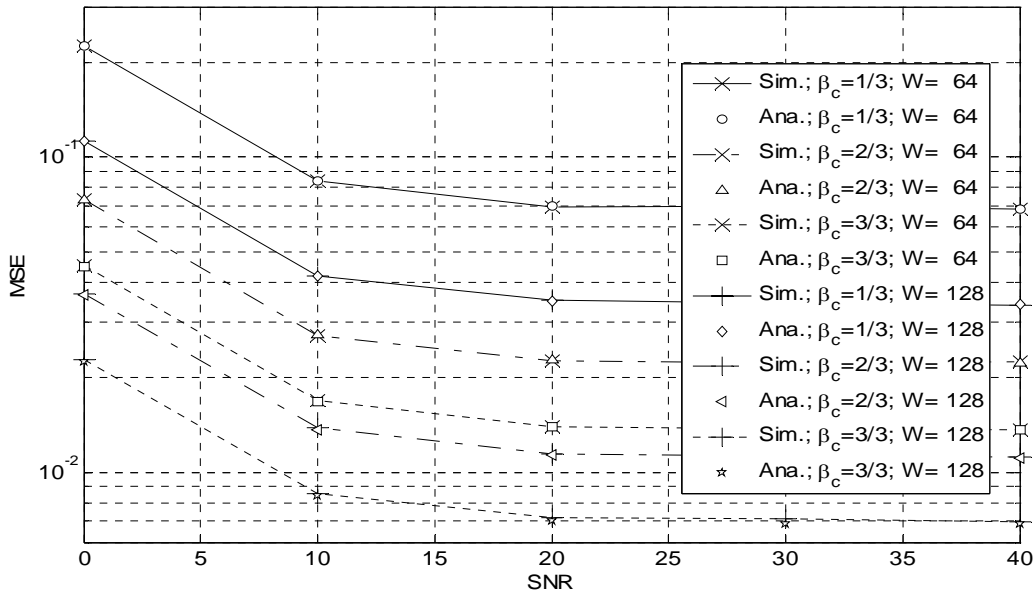


Fig. 3-10 MSE of channel estimates with various SNRs, flat Rayleigh fading channel, $PDR=1.0$, $G=1$.

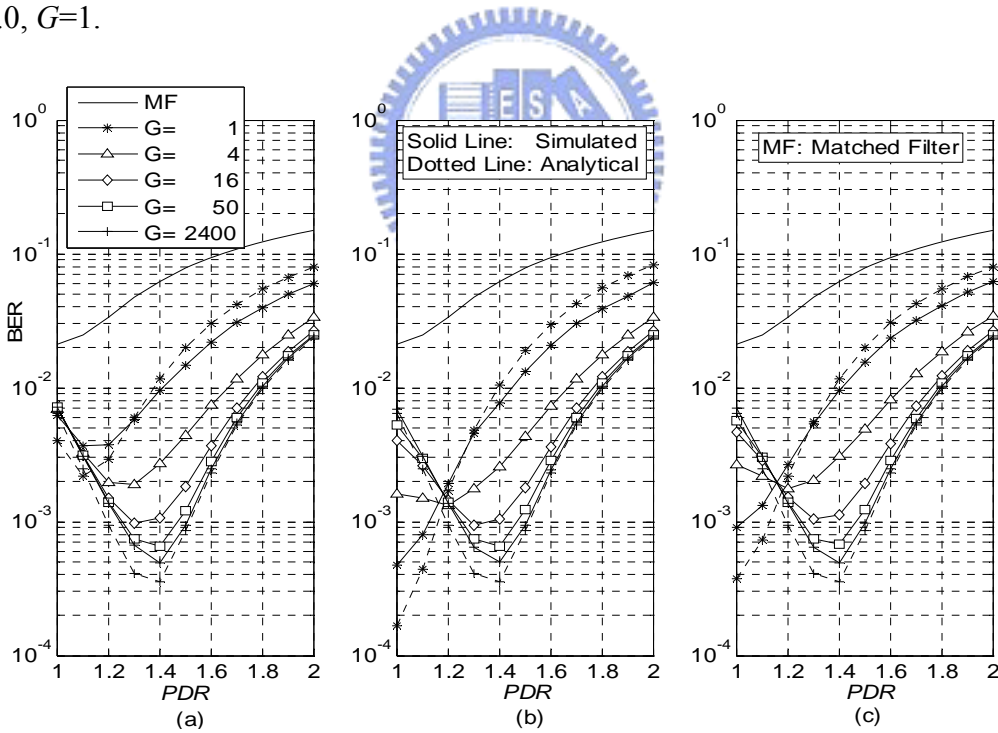


Fig. 3-11 BER versus PDR with different grouping interval G for (a) SIC I, (b) SIC II, (c) SIC III; AWGN, know channel parameters, with PCSR.

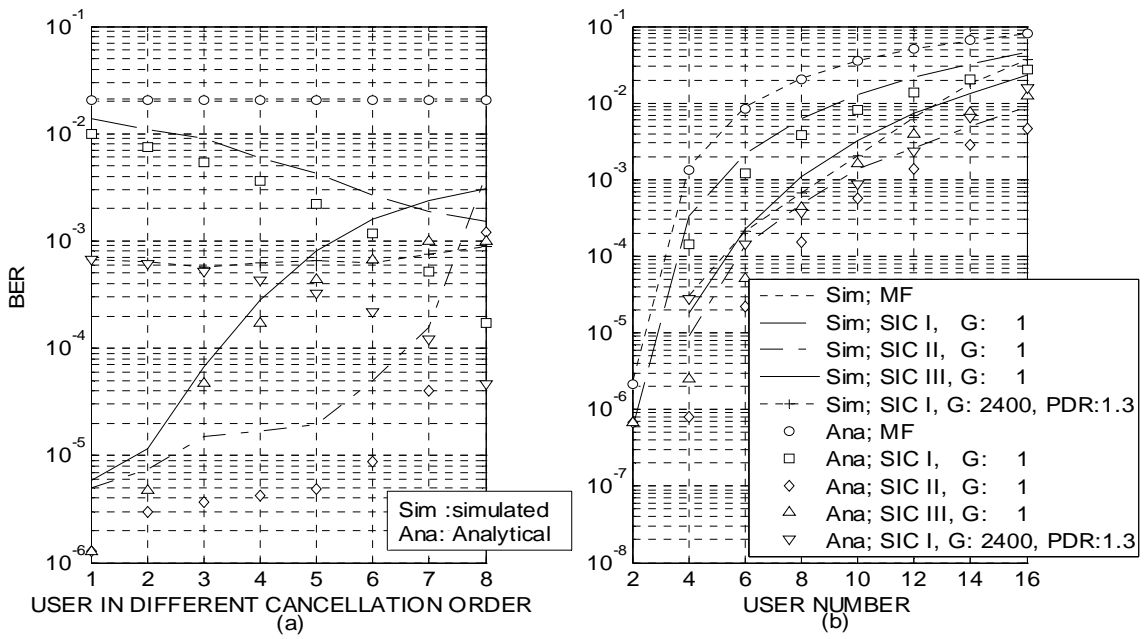


Fig. 3-12 Simulated and analytical results of SICs with PCSR (a) individual BER in an eight-user system, (b) average BER.

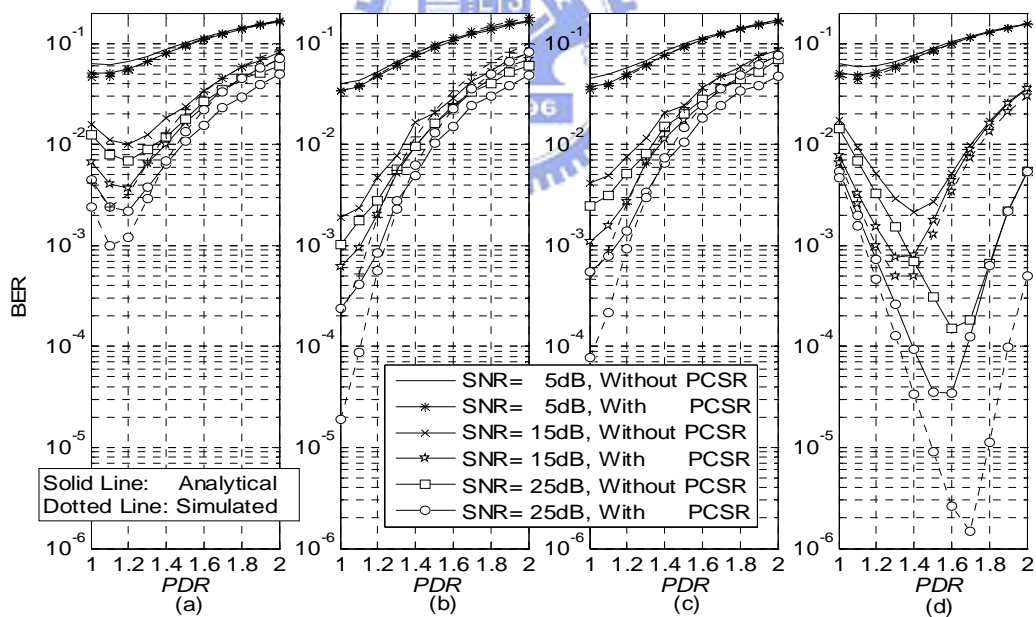


Fig. 3-13 BER comparison with different PDRs and SNRs with/without PCSR for (a) SIC I with $G=1$, (b) SIC II with $G=1$, (c) SIC III with $G=1$, (d) SIC I with $G=2400$; AWGN, channel estimation with $W=128$.

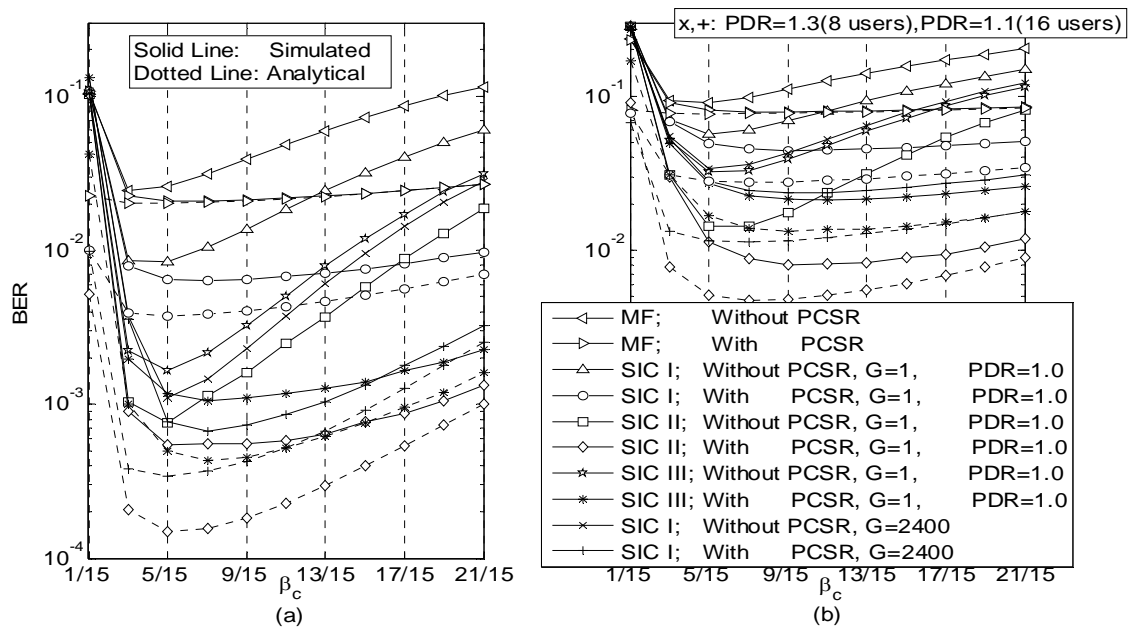


Fig. 3-14 BER versus β_c with/without PCSR when there are (a) 8 users, (b) 16 users in the system; AWGN, channel estimation with $W=128$.

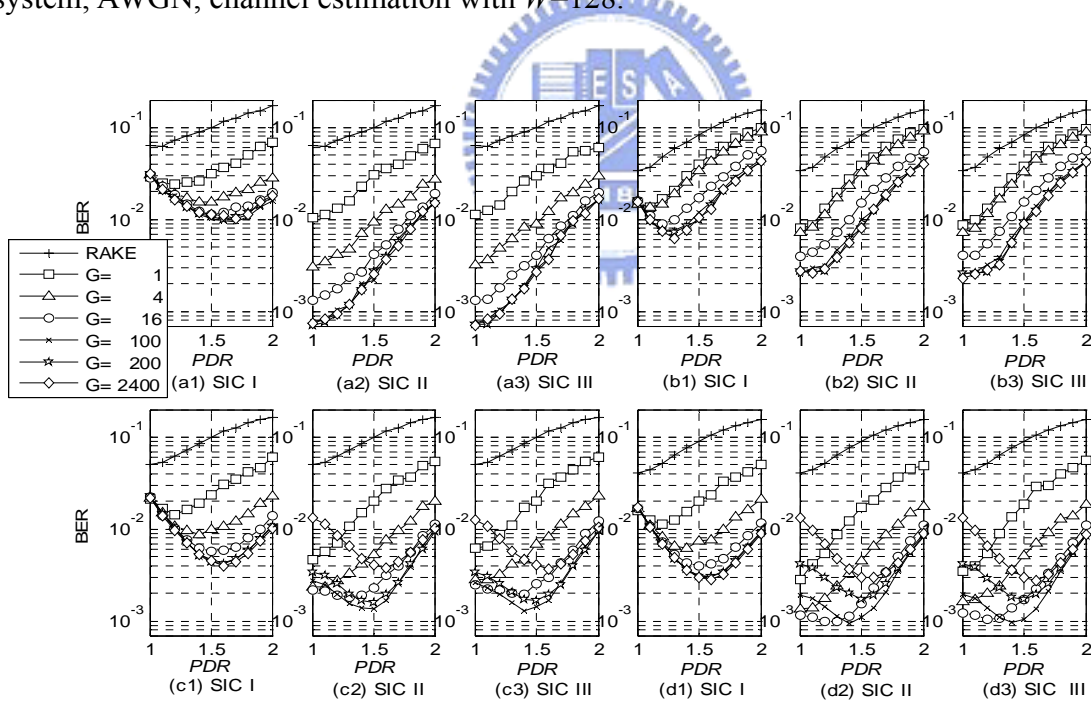


Fig. 3-15 BER versus PDR for the three SICs in multipath fading channels (a) Case 1, (b) Case 2, (c) Case 3, (d) Case 4; with PCSR, known channel parameters.

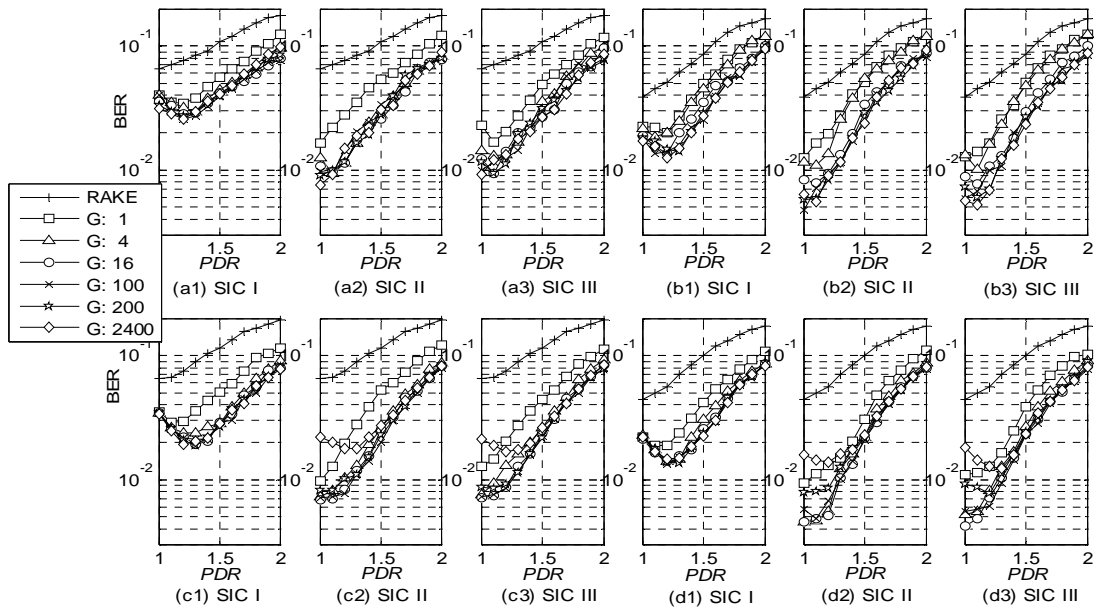


Fig. 3-16 BER versus PDR for the three SICs in multipath fading channels (a) Case 1, (b) Case 2, (c) Case 3, (d) Case 4; channel estimation with $W=128$ and timing estimation error with variance 2 samples at $1/32$ chips resolution.

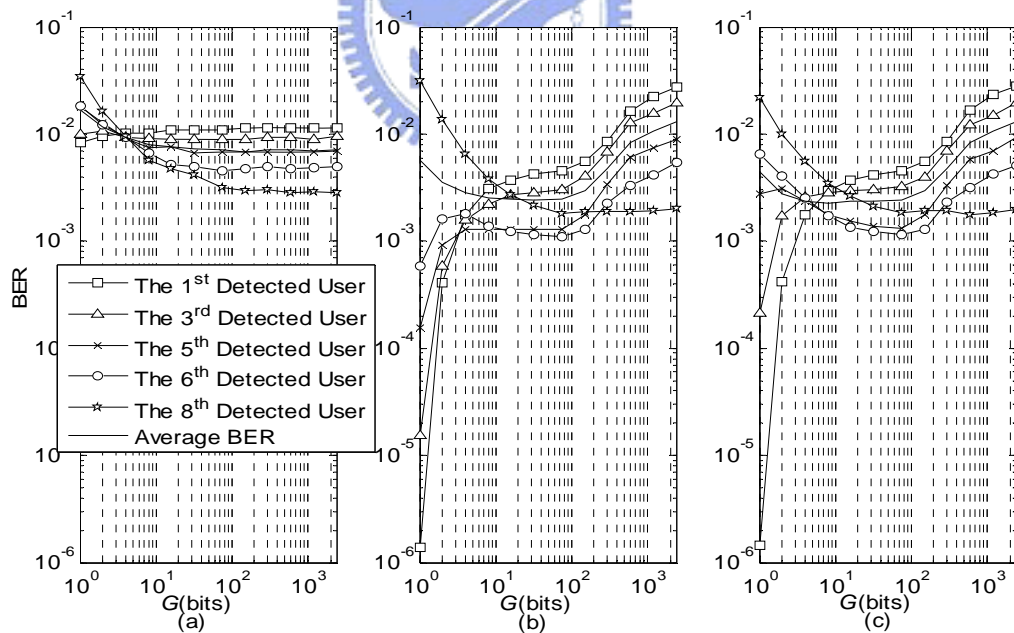


Fig. 3-17 BER versus grouping interval G for user in different detection order for (a) SIC I with $PDR=1.3$, (b) SIC II with $PDR=1.0$, (c) SIC III with $PDR=1.0$; channel case 3, known channel parameter, with PCSR.

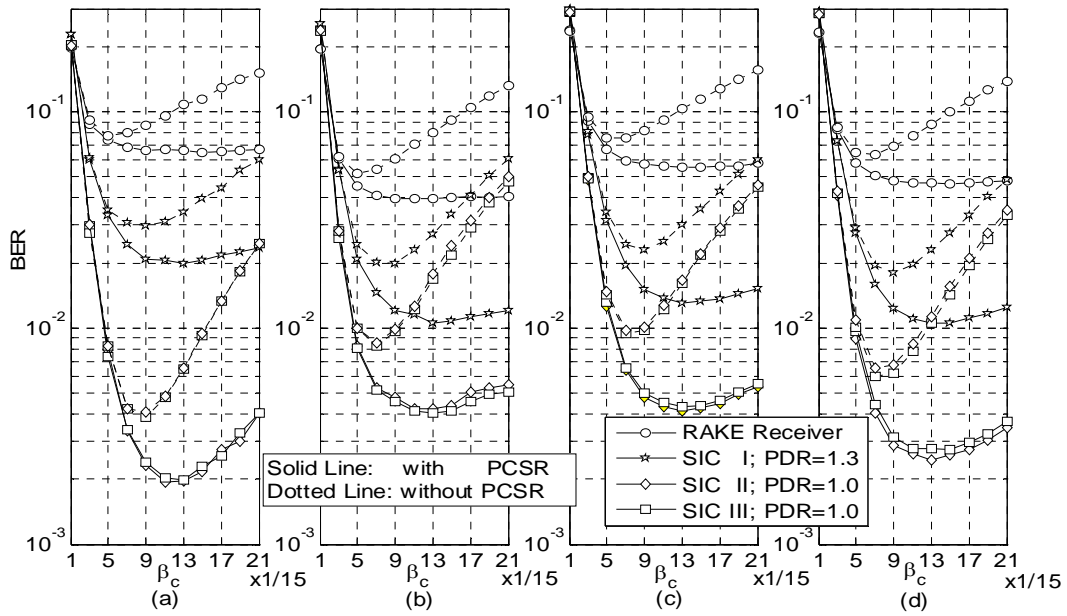


Fig. 3-18 BER versus β_c for multipath fading channels (a) Case 1, (b) Case 2, (c) Case 3, (d) Case 4; channel estimation with $W=128$.

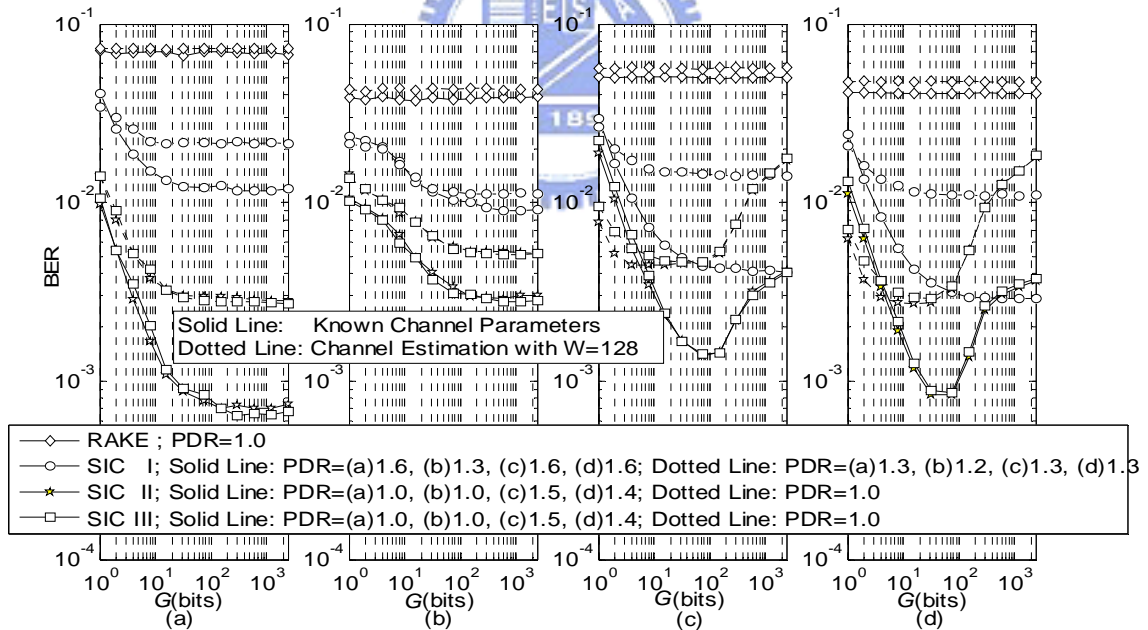


Fig. 3-19 BER versus grouping interval G for multipath fading channels (a) Case 1, (b) Case 2, (c) Case 3, (d) Case 4; with PCSR

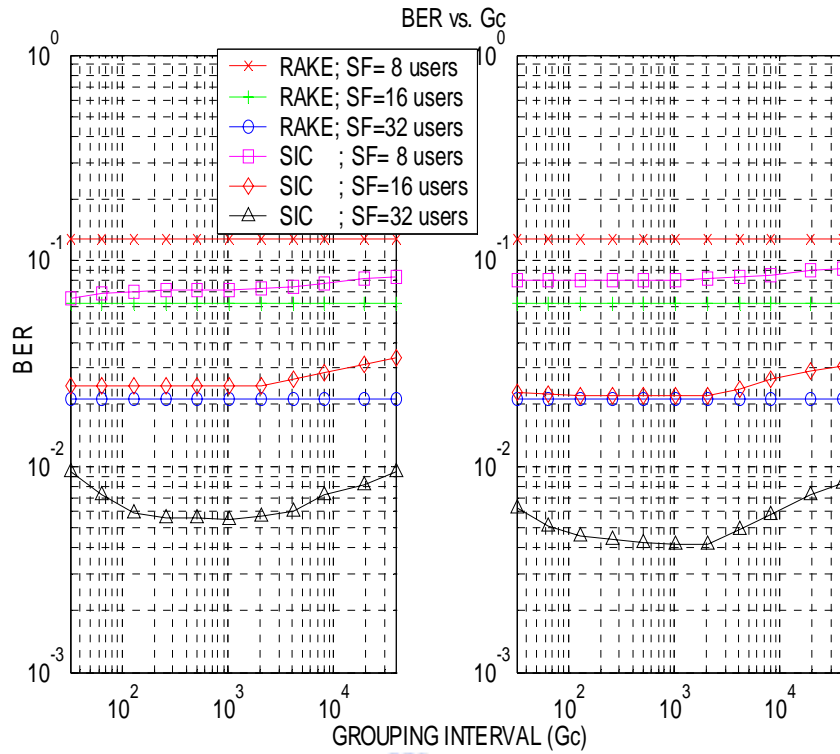


Fig. 3-20 BER vs. grouping interval G_c , $f_d=222\text{Hz}$ for (a) multirate systems and (b) single rate systems.

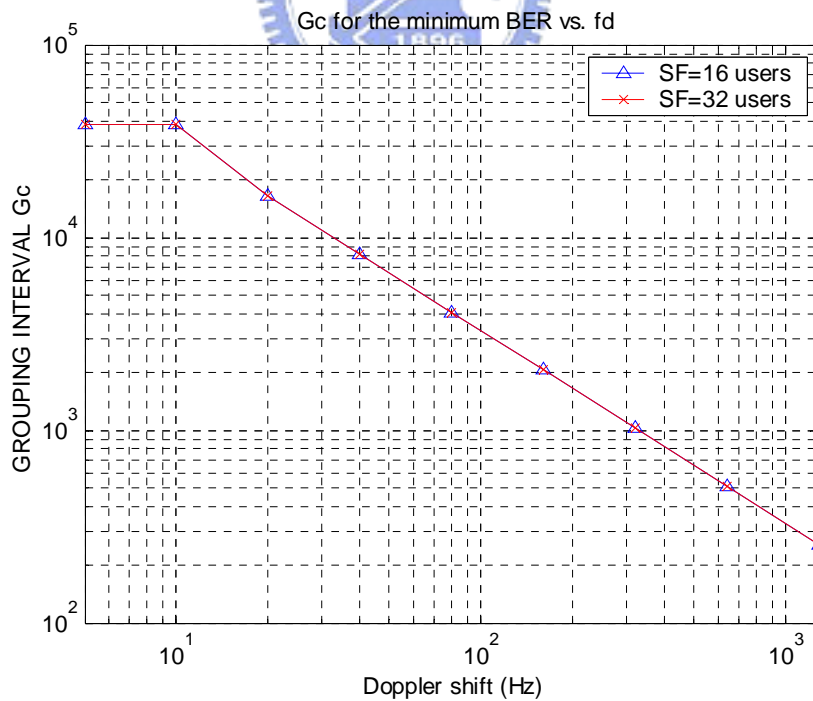


Fig. 3-21 Grouping interval G_c for the minimum BER vs. Doppler shift

Chapter 4

Advanced Techniques for Pilot-Channel

Aided Interference Cancellation

4.1 Overview

In the uplink of WCDMA systems, traffic-channel signal and pilot-channel signal are multiplexed in I and Q channel, respectively. In the former chapter, pilot-channel signal are removed before data detection is performed to acquire better performance. In this chapter, the channel estimation accuracy is further improved. Additionally, we find that the SIC outperforms PIC under fading channels but faces the problem of power reordering and longer processing delay. In this chapter, we propose techniques to overcome this drawback.

In the first part of this chapter, we propose a pipelined structure to reduce the latency, i.e. a pilot-channel aided pipeline scheme for interference cancellation (IC) in uplink wideband DS/CDMA system is proposed. Generally speaking, pipelined implementation is inherent in SIC but not in channel estimation. This scheme combines channel estimation and user data detection into sequential type with low complexity and leads to pipeline implementation. Besides, interference between data channel signals and pilot channel signals under multipath fading channel are also taken into consideration. Compared with conventional channel estimation using correlator output and SIC without pilot channel signal removal, the proposed scheme shows better quality both on channel estimation and user data detection.

In the second part of this chapter, we further propose an adaptable scheme which has the ability to perform better than SIC discussed in Chapter 3 as well as adapt its structure

according to the environment and channel condition. The pilot-channel aided adaptable IC scheme combines successive (SIC) and parallel (PIC) interference cancellation to adapt to different services under different circumstances for uplink wideband CDMA system. The processing delay and computational complexity can be adjusted based on system loading and required performance. The interference between data channel signals and pilot channel signals under multipath fading channel are also taken into consideration. This results in better quality both on channel parameter estimation and user data detection. Compared with SIC and PIC, the proposed scheme shows better performance with reasonable hardware while it needs shorter processing delay than SIC.

4.2 Pilot-Channel Aided Pipeline Interference Cancellation Scheme

Previous research has shown the characteristics of the SIC detector with binary (BPSK) and quadrature (QPSK) phase shift keying modulations [53], [54], and pipelined architecture was proposed to compensate large delay [35], [55]. In our proposed scheme, the pilot-channel signals from the received signal are cancelled before they enter next detection unit, while the respreaded estimated data are subtracted from the received signal to obtain more accurate channel parameters for further data detection. Except the coarse channel estimation used in RAKE bank for ordering at initial, all procedures are pipelined to cope with the problem of long processing delay of SIC.

4.2.1 The Proposed Scheme

We assume the n -th bit interval of the J -th user to be the bit and user of interest. For simplicity, the n -th bits of all user signals are supposed to overlap in some time interval as shown in Fig. 3-1 and all paths' delay are perfectly estimated. From (2-3), we can observe that the data

estimates are corrupted by interference including traffic-channel signal and pilot-channel signal of other users. In order to alleviate the interference with shorter delay, we can use the proposed method as shown in Fig. 4-1. In the beginning, the coarse channel estimation are performed with a bank of PiIC # ua block. The PiIC # ua block is shown in Fig. 4-2(a). Inputs to PiIC # ua is $r_{pi2,1}(t) = r(t)$ while the outputs are channel estimates $\alpha_{u,f}^{(n)} = \hat{\alpha}_{k,f}^{(n)}$, $u=k+1$ where $1 \leq f \leq F$, $1 \leq u \leq K$ and $0 \leq k < K$. The channel parameters of all users are estimated with correlators followed by a moving average filter as depicted in (3-1). $\mu_{k,l;J,p}^{(n)}(\tau) = 1$ occurs only when $k=J$ and $l=p$ and thus leads to the desired channel estimates. All the other terms of $\mu_{k,l;J,p}^{(n)}(\tau)$ are caused by MAI or self-interference due to multipath, while all terms of $\lambda_{k,l;J,p}^{(n)}(\tau)$ are caused by traffic-channel signal. These interferences result in worse estimates. At stage 1, the received signal goes through a bank of MRC RAKE receiver and the output $\hat{Y}_k^{(n)}$ of user k is shown in (2-3). We choose the user with the maximum $\hat{Y}_k^{(n)}$ as the desired user where $J=k$. Fig. 4-3(a) shows the block diagram of UdIC # ua block where u denotes the cancellation order. In UdIC #1a block, the inputs are user index J , $r_{dia,1}(t) = r(t)$, and $\tilde{\alpha}_{<1>,f}^{(n)} = \hat{\alpha}_{av;J,f}^{(n)}$ in (3-1) where $1 \leq f \leq F$, and the corresponding outputs are data decision $\tilde{b}_{<1>}[n] = \text{sgn}\{\tilde{Y}_J^{(n)}\}$ where $\tilde{Y}_J^{(n)}$ is obtained from (2-3), the respreaded data $\tilde{C}_{data;<1>}(t)$ and the remained received signal $r_{do1a,1}(t)$ and $r_{do2a,1}(t)$ where

$$r_{do1a,1}(t) = r(t) - \tilde{C}_{pilot;<1>}(t) - \tilde{C}_{data;<1>}(t) \quad (4-1)$$

$$r_{do2a,1}(t) = r(t) - \tilde{C}_{data;<1>}(t) \quad (4-2)$$

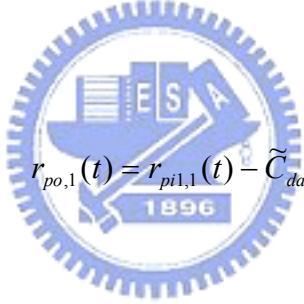
$$\tilde{C}_{pilot;<1>}(t) = \sum_{p=1}^F j\beta_p \tilde{\alpha}_{<1>,p}^{(t-\tau_{<1>,p}/T_b)} a_{pilot} \left[\left\lfloor \frac{t-\tau_{<1>,p}}{T_b} \right\rfloor \right] C_{<1>}(t-\tau_{<1>,p}) \quad (4-3)$$

$$\tilde{C}_{data;<1>}(t) = \sum_{p=1}^F \beta_d \tilde{\alpha}_{<1>,p}^{(t-\tau_{<1>,p}/T_b)} \tilde{b}_{<1>} \left[\left\lfloor \frac{t-\tau_{<1>,p}}{T_b} \right\rfloor \right] C_O(t-\tau_{<1>,p}) C_{<1>}(t-\tau_{<1>,p}) \quad (4-4)$$

where $\langle 1 \rangle$ means the first cancelled user.

Inputs to the PiC # un block as shown in Fig. 4-2(b) at stage 1 are user index J , $r_{pi1,1}(t) = r(t)$ and $r_{pi2,1}(t) = r_{do,1}(t)$, while the outputs are refined channel estimates $\alpha'_{<1>,f}{}^{(n)}$ where $1 \leq f \leq F$, respreaded pilot-channel signal $C'_{pilot;<1>}(t)$, and the remained signal $r_{po,1}(t)$

where



$$r_{po,1}(t) = r_{pi1,1}(t) - \tilde{C}_{data;<1>}(t)$$

and

$$C'_{pilot;<1>}(t) = \sum_{p=1}^F j\beta_p \alpha'_{<1>,p}^{(t-\tau_{<1>,p}/T_b)} a_{pilot} \left[\left\lfloor \frac{t-\tau_{<1>,p}}{T_b} \right\rfloor \right] C_{<1>}(t-\tau_{<1>,p})$$

where $\alpha'_{<1>,f}{}^{(n)}$ can be obtained from (3-1) by replacing $r(t)$ with $r_{pi2,1}(t)$.

Meanwhile, another output of the UdIC #1a block, i.e. $r_{do1a,1}(t)$, is sent to RAKE bank in stage 2 to find the user with maximum power. Signal without pilot-channel interference from PiC block of the I^{st} user, $r_{po,1}(t)$, is sent to UdIC #1b block, this time we use refined channel parameters instead of coarse channel parameters.

For the UdIC #1b block shown in Fig. 4-3(b), inputs are user index J , $r_{dib,1}(t) = r_{po,1}(t)$, and $\tilde{\alpha}_{<1>,f}{}^{(n)} = \alpha'_{J,f}{}^{(n)}$ where $1 \leq f \leq F$, and the corresponding outputs are data decision

$\tilde{b}_{<1>}[n] = \text{sgn}\{\tilde{Y}_J^{(n)}\}$ where $\tilde{Y}_J^{(n)}$ is obtained from (2-3) by replacing $r(t)$ with $r_{po,1}(t)$,

the respreaded data $\tilde{C}_{data;<1>}(t)$ and the remained received signal $r_{do2b,1}(t)$ as defined in

(4-2) with refined channel estimates. $r_{do2b,1}(t)$ is then sent to UdIC #2a block in the stage 2

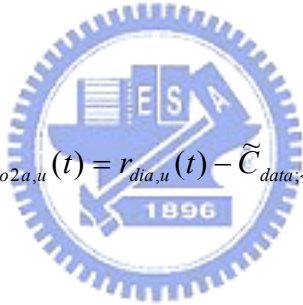
where $r_{dia,2}(t) = r_{do2b,1}(t)$ to perform the 2^{nd} user data decision and signal removing.

For the n -th bit interval signal at the u -th stage, relation among all the above signals can be

written as follows. From $u > 1$, for UdIC # ua block,

$$r_{dia,u}(t) = r_{do2b,u-1}(t)$$

$$r_{do1a,u}(t) = r_{dia,u}(t) - \tilde{C}_{pilot;<u>}(t) - \tilde{C}_{data;<u>}(t)$$



$$r_{do2a,u}(t) = r_{dia,u}(t) - \tilde{C}_{data;<u>}(t)$$

$$\tilde{C}_{pilot;<1>}(t) = \sum_{p=1}^F j\beta_p \tilde{\alpha}_{<u>,p}^{(t-\tau_{<u>,p}/T_b)} a_{pilot}[\lfloor (t-\tau_{<u>,p})/T_b \rfloor] C_{<u>}(t-\tau_{<u>,p})$$

$$\tilde{C}_{data;<u>}(t) = \sum_{p=1}^F \beta_d \tilde{\alpha}_{<u>,p}^{(t-\tau_{<u>,p}/T_b)} \tilde{b}_{<u>}[\lfloor (t-\tau_{<u>,p})/T_b \rfloor] C_o(t-\tau_{<u>,p}) C_{<u>}(t-\tau_{<u>,p})$$

where $\tilde{\alpha}_{<u>,f}^{(n)} = \hat{\alpha}_{av;J,f}^{(n)}$ obtained from (3-1) and $\tilde{b}_{<u>}[n] = \text{sgn}\{\hat{Y}_J^{(n)}\}$ where $\hat{Y}_J^{(n)}$ is

obtained from (2-3) by replacing $r(t)$ with $r_{do1a,u-1}(t)$. For PiIC # ub block

$$r_{pi1,u}(t) = r_{do2b,u-1}(t)$$

$$r_{po,u}(t) = r_{pi1,u}(t) - C'_{pilot;<u>}(t)$$

where

$$C'_{pilot;<u>}(t) = \sum_{p=1}^F j\beta_p \alpha'^{(\lfloor (t-\tau_{<u>,p})/T_b \rfloor)} a_{pilot}[\lfloor (t-\tau_{<u>,p})/T_b \rfloor] C_{<u>}(t-\tau_{<u>,p}).$$

And

$$r_{pi2,u}(t) = r_{do2a,u}(t)$$

where $\alpha'^{(n)}$ can be obtained from (3-1) by replacing $r(t)$ with $r_{pi2,u}(t)$. And for UdIC # ub block,

$$r_{do2b,u}(t) = r_{dib,u}(t) - \tilde{C}_{data;<u>}(t) \quad (4-9)$$

$$\tilde{C}_{data;<u>}(t) = \sum_{p=1}^F \beta_d \alpha'^{(\lfloor (t-\tau_{<u>,p})/T_b \rfloor)} \tilde{b}_{<u>}[\lfloor (t-\tau_{<u>,p})/T_b \rfloor] C_O(t-\tau_{<u>,p}) C_{<u>}(t-\tau_{<u>,p}) \quad (4-10)$$

where $\tilde{b}_{<u>}[n] = \text{sgn}\{\tilde{Y}_J^{(n)}\}$ where $\tilde{Y}_J^{(n)}$ is obtained from (2-3) by replacing $r(t)$ with $r_{dib,u}(t)$. The process repeats until all K user data are detected.

4.2.2 Computational Complexity Analysis

In Fig. 4-1, we can find that there are two more blocks per stage in the proposed scheme in comparison with SIC II in Chapter 3, i.e. PiIC # b unit and UdIC # b blocks. Although the hardware complexity increases, the throughput is K times the normal SIC and the latency only increases with the time spent for signal processing through PiIC unit and UdIC one

time. Table 4-1 lists the computational complexity analysis. In the following, it is shown that the extra blocks in our proposed scheme can help to achieve better performance than other interference cancellation schemes and RAKE receiver.

4.2.3 Simulation Results and Discussions

The simulation parameters are the same as those in Table 3-2 except that the $\beta_c=1$, $G=1$ bit and $PDR = 1$. We simulate four kinds of detectors with multipath fading channel Case 3 in Table 3-3 and total power of all paths are normalized to unity. A 4-finger rake receiver is used for path combination. The path delay is assumed to be perfectly known. Fig. 4-4 shows performance comparison among the proposed pipelined scheme, rake receiver, SIC without pilot signal remover, and PPIC [22] with coefficient 0.6 at the first stage under different users. At the same BER, the proposed method has larger user capacity. Besides, note that the proposed scheme performs better at SNR=10dB than SIC at SNR=15dB when there are more than about 10 users in the system. Thus, we can achieve the same BER at lower SNR by using the proposed scheme. Fig. 4-5 shows the performance of detectors under different SNRs. We can find that the proposed scheme performs slightly better than SIC at low SNR while it performs much better than any other scheme in the simulation when the SNR is high. The reason is that the noise term dominates the system performance at low SNR while the interferences we dealt with between different users and paths play a relatively important role at high SNR. Besides, channel parameters can be estimated precisely when data interferences are eliminated at high SNR. Therefore, the proposed scheme is recommend for interference cancellation at higher SNR as a result of hardware complexity.

4.3 Pilot-Channel Aided Adaptable Interference Cancellation Scheme

Not only the data-channel symbols but the pilot channel symbols are also interfered with other user signals, especially when the cross-correlation between each user's codes is high. In our proposed scheme, the pilot channel signals from the received signals are cancelled before they enter to next detection unit, while the respread traffic-channel signals are subtracted from the received signals to obtain more accurate channel parameters.

4.3.1 The Proposed Scheme

The structure of Pilot-Channel Aided Adaptable IC is shown in Fig. 4-9. The proposed scheme has four main blocks to make the system performance better. These blocks are channel estimation plus pilot signal regenerator (Block 1), SIC with two different ordering methods (Block 2), refined successive channel estimation (Block 3), and PPIC (Block 4). Each of the blocks can be chosen on or off depending on the system loading and environmental condition. Block1 in Fig. 4-9 are equivalent to Part I in either Fig. 3-8 or Fig. 3-9 while the block diagram of the pilot signal regenerator is shown in Fig. 3-5. The input signal to Block2 in Fig. 4-9 is $\hat{r}(t)$ in (3-6). As shown in Chapter 3, SIC with different power ordering methods have different computational complexity as well as error performance. In Block2, we can choose one of the methods based on system loading and/or performance requirement. The unit in Block2 in Fig. 4-9 is equivalent to an iteration of the Part II in Fig. 3-8 or Fig. 3-9. The cancellation process is serially repeated until the desired U -th iteration is performed. It depends if all K users are detected in SIC unit. The detail structure of Data Respread and RAKE bank in Part II in Fig. 3-8 or Fig. 3-9 is shown in Fig. 3-4 and Fig. 2-22, respectively. The output signal $\hat{r}_{SIC;u}(t)$ at u -th iteration is given in (3-13). When the first unit of Block2 is performed, the regenerated signal $\check{C}_{data;<1>}(t)$ dedined in (3-14) where $k=<1>$ is subtracted from the received signal and enters the unit 1 of Block3 to obtain

$$\bar{r}_1(t) = r(t) - \check{C}_{data;<1>}(t)$$

The advanced channel estimation for the chosen user is performed with $\bar{r}_1(t)$ in Block3 as shown in Fig. 4-10. Functions of units in Block3 is equivalent to that of PiIC #b in Fig. 4-2(b) Due to cancellation of the strongest signal in data channel, the interference term in (3-1) becomes smaller, and more accurate channel parameters can be expected. The output signal $C''_{pilot;<1>}(t)$ of unit 1 in Block3 is the regenerated pilot signal with new channel parameters and can be obtained from (3-7) where $\hat{\alpha}_{av;J,f}^{(n)}$ is replaced by $\alpha_{J,f}^{(n)}$ as shown in Fig. 4-10. Then $C''_{pilot;<1>}(t)$ is subtracted from Block3 input signal $\bar{r}_1(t)$.

After the operation of unit 2 of Block2 is completed, the output also needs to be removed, i.e. the signal entering unit 2 of Block3 is

$$\bar{r}_2(t) = \bar{r}_1(t) - \check{C}_{data;<2>}(t) - C''_{pilot;<1>}(t).$$

The process is repeated until the desired U -th iteration is performed. From $(U+1)$ -th to K -th stage, RAKE bank with input_enable signal is used in Block2 as shown in Fig. 4-10. In this way, redundant computation can be saved and processing dela can be shorter. This is equivalent to performing conventional detection to the remaining users, but the detector input signal becomes less interfered as compared with the input signal in (3-6). At the input of the $(U+1)$ -th to the K -th stage in Block 3, the signal becomes

$$\bar{r}_{U+1}(t) = \bar{r}_U(t) - \sum_{k=<U+1>}^{<K>} \check{C}_{data;k}(t) - C''_{pilot;<U>}(t).$$

Finally, the new channel estimates $\alpha_{k,f}^{(n)}$, $1 \leq f \leq F$, and tentative decision $\hat{b}_{SIC;k}[n]$ of all users are fed into the partial PIC (PPIC). The PIC receiver is often called multistage cancellation [78], and it processes signals of K users at the same time. The multistage PIC

scheme is shown in Fig. 4-6. The PIC has the advantage of having shorter latency than SIC at the expense of approximately K times more hardware required. Since the estimation of MAI in PIC may not be reliable in the early stages, the well-known partial PIC [22] uses partial coefficients (often estimated from experience) partially cancels the estimated MAI to alleviate errors when the estimation of interference is poor in early stages. Fig. 4-7 shows the block diagram of one stage partial PIC for uplink dedicated channel. The tentative decision made from correlator outputs of all users are respread (shown in Fig. 3-4) and removed from the received signal except the desired user data. The remaining signals are passed through the correlator again to acquire a new output with less MAI. After that, the new decision is made with the combination of the old output times $1-p_s$ and new outputs times p_s where s is the stage index. The iterative manner of PPIC is based on the likelihood concept. However, the update of the likelihood information becomes unreliable when the system is in heavy load. A linear version of this PPIC is presented in [20]. In [90], the authors proposed an adaptive multistage PIC, which adaptively decides the cancellation weight of each user by minimizing the mean-square error between the received signal and its estimates according to the least-mean-square (LMS) algorithm. The adaptive multistage PIC is suitable for the system with short scrambling code, and it can achieve better performance than the PPIC. But it has computational complexity $O(KSF)$ per stage where K is the user number and SF is the spreading gain.

In our proposed scheme, the RAKE bank at initial stage in Fig. 4-6 are omitted, and a better initial decision is used, i.e. $\hat{b}_{PIC,k}^0[n] = \hat{b}_{SIC,k}^0[n]$. The other input of PIC is the signal $\tilde{r}_0(t)$, which removes all pilot signals respreaded with new channel parameters from the received signal.

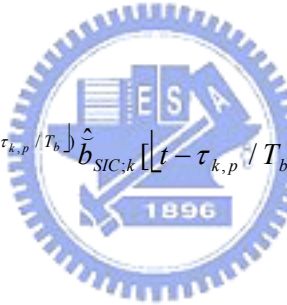
$$r_{U+1}''(t) = r(t) - \sum_{k=1}^K C_{pilot;k}''(t)$$

(4-11)

Compared $r_{U+1}''(t)$ with $\hat{r}(t)$ in (3-6), because $C_{pilot;k}''(t)$ is respread by new channel estimates with fewer interference from traffic-channel, we can expect $C_{pilot;k}''(t)$ a better approximation to real $C_{pilot;k}(t)$ than $\hat{C}_{pilot;k}(t)$ in (3-7). For user J with F paths combining at the output of PPIC's first stage, the tentative decision can be written as

$$\begin{aligned} \hat{b}_{PIC,J}^1[n] = & \text{sgn}\{(1-p_1)\hat{b}_{SIC;k}[n] \\ & + p_1 \sum_{f=1}^F \text{Re} \left\{ \frac{1}{2\beta_d T_b} \int_{nT_b+\tau_{J,f}}^{(n+1)T_b+\tau_{J,f}} (\alpha_{J,f}''(n))^* (r_{U+1}''(t) - \sum_{k=1, k \neq J}^K C_{0\data,k}''(t)) C_O(t-\tau_{J,f}) C_J^*(t-\tau_{J,f}) dt \right\} \} \end{aligned} \quad (4-12)$$

where

$$C_{0\data,k}''(t) = \sum_{p=1}^F \beta_d \alpha_{k,p}'' \left(\frac{t-\tau_{k,p}}{T_b} \right) \hat{b}_{SIC;k} \left[\left\lfloor \frac{t-\tau_{k,p}}{T_b} \right\rfloor \right] C_O(t-\tau_{k,p}) C_k(t-\tau_{k,p}) \quad (4-13)$$


and p_l is the partial cancellation coefficient. At the second stage of PPIC, it performs the same calculation as (4-12) and (4-13) except that $\hat{b}_{PIC,J}^1[n]$ is replaced by $\hat{b}_{PIC,J}^2[n]$, $\hat{b}_{SIC;k}[n]$ is replaced by $\hat{b}_{PIC,J}^1[n]$ and $C_{0\data,k}''(t)$ is replaced by $C_{1\data,k}''(t)$. The process can keep on until to the stage (often 2~4 stages) we want to stop.

Also there are K sets of units in Fig. 4-9, the hardware of all blocks used in the adaptable scheme can be ranging from having only one set for processing one user a time to having K sets for processing all users at the same time with different bit index n .

4.3.2 Simulation Results and Discussion

In this section, we compare the performance of the proposed detector with that of PIC and

SIC mentioned above. The data channel and the pilot channel are assumed to have equal transmitting power. We simulate these detectors under multipath fading channel Case 3 in Table 3-3 and total power of all paths are normalized to unity. A 4-finger RAKE receiver is used for path combination. We assume path delay is perfectly known. The simulation parameters are similar to the parameters in Table 3-2 for performance evaluation except that $SF=32$, $\beta_c=1$, $PDR=1$, $G=1$ and $SNR=13\text{dB}$. We adopt PPIC in [4] with partial coefficient 0.6 at the first stage in Block 4.

Fig. 4-11 shows the average BER versus iteration number of Block2 marked in Fig. 4-9 with different combination of other blocks. The capital letter B in the figure means Block. There are 20 users in the system. When all blocks are used, we can see that a single-stage PIC of Block4 can outperform the traditional PPIC. The property means that although Block2 and Block3 are the additional structures compared with PPIC, we can save the required stage in the succeeding Block4 working with Block2 and Block3. The figure also shows that B1+B2+B3+B4 converges fast, 2-stage PIC almost has equal BER as 4-stage PIC in Block4.

Fig. 4-12 and Fig. 4-13 show the average BER versus user numbers. The difference between these two simulations is that Fig. 4-12 uses one stage of PPIC in Block4 and half of user number as iteration number in Block2 and Block3 while Fig. 4-13 finds the minimum BER when the stage in Block4 is limited up to three. Comparing Fig. 4-12 with Fig. 4-13, we can see that there is little difference in these two figures. Note that in Fig. 4-12 several schemes have better performance than three-stage pure PPIC and pure SIC while these schemes only take about half of the processing time of SIC and about $2/3$ computational complexity of PPIC. Fig. 4-12 and Fig. 4-13 also show that with the same BER, more users can be served in the system when we use the proposed adaptable scheme. For example, the user number in system can be up to 24 when the BER is at $2*10^{-2}$. It also means energy will be saved if proper blocks are chosen to achieve the desired BER.

Fig. 4-14 shows the best performance (lowest BER) each scheme can achieve versus signal-to-noise ratio, the stage in Block4 is limited to not more than three. With the same BER, the required SNR becomes smaller. This means that the adaptable scheme can perform well even the environment is noisier. The figure also shows that the proposed schemes outperform pure PPIC and SIC under different SNR.

4.4 Summary

In this chapter, we propose two advanced IC techniques for the pilot-channel aided systems. At first, a pilot channel aided pipelined interference cancellation scheme is introduced to cope with interferences due to multiuser, multipath as well as long delay due to inherent property of SIC. It is shown to have better performance when compared with RAKE receiver, SIC and PPIC under the same SNR and user capacity while it maintains the same throughput and slightly longer latency than SIC owing to the pipelined format.

In the second part, we proposed an adaptable interference cancellation scheme for multiuser detection and channel estimation. Due to its flexibility, the scheme can be used in a changing environment with corresponding computational complexity. Simulation results show that it outperforms the traditional SIC and PPIC with reasonable hardware, and the processing delay can be shorter than SIC.

Table 4-1 Implementation issues with the proposed pipelined SIC

Reordering Frequency	Throughput (per unit)	Latency (units)	Hardware Required for Minimum Delay	Computational Complexity $C(\cdot)$
$K/(GT_b)$	1/3	$2+3K+2$	As shown in Fig. 4-1	$K*C(CE)+K*C(FM)+K(K-1)/2*C(RAKE)+K*C(PiC)+2K*C(UdIC)$

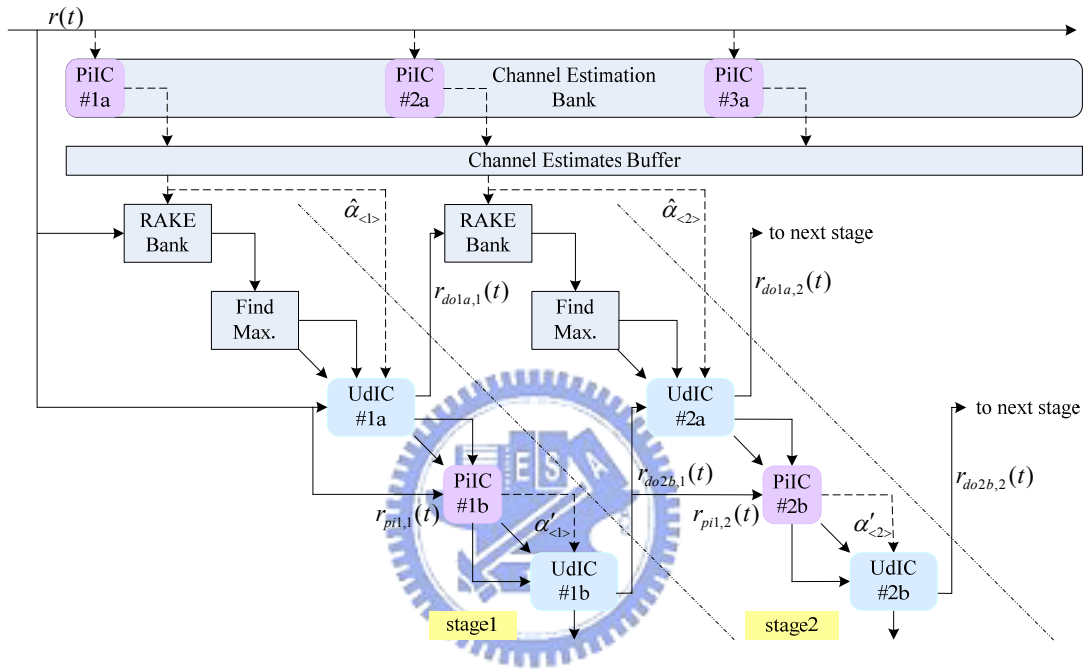


Fig. 4-1 The proposed pipelined scheme for interference cancellation scheme

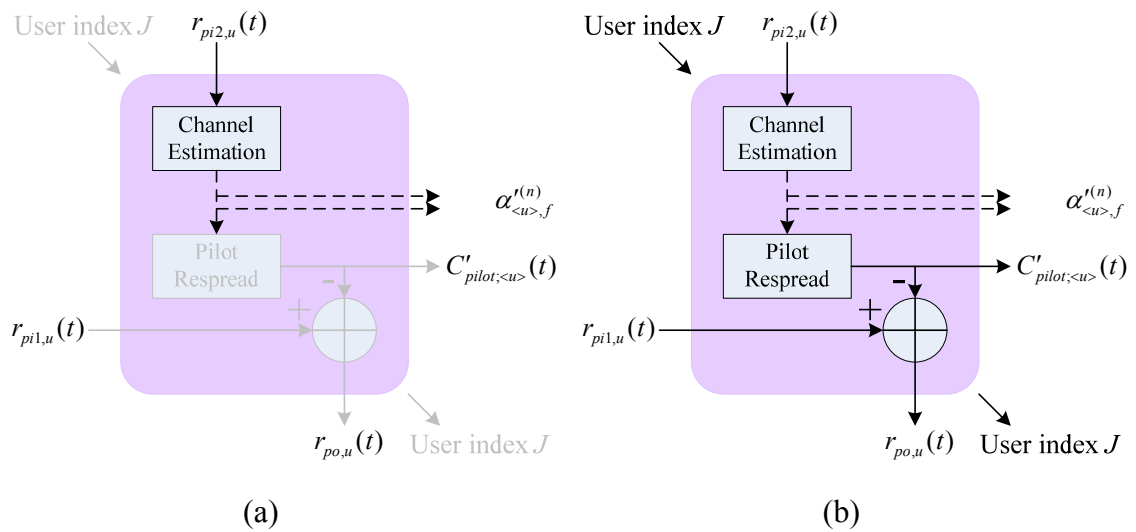
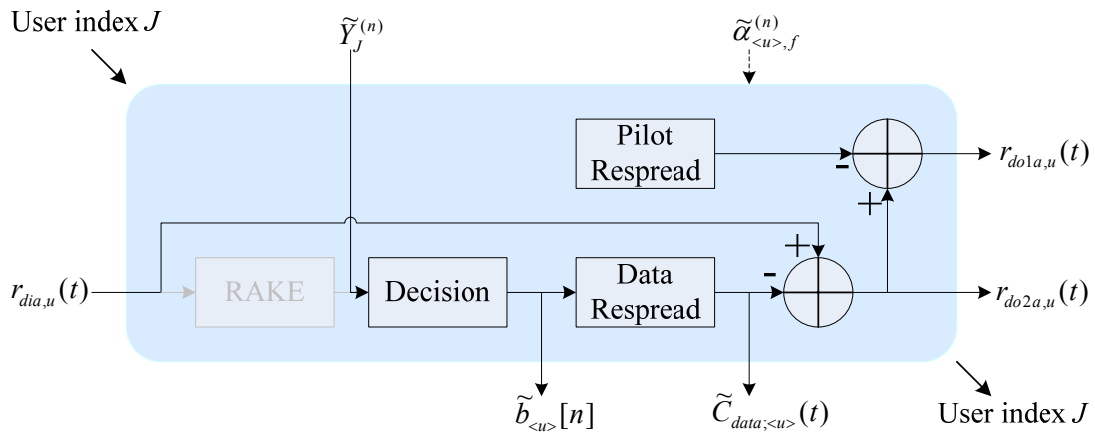
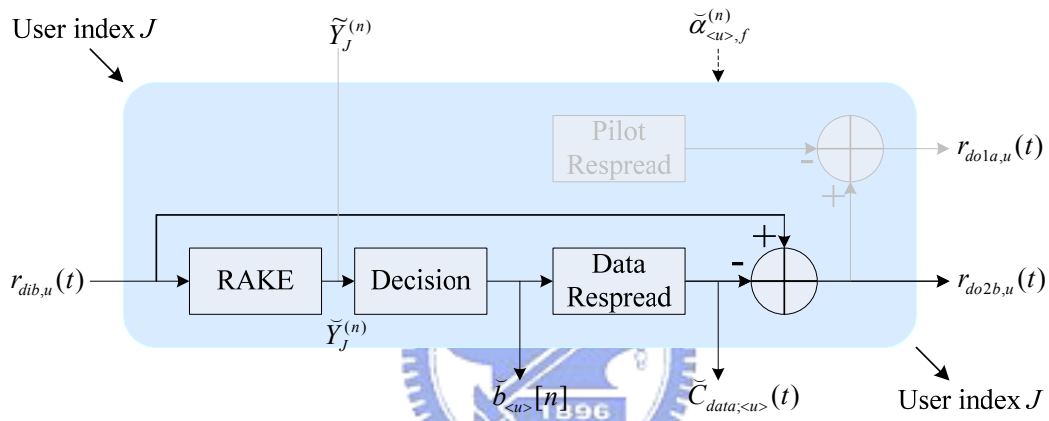


Fig. 4-2 PiC (a) #ua block and (b) #ub block in Fig. 4-1, $1 \leq u \leq K$



(a)



(b)

Fig. 4-3 UdIC (a) $\#ua$ block and (b) $\#ub$ block in Fig. 4-1, $1 \leq u \leq K$

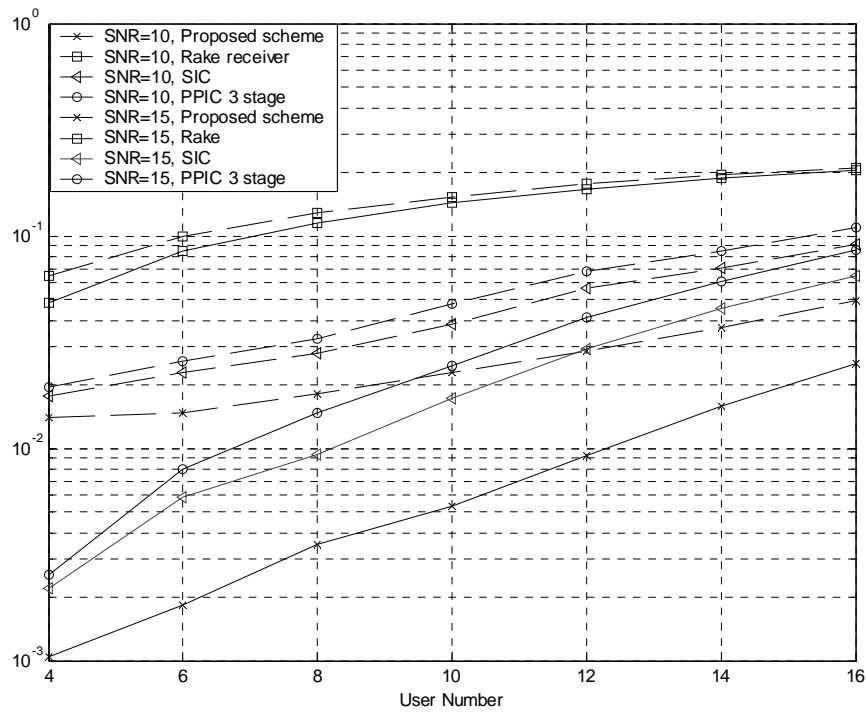


Fig. 4-4 Average BER versus user number with different schemes

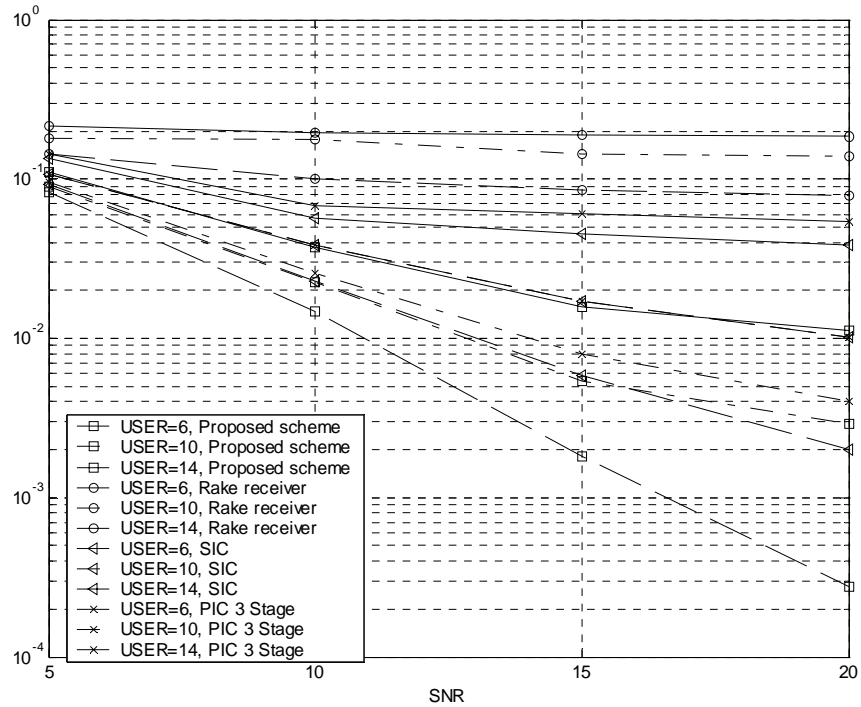


Fig. 4-5 Average BER versus SNR with different schemes and user numbers

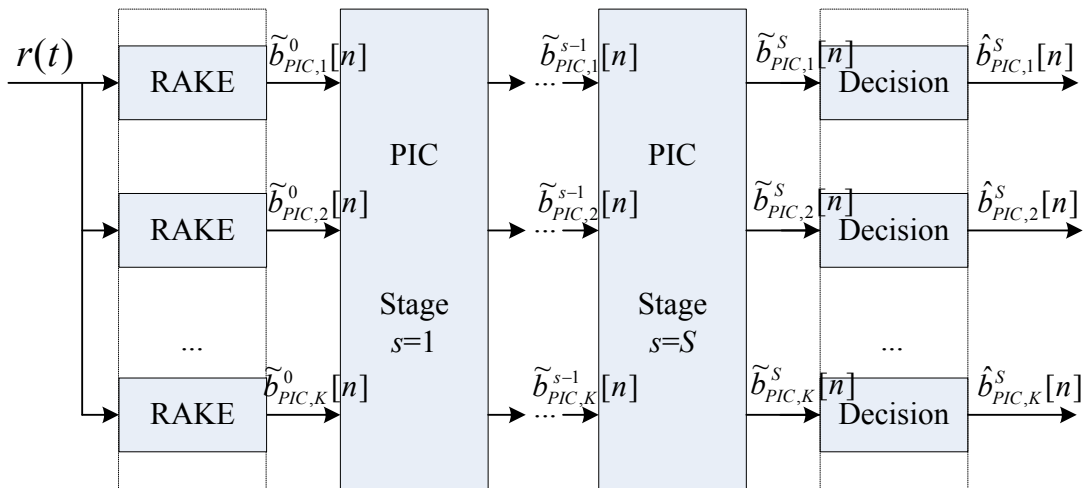


Fig. 4-6 Multistage PIC scheme

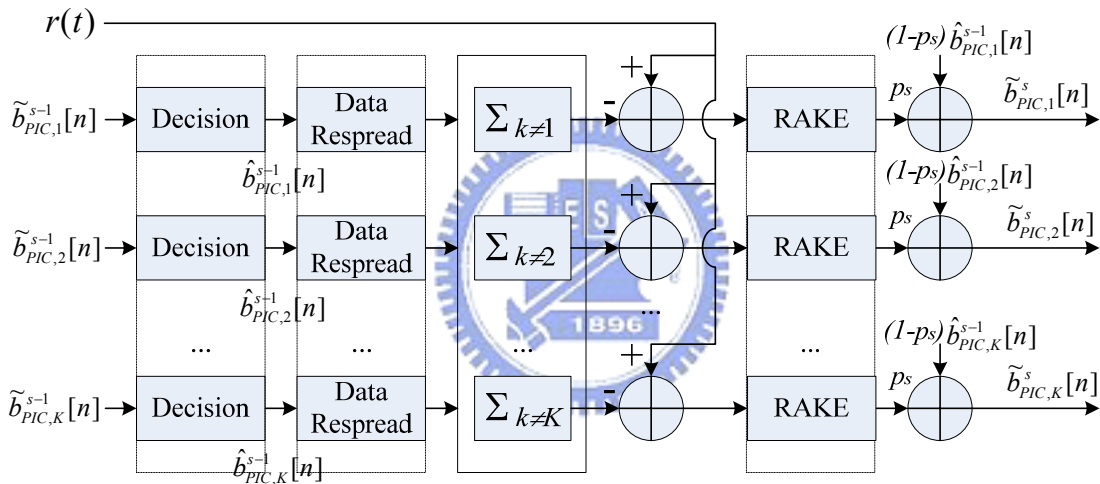


Fig. 4-7 The s -th stage of PPIC

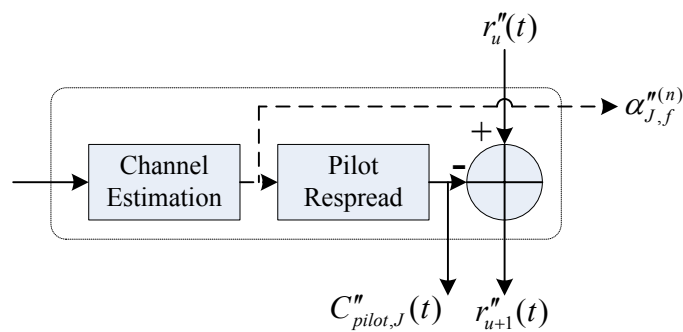


Fig. 4- 8 Detail structure of unit in Block3 in Fig. 4-9

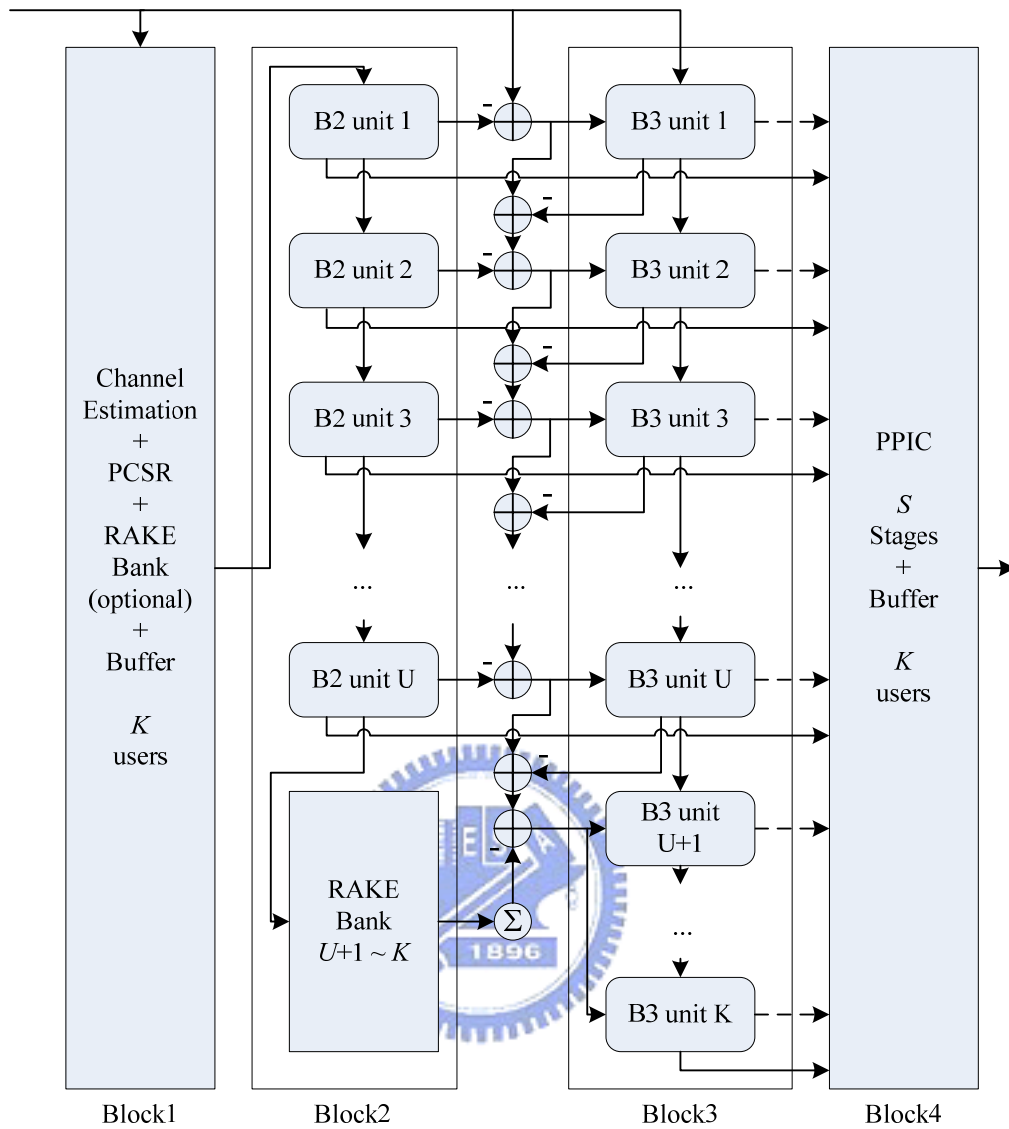


Fig. 4-9 The proposed adaptable IC scheme

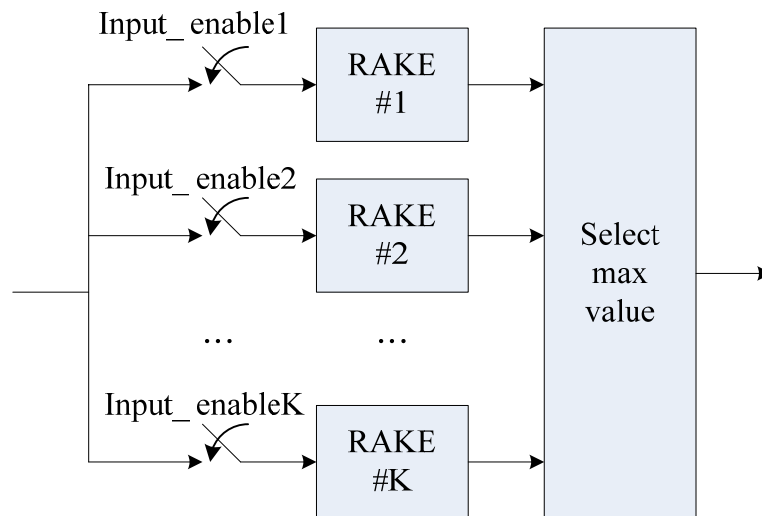


Fig. 4-10 Structure of the RAKE bank with input enables

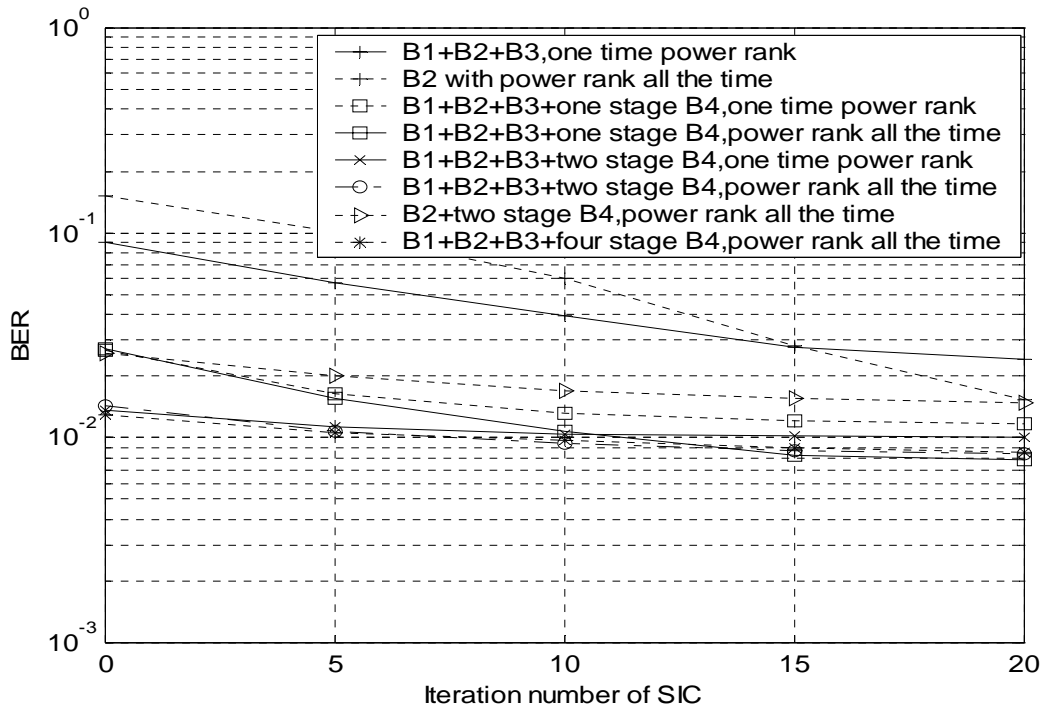


Fig. 4-11 Average BER versus iteration of SIC in Block2 in Fig. 4-9, 20 users, 10dB

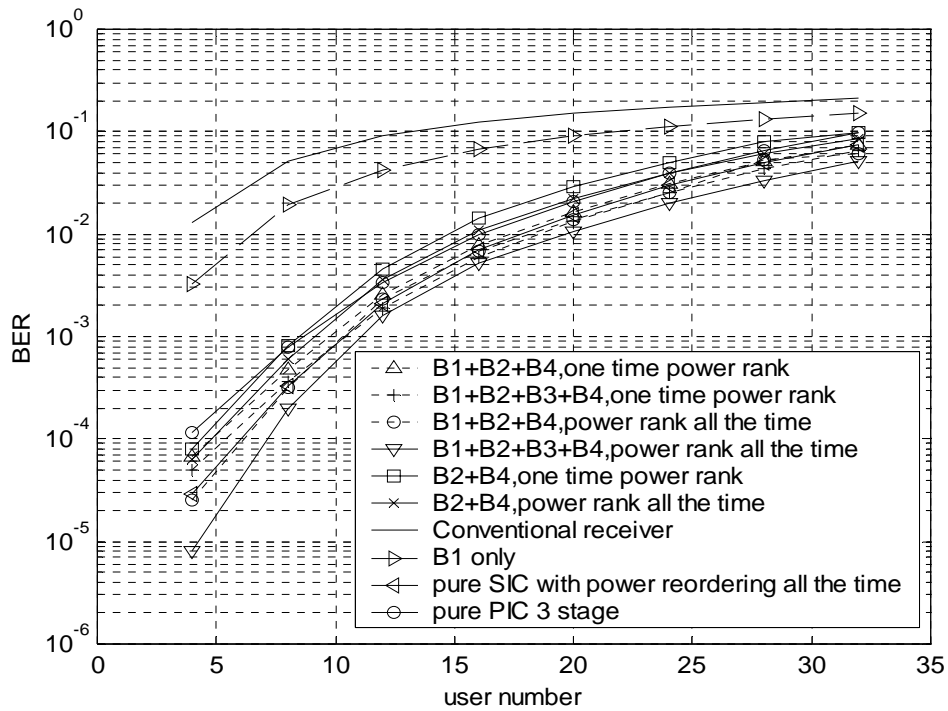


Fig. 4-12 Average BER versus user number, iteration in Block2 equals to user number divide by 2, stage in Block4 is limited to 1

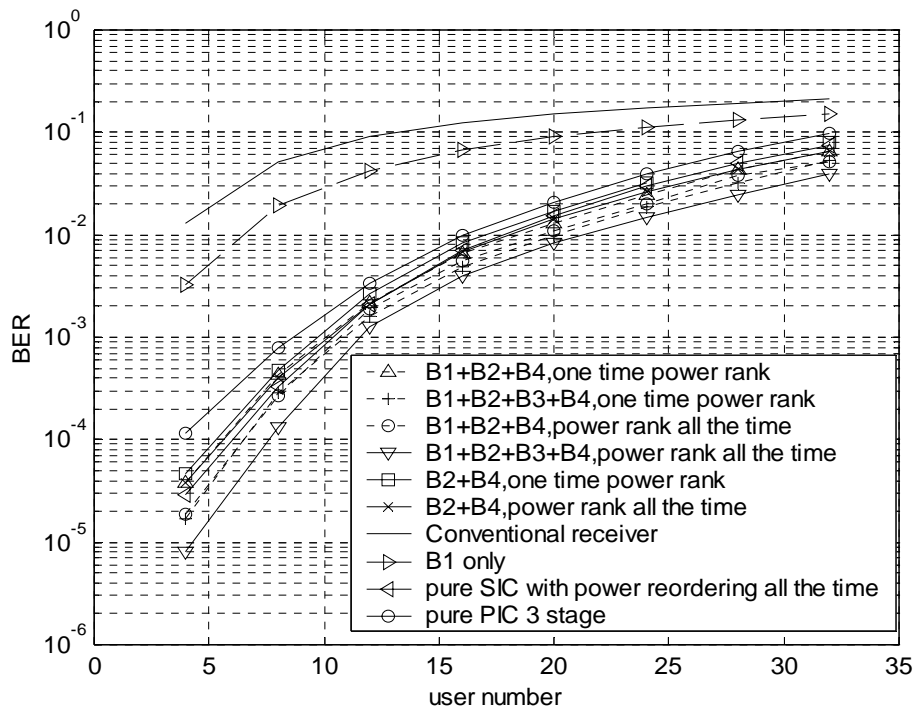


Fig. 4-13 Minimum average BER versus user number, PIC stage in Block4 can be up to 3, 10dB

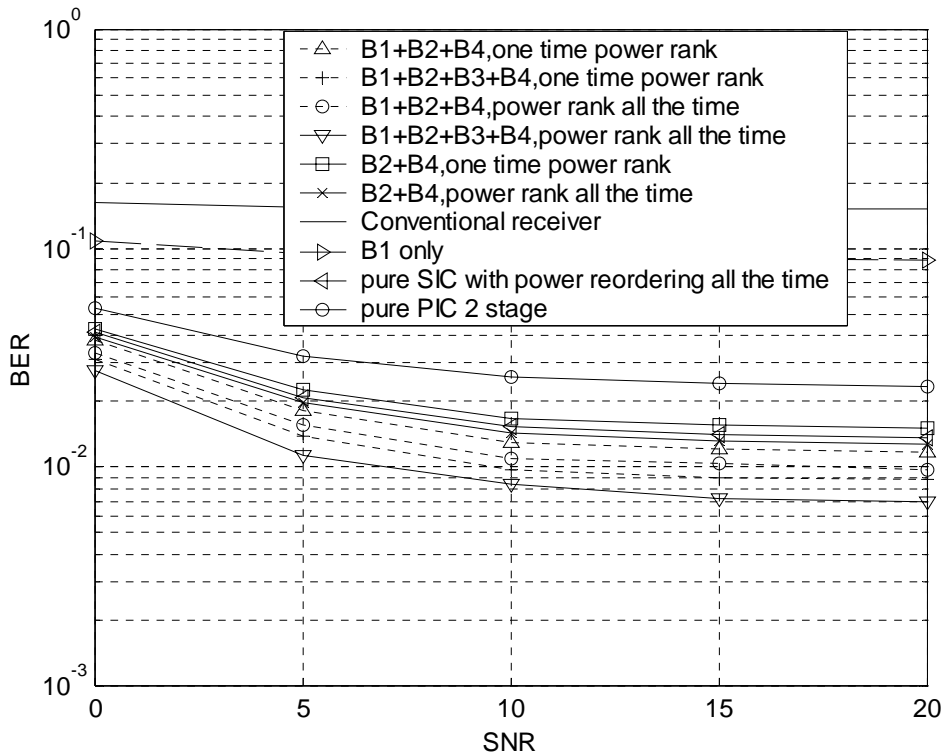


Fig. 4-14 Average BER versus different SNR, 20 users

Chapter 5

Pilot-Channel Aided Iterative Interference Cancellation in Turbo-Coded Systems

5.1 Overview

Both channel decoding and MUD are important techniques in CDMA systems. In wireless communications, channel coding protects data passing through fading channel by adding redundant bits in the transmitted message. With MUD at receiver end, error control coding, such as convolutional codes and Turbo codes, can be used to cope with residual interferences from all sources including AWGN in CDMA systems. In Chapter 3, we present pilot-channel aided SIC for asynchronous fading environment with varying performance according to the ordering method. In this chapter, we consider MUD in WCDMA systems with Turbo coding.

Turbo codes, first introduced by Berrou, Glavieux, and Thitimajshima in 1993 [11], are a class of error correcting codes generated from the parallel concatenation of two or more recursive systematic convolutional (RSC) codes to different interleaved versions of the same information sequence. Turbo codes are suitable for data communications as they exhibit a very good error performance from low to high SNR with large decoding delay. The performance of Turbo codes can be near Shannon limit capacity by performing iterative maximum a posteriori (MAP) probability algorithm [13], i.e. iteratively passing probabilistic estimates between two decoders with long codeword. It is known that most improvements in SNR are achieved in the first few iterations. Detection of early

convergence or non-convergence of iterative decoder is essential to save power consumption and processing delay. Recently, techniques known as early-stopping criteria are introduced to examine if the iteratively decoding process could be terminated when the CB is correctly decoded, [24], [29], [30], [32], [37], [44], [47], [62], [83], [85], [86], [93], [94].

A class of receivers known as iterative/turbo MUD combines MUD and channel decoding with excellent error performance via an iterative process [3], [4], [14], [28], [50] [51], [64], [84]., [91] The channel encoder of Turbo MUD is not necessary Turbo codes. The term “turbo” in Turbo MUD describes the iterative information transition between MUD and channel decoder. Based on the realization that multiuser CDMA signals combined with forward-error control (FEC) coding can be viewed as the serial concatenation of two coding systems, the iterative MUD takes two operations: (1) a posteriori probability (APP) estimation of the coded symbols and (2) parallel single-user FEC soft decoding. Soft informations are passed back and forth between these two soft-input soft-output (SISO) decoders with interleaving. Although it has been shown that near-single-user performance can be achieved, many iterative MUD receivers need complex implementation with significant computational complexity. The generalized iterative MUD tends to removed or factor out all MAIs from other users and/or other noise based on different criterion. However, non-perfect parameters estimation obscures the efficiency of sophisticated operations for low error rate, especially at low SNR. Cancellation of the estimated MAI at low SNR can bring large performance degradation. Efforts to find a practical iterative MUD with performance improvement from low to high SNR for concurrent communication systems are needed.

The SIC II in Chapter 3 explores variation of the received data grouping bits by grouping bits, and removes MAI only from users with more reliable estimated data than

that of the desired user. These properties are especially suitable for signal detection at low SINR. In 5.2, the SIC II front-end with $PDR=1.0$ and $G=1$ followed by MAP algorithm for turbo decoding is employed. (If the required SNR is higher, such as punctured codes are used, the optimal PDR and G increase. In this case, SIC III is chosen.) Variance estimation used for MAP algorithm in turbo decoding is acquired from pilot-channel signal. This scheme is shown to be superior to the one with PPIC at front-end in BER and computational complexity. In addition, with the ordering information obtained from SIC front-end, we propose a new stopping criterion which requires low complexity and data buffer.

In 5.3, a novel iterative IC with the turbo-coded SIC presented in 5.2 as part of the first outer iteration is proposed. With the information obtained from stopping criterion, the correct CBs are hard-decisioned, re-encoded, respread and then removed from the signal to the next outer iteration. In this way, huge amount of redundant computational complexity and processing delay can be saved when compared to the generalized Turbo-coded iterative MUD. In addition, channel estimates from pilot-channel signal are refined from the second outer iteration with estimated traffic-channel signal removal. With the analyses in complexity and computer simulations in BER, this scheme is shown to be superior and practical in current communication systems.

5.2 Stopping Criterion for Turbo Decoding with SIC at Front End

The performance of Turbo codes can be near Shannon-limit capacity by iteratively passing probabilistic estimates between two decoders with long codeword, i.e. iterative maximum a posteriori (MAP) probability algorithm [13]. Recently, for practical use, techniques called early-stopping criterion are introduced to see if the iteratively decoding process could be terminated to avoid unnecessary iterations and save computational power

as well as processing delay [37], [44], [83], [93]. In this section, the SIC II presented in Chapter 3 is used as the front-end of a receiver in Turbo coded systems. This scheme is shown to outperform the one with PPIC at front end in multipath fading channels. In addition, with the characteristics of logarithm likelihood ratios (LLR) and ordering information from SIC, we propose a high efficient stopping criterion with low complexity.

5.2.1 Turbo Decoding

An important feature of Turbo codes is the iterative decoder with SISO algorithms, such as MAP algorithm [9], log-MAP algorithm [60], Max-Log-MAP algorithm [25], [43], and soft-output Viterbi algorithm (SOVA) [12], [30]. The MAP algorithm, also known as BCJR algorithm, was first presented by Bahl, Colcke, Jelinik and Raviv in 1974 for both convolutional codes and block codes [9]. The algorithm attempts to minimize the BER by estimating the a posteriori probabilities (APP) of the individual bits in the codeword, and it examines every possible path through the convolutional decoder trellis. For the user with index k , we have the following definitions [61]:

S is the set of all 2^m constituent encoder states where m is the encoder memory

$$\mathbf{u}_k^s = (u_k^s[1], u_k^s[2], \dots, u_k^s[M_K + m])$$

$$\mathbf{u}_k^{px} = (u_k^{px}[1], u_k^{px}[2], \dots, u_k^{px}[M_K + m])$$

where x , which can be 1 or 2, denotes one of the constituent encoder E1 or E2.

$$\mathbf{y}_k^{(n)} = (y_k^{s(n)}, y_k^{p(n)})$$

is the noisy version of $(x_k^{s(n)}, x_k^{p(n)})$,

$$\mathbf{y}_k^{(x,y)} = (y_k^{(x)}, y_k^{(x+1)}, \dots, y_k^{(y)}),$$

$$\mathbf{y}_k = \mathbf{y}_k^{(1, M_k)} = (y_k^{(1)}, y_k^{(2)}, \dots, y_k^{(M_k)})$$

is the noisy received codeword. Without loss of generality, the index k is temporarily omitted for simplicity. We would like to make decision of $u[n]$ as

$$\hat{u}[n] = (\text{sign}[L(u[n])] + 1) / 2 \quad (5-1)$$

with the log APP

$$L(u[n]) \stackrel{\Delta}{=} \log \left(\frac{P(u[n] = 1 | y)}{P(u[n] = 0 | y)} \right) = \log \left(\frac{\sum_{S^1} p(s', s, y) / p(y)}{\sum_{S^0} p(s', s, y) / p(y)} \right) \quad (5-2)$$

where S^0 denotes all states s from $u[n]=0$, and S^1 denotes all states s from $u[n]=1$.

$$p(s', s, y) \stackrel{\Delta}{=} p(s_n = s', s_n = s, y) \quad (5-3)$$

$$\alpha_n(s) \stackrel{\Delta}{=} p(s_n = s, y^{(1, n)})$$

$$\beta_n(s') \stackrel{\Delta}{=} p(y^{(n+1, M)} | s_n = s')$$

$$\gamma_n(s', s) \stackrel{\Delta}{=} p(s_n = s, y^{(n)} | s_{n-1} = s')$$

■ Iterative MAP algorithm

The MAP algorithm provides not only the estimated information bits, but also the probability for each bit. This is essential for the iterative decoding of Turbo codes. With the encoder shown in Fig. 2-4, the corresponding iterative MAP decoder with two

interconnected elementary decoders is shown in Fig. 5-1. The decoder has three inputs. For SISO decoder D1, inputs are the systematically encoded channel output bit $y^{s^{(n)}}$, the parity bit $y^{p1^{(n)}}$ and the extrinsic information $L_{2ex}^{i-1}(u[n])$. For SISO decoder D2, inputs are the interleaved version of $y^{s^{(n)}}$, $y^{p2^{(n)}}$ and $L_{1ex}^i(u[n])$ from D1. For decoder D1 at the i -th inner iteration. $p(s', s, y)$ in (5-3) is defined as

$$p(s', s, y) = \alpha_{n-1}(s') \cdot \gamma_n(s', s) \cdot \beta_n(s)$$

with

$$\alpha_n(s) = \sum_{s' \in S} \alpha_{n-1}(s') \gamma_n(s', s),$$

$$\beta_n(s') = \sum_{s \in S} \beta_{n+1}(s) \gamma_{n+1}(s', s),$$

and the initial conditions

$$\alpha_0(0) = 1 \text{ and } \alpha_0(s \neq 0) = 0,$$

$$\beta_M(0) = 1 \text{ and } \beta_M(s \neq 0) = 0.$$

To avoid numerically unstable results, we define

$$\tilde{\alpha}_n(s) = \alpha_n(s) / p(\mathbf{y}^{(1,n)}) = \frac{\sum_{s'} \tilde{\alpha}_{n-1}(s') \cdot \gamma_n(s', s)}{\sum_s \sum_{s'} \tilde{\alpha}_{n-1}(s') \cdot \gamma_n(s', s)},$$

$$\tilde{\beta}_{n-1}(s) = \beta_{n-1}(s) / p(\mathbf{y}^{(n,M)} | \mathbf{y}^{(1,n-1)}) = \frac{\sum_{s'} \tilde{\beta}_n(s') \cdot \gamma_n(s', s)}{\sum_s \sum_{s'} \tilde{\alpha}_{n-1}(s') \cdot \gamma_n(s', s)}$$

and the Log-APP in (5-2) becomes

$$L(u[n]) = \log \left(\frac{\sum_{s^1} \tilde{\alpha}_{n-1}(s') \cdot \gamma_n(s', s) \cdot \tilde{\beta}_n(s)}{\sum_{s^0} \tilde{\alpha}_{n-1}(s') \cdot \gamma_n(s', s) \cdot \tilde{\beta}_n(s)} \right)$$

For decoder D1, the transition probability $\gamma_{1n}(s', s)$ can be written as

$$\begin{aligned} \gamma_{1n}(s', s) &= P(s|s')p(y^{(n)} | s', s) \\ &= P(u[n])p(y^{(n)} | u[n]) \\ &= \exp \left[\frac{1}{2} u[n] \left(L_{1in}^i(u[n]) + L_c y^{s^{(n)}} \right) \right] \cdot \gamma_n^e(s', s) \end{aligned}$$

(5-4)

where the event $u[n]$ corresponds to the event of state transition $s' \rightarrow s$. $L_c = 4E_b / N_0$ with noise variance $N_0/2$. The intrinsic information is defined as

$$L_{1in}^i(u[n]) = L_{2ex}^{i-1}(u[n]) = \log \left(\frac{P(\hat{u}[n] = 1)}{P(\hat{u}[n] = 0)} \right),$$

and $\gamma_{1n}^e(s', s)$ is defined as

$$\gamma_{1n}^e(s', s) = \exp \left[\frac{1}{2} L_c y^{p^1(n)} u^{p^1}[n] \right]$$

where $u^{p^1}[n]$ is the encoder output with state transition $s' \rightarrow s$. Thus we can have

$$L_1^i(u[n]) = L_c y^{s^{(n)}} + L_{2ex}^{i-1}(u[n]) + \log \left(\frac{\sum_{s^1} \tilde{\alpha}_{n-1}(s') \cdot \gamma_{1n}^e(s', s) \cdot \tilde{\beta}_n(s)}{\sum_{s^0} \tilde{\alpha}_{n-1}(s') \cdot \gamma_{1n}^e(s', s) \cdot \tilde{\beta}_n(s)} \right)$$

(5-5)

The first term in (5-5) is called the channel value, the second term is the a priori information provided by decoder D2 which is equal to 0 at the first inner iteration, and the third term is the extrinsic information $L_{1ex}^i(u[n])$ that can be passed on to the subsequent

decoder D2. For D2, the LLR of APP in (5-2) can be written as

$$L_2^i(u[n]) = L_c y^{s^{(n)}} + L_{1ex}^i(u[n]) + \log \left(\frac{\sum_{s^1} \alpha_{n-1}(s') \cdot \gamma_{2n}^e(s', s) \cdot \beta_n(s)}{\sum_{s^0} \alpha_{n-1}(s') \cdot \gamma_{2n}^e(s', s) \cdot \beta_n(s)} \right) \quad (5-6)$$

where

$$\gamma_{2n}^e(s', s) = \exp \left[\frac{1}{2} L_c y^{p2(n)} \hat{u}^{p2}[n] \right].$$

Hence, final decision of $u[n]$ in (5-1) at the D2 output of the i -th inner iteration thus becomes

$$\hat{u}[n] = (\text{sign}[L_2^i(u[n])] + 1) / 2 \quad (5-7)$$

By iterative decoding, each decoder passes the updated extrinsic information to the other decoder, and we can expect that the BER of the decoded bits tends to become lower and lower. Further improvement in BER decreases as the number of iterations increases. To reduce the decoding computational complexity, data memory and power consumption, dynamically control of the iteration number is inevitable.

■ Literature overview of stopping criteria

Many criteria have been proposed in recent years for early stopping in turbo decoding. The variables generally used in literature for decision making are the extrinsic/intrinsic information and the LLR of APPs as shown in Fig. 5-1. For the i -th inner iteration, the LLR of APP in decoder D1 and decoder D2 defined in (5-5) and (5-6) are re-written as follows.

$$L_1^i(u[n]) = Y_s(u[n]) + L_{1in}^i(u[n]) + L_{1ex}^i(u[n])$$

and

$$L_2^i(u[n]) = Y_s(u[n]) + L_{2in}^i(u[n]) + L_{2ex}^i(u[n])$$

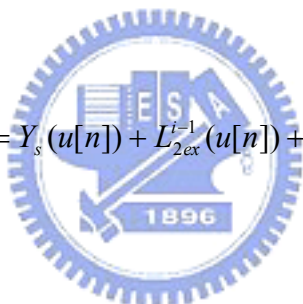
where $Y_s(u[n]) = L_c y^{s(n)}$. The relationship between the intrinsic and extrinsic information of decoder D1 and decoder D2 are as follows.

$$L_{1in}^i(u[n]) = L_{2ex}^{i-1}(u[n])$$

and

$$L_{2in}^i(u[n]) = L_{1ex}^i(u[n]).$$

We then have

$$L_1^i(u[n]) = Y_s(u[n]) + L_{2ex}^{i-1}(u[n]) + L_{1ex}^i(u[n])$$

(5-8)

and

$$L_2^i(u[n]) = Y_s(u[n]) + L_{2ex}^i(u[n]) + L_{1ex}^i(u[n])$$
(5-9)

The stopping criteria mentioned in literature are briefly described as follows.

Cross Entropy (CE) Criterion. Hagenauer et al. [30] used a threshold value on the Cross entropy between the output distributions of the two SISO decoders. For a Turbo decoder, it is shown that the CE of iteration i can be approximated by,

$$T(i) \approx \sum_{n=1}^{M_k} \frac{L_{2ex}^i(u[n]) - L_{2ex}^{i-1}(u[n])}{e^{|L_1^i(u[n])|}}$$

where M_k is the block size of user k . The decoding process is stopped after iteration i for $i > 1$,

$$T(i)/T(1) < \theta$$

where $T(I)$ is the approximated CE after the first iteration.

Sign-Change Ratio (SCR) Criterion. Based on the concept of CE, Shao et al. [62] presented two simple and effective criteria, known as SCR and hard-decision aided (HDA), respectively. SCR evaluates the number of sign changes in the extrinsic information between successive iterations, and the decoding process is stopped after iteration i for $i > 1$, if

$$\frac{1}{M_k} \sum_{n=1}^{M_k} (S(L_{2ex}^i(u[n])) \oplus S(L_{2ex}^{i-1}(u[n]))) < \theta$$

where $S(x)$ denotes the sign part of x and \oplus denotes the XOR operation.

Hard-Decision Aided (HDA) Criterion. This criterion is proposed in [62]. It compares the decoded bits of the two successive iterations. The decoding process is stopped after iteration i for $i > 1$, if

$$S(L_2^i(u[n])) = S(L_2^{i-1}(u[n])), \quad \forall n \in 1 \dots M_k$$

HDA2 Criterion. The idea of HDA criterion is extended in [47]. The decoding process is stopped after iteration i for $i > 1$, if

$$S(L_1^i(u[n])) = S(L_2^i(u[n])), \quad \forall n \in 1 \dots M_k$$

where $j=1$ or 2 . In this way, about half of the iteration number can be saved.

Sign Difference Ratio (SDR) Criterion. Extending the SCR method, a new criterion called SDR is proposed in [24]. SDR evaluates the number of sign differences between the intrinsic information and the extrinsic information for the same SISO decoder in the same

iteration, and the decoding process is stopped after iteration i for $i > 1$, if

$$\frac{1}{M_k} \sum_{n=1}^{M_k} (S(L_{jin}^i(u[n])) \oplus S(L_{jex}^i(u[n]))) < \theta$$

Min-LLR Criterion. The minimum of the absolute values of the LLRs is first used in an early stopping criterion in [85], [86] and is later presented in [47], [93]. The decoding process is stopped after iteration i for $i > 1$, if

$$\min_{1 \leq n \leq M_k} |L_2^i(u[n])| > \theta$$

Mean-LLR and Sum-LLR Criteria. The stopping criterion based on the mean of the absolute values of the LLRs is presented in [32], [47], [94]. The decoding process is stopped after iteration i for $i > 1$, if

$$\frac{1}{M_k} \sum_{n=1}^{M_k} |L_2^i(u[n])| > \theta$$

In [29], the sum of the absolute values of the LLRs is calculated to avoid a costly division operation in the Mean-LLR criterion,

$$S_i = \sum_{n=1}^{M_k} |L_2^i(u[n])|$$

The decoding process is stopped after iteration i for $i > 1$, if

$$S_i - S_{i-1} \leq 0$$

Cyclic Redundancy Check (CRC) Criterion. CRC is introduced as a stopping criterion in several papers. The CRC criterion takes extra resource. In WCDMA, CRC is attached before channel coding. All bits in a decoded CB should be checked to know its correctness.

Recently, it is shown that more than one parameter in stopping criterion provides better performance. An example of this kind of criterion is as follows.

Comb. Min-LLR and Sum-LLR Criterion. Min-LLR and Sum-LLR criteria are combined in [29]. The decoding process is stopped after iteration i for $i > 1$, if

$$(S_i - S_{i-1} \leq 0) \parallel \left(\min_{1 \leq n \leq M_k} |L_2^i(u[n])| > \theta \right)$$

where \parallel denotes the *OR* operation.

5.2.2 Turbo-Coded SIC with Low-Complexity Stopping Criterion

The block diagram of turbo-coded SIC is shown in Fig. 5-4 with the transmitter model shown in Fig. 2-19. The input to the de-interleaver Π^{-1} followed by K single-user turbo decoder is soft value $\hat{Y}_{SIC\langle u \rangle}^{(n)}$ of the SIC shown in (3-12). $\hat{Y}_{SIC\langle u \rangle}^{(n)}$ is separated to systematic part $y_{\langle u \rangle}^s{}^{(n_b)}$, and parity part $y_{\langle u \rangle}^{p1}{}^{(n_b)}$, $y_{\langle u \rangle}^{p2}{}^{(n_b)}$ where $0 \leq n_b < M_{\langle u \rangle} + 3$. The iterative decoding algorithm of the turbo decoder is described in 5.2.1. Although the output of SIC II and SIC III in different order are different in mean and variance, according to the central limit theorem, whatever of these outputs in different order are independent random variables, the outputs $\hat{Y}_{SIC,k}^{(n)}$ can be approximated as Gaussian distributed random variables with $\sim \mathcal{N}(m_k, \sigma_k^2)$ in both power-balanced and power-unbalanced systems, especially when K is large. For practical use, estimation of the residual interference plus noise is done with the aid of pilot-channel signal. The block diagram of variance estimation is shown in Fig. 5-7. In traffic-channel signal remover (TCSR), all user data respread in SIC for data are summed and removed from $r(t)$, i.e. the output of TCSR is

$$r_{SIC,pilot}(t) = r(t) - \sum_{k=1}^K \tilde{C}_{data,k}(t)$$

where

$$\tilde{C}_{data;k}(t) = \sum_{p=1}^F \beta_d \hat{\alpha}_{av;k,p}^{(\lfloor (t-\tau_{k,p})/T_b \rfloor)} \hat{b}_{SIC;k}[\lfloor (t-\tau_{k,p})/T_b \rfloor] C_{OVSF}(t-\tau_{k,p}) C_{scramb,k}(t-\tau_{k,p}). \quad (5-10)$$

SIC for pilot is then performed with $r_{SIC;pilot}(t)$. The mean of the soft output $\hat{Y}_{pilot;SIC,k}^{(n)}$ is thus calculated as follows.

$$m_{pilot,k} = \frac{1}{N_{b,k}} \sum_{n=1}^{N_{b,k}} \hat{Y}_{pilot;SIC,k}^{(n)} \quad (5-11)$$

where $N_{b,k}$ is defined in 2.2.1 and the variance of $\hat{Y}_{pilot;SIC,k}^{(n)}$ is defined as.

$$\sigma_{pilot,k}^2 = \frac{1}{N_{b,k}} \sum_{n=1}^{N_{b,k}} (\hat{Y}_{pilot;SIC,k}^{(n)} - a_{pilot}[n]m_{pilot,k})^2. \quad (5-12)$$

After i_k iterations, the transmission data sequence of the k -th user is recovered by the hard-decision and demapper of the LLR $L_2^{i_k}(u[n])$ as shown in (5-6).

From 5.2.1, we can find that most stopping criteria in literature take information from all bits in a CB as measurement bases. The processing delay and required data buffer thus become large when the block length increases. According to the characteristic of SIC II & SIC III, bits in later detected order have smaller soft outputs, or say, smaller SNR than that in the former detected order. In addition, the LLR of APP is a function of soft outputs of SIC, and systematic bit takes the most important part in LLR of APP. As a result, the decoded bit with the minimum LLR of APP is most probably the one in later detected order. Also, errors are easier to occur in decoded bits with later detected order. According to these properties, we propose to consider only part of the APP LLRs in a CB. The APP LLRs of a CB are divided into K groups, i.e. for the n -th bit of user with index k detected at the u -th

order,

$$\Lambda_u = \{n : \langle u \rangle_n = k, 0 \leq n < M_k\}$$

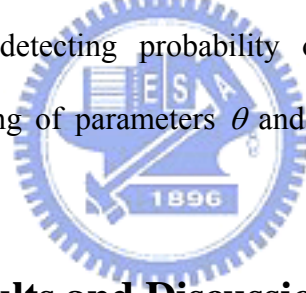
where $0 \leq u < K$ and

$$\Lambda = \{n : n \in \Lambda_u, u \geq x, 0 \leq x < K\}.$$

For example, if the stopping criterion is the combination of HDA2 and Min-LLR, i.e. the decoding process is terminated at the $I_{i,k}$ -th inner iteration if

$$\min_{0 \leq n < M_k} |L_2^{i,k}(u_k[n])| > \theta \quad \& \quad S(L_2^{i,k}(u_k[n])) = S(L_1^{i,k}(u_k[n])) \quad \text{for all } n \in \Lambda \quad (5-13)$$

The resultant computational complexity and used buffer become x/K times of the original one. The tradeoff between detecting probability of correct CB and computational complexity relies on the setting of parameters θ and x . Impacts of these parameters are examined in the next section.



5.2.3 Simulation Results and Discussions

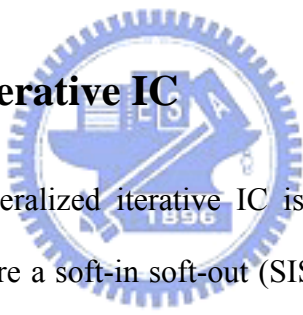
The simulation parameters listed in Table 3-2 with multipath fading channel Case 3 shown in Table 3-3 is used for performance evaluation. We first compare the performance of our proposed SIC front-end and the one with PPIC [22] with three stages where the partial coefficient is 0.6 at the first two stages. The turbo iteration number is limited to 10 and the CB length is $M=196$. In Fig. 5-2, the SIC frond-end is shown to outperform PPIC from 0.25dB with BER at $2 \cdot 10^{-2}$ to more than 1dB with BER at 10^{-3} .

In Table 5-1, it is shown that our proposed stopping criterion performs almost the same as the full-block-checking criterion with much less computational complexity needed, and about half of the computational complexity can be saved. In addition, the combination of HDA2 and min-LLR can results in less iteration number needed.

5.3 A Novel Iterative IC

In 5.2, LLRs of turbo decoder output is used to determine if a CB is correctly decoded. With this useful information, in the section, a novel iterative IC is presented. In the proposed scheme, process propagates to the next outer iteration or not depending on the correctness of the CB in current outer iteration. Bits of the correct decoded CBs are hard-decisioned, re-encoded to form the coded bits including systematic bits, parity bits, and tail bits. Then these bits are respread and removed from the received signal. MAI from these correct blocks is thus removed correctly, and we can expect better BER than those with estimated parity bits and tail bits. In addition, large amount of computational complexity and processing time can be saved.

5.3.1 The Generalized Iterative IC



The block diagram of the generalized iterative IC is shown in Fig. 5-8. The basic building blocks of an iterative IC are a soft-in soft-out (SISO) MUD and a bank of K user SISO channel decoder. The function of these blocks is to compute the posterior probabilities based on the given prior probabilities and on the given signal. For the SISO MUD [57], it has two sets of inputs: the MF output, and the *a priori* information obtained from channel decoder. In the first outer iteration, no *a priori* information is actually available at the receiver on the transmitted bits. From the 2nd outer iteration, the set of is fed back from the channel decoders. We refer to the set of the feedback LLR as the current bit statistics. The SISO-US outputs another set of LLR and then deinterleaved according to permutation and sent as input to the SISO channel decoder, which performs the same algorithm, i.e. BCJR, as in turbo decoding. Details on the algorithm can be found in 5.2.1. The output of the SISO channel decoder in current outer iteration, after interleaving, becomes the set of current bit statistics for user in the next outer iteration. In the last iteration, each SISO decoder must also

supply the final estimate of the corresponding information bit stream, which represents the output of the whole receiver.

5.3.2 The Proposed Iterative IC

The structure of our proposed iterative IC is shown in Fig. 5-3. The block diagram of the first outer iteration is shown in Fig. 5-5. Parts of these blocks are introduced in 5.2 as shown in Fig. 5-4 which perform SIC and turbo decoding with stopping criterion, and new blocks added in Fig. 5-5 are used for the next outer iterative processing. At the turbo decoder output, all blocks are separated into two parts. The first part is composed of the detected correct blocks and the other part is composed of the remaining blocks. LLRs of the first part are passing through the block of hard decision followed by the turbo encoder to reconstruct the parity bits and tail bits. All bits are mapped, interleaved and respread, and then removed from the received signal, and the remaining signals are sent as one of the inputs to the second iteration. For the bits in the first part, no further processing is needed. Only the LLRs of the CBs in the second part are interleaved as one input to the second outer iteration. To re-build the parity bits $u^{px}[n]$ of the incorrect CB, we should utilize the LLR of parity bits where

$$L(u^{px}[n]) = \log \left(\frac{\sum_{s^1} \alpha_{n-1}(s') \cdot \gamma_n(s', s) \cdot \beta_n(s)}{\sum_{s^0} \alpha_{n-1}(s') \cdot \gamma_n(s', s) \cdot \beta_n(s)} \right)$$

The block diagram of the second to the $I_{o,k}$ -th outer iteration is shown in Fig. 5-6. From the second outer iteration, input to refined channel estimation is the output of TCSR in which all estimated respread user data are cancelled. The SISO user data separator can be MUD such as PPIC, MMSE and etc. with the remaining signal form the first outer iteration and LLRs as input. Here the SISO PPIC [4] with two stages is used. The Decision block

performs soft-decision and the estimated bits at initial stage are as follows.

$$\hat{b}_{PIC,J}^0[n] = E\{u_J[n']\} = \tanh\left(\frac{L_2^{I_i}(u_J[n'])}{2}\right) \quad (5-14)$$

where $b_J[n] = u_J[n']$. And the data estimates of the desired user J at the s -th are

$$\hat{b}_{PIC,J}^s[n] = (1 - p_s) \sum_{f=1}^F |\hat{\alpha}_{J,f}^{(n)}|^2 \hat{b}_{PIC,J}^{s-1}[n] + p_s \{r'(t) - \sum_{k=1, k \neq J}^K \hat{b}_{PIC,k}^s[n]\} \quad (5-15)$$

Outputs of the PPIC are de-interleaved, then the LLR as computed for RAKE in [45] are inputs to turbo decoder. Again, variance estimation is done with the aid of pilot-channel signal. The stopping criterion is the same as that in the first outer iteration with the same ordering information. When the decoding (inner) iteration reaches the predefined limit, the process continues to the next outer iteration. To decide if the next outer iteration should be done, a simple method is to discriminate if the bits of a newly-detected correct decoding block are overlapped with the bits in an incorrect CB of other users. The concept of dividing correct and incorrect decoded CBs into two parts has been proposed [8], [41], [46]. In [46], bits in correct CBs are given a high LLR value for equalization in MIMO systems. However, soft information of bits other than information bits in a correct CB not necessary has the same sign as the original ones. The same problem arises in [8] where only the information bits in a CRC-checked correct CB are soft decision with $+1/-1$, reconstruct and removed from the correlated signal in orthogonal frequency-division multiple-access code-division multiplexing (OFDMA-CDM) systems. Our proposed method can be viewed as the solution to generate the “genie” re-encoded bits depicted in [41].

5.3.3 Simulation Results and Discussions

In this section, we compare the performance of our proposed iterative IC and the generalized iterative IC which performs turbo decoding with 10 inner iterations, and no correct CB is removed from the received signal. From the 2nd outer iteration, both iterative IC adopt two-stage SISO PPIC with partial coefficient 0.6. The simulation parameters are the same as those in 5.2.3. It is shown in Fig. 5-9 that our proposed iterative IC outperforms the generalized one with 0.5 dB gain at BER=10e-4.

In Table 5-2, the average inner iteration number for turbo decoding used in our proposed method and the generalized method are listed at SNR=5.9 dB. It is shown that large amount of iteration number can be saved.

5.4 Summary

In this chapter, we propose a novel iterative IC with high performance. The SIC front-end at the first outer iteration provides lower BER than PPIC with three stages, and thus better performance can be expected after turbo decoding. A highly efficient and low-complexity stopping criterion utilized the ordering information of SIC is used to find the correct CB and decide if the decoding process can be terminated. Only the bits in incorrect CBs should proceed to the next outer iteration. As a result, huge amount of computational complexity can be saved. When the outer iteration number increases, the improvement in correct decoding becomes smaller. A simple method is proposed to decide if the next outer iteration should be done. Except the timing information, all parameters used in the proposed scheme are estimated from the received signal. Our proposed iterative IC is shown to have smaller computational complexity than the generalized iterative IC with much BER improvement.

Table 5-1 Average redundant iteration number of deciding correct CB versus average false alarm probability at SNR = 6.9dB, 8 users

			Average redundant iteration number	Average false alarm probability
Genie			0	0
Min-LLR	Checking full block	$\theta=3$	5.6e-2	2.2e-3
		$\theta=4$	7.1e-2	0
	Proposed (x= 4)	$\theta=3$	5.5e-2	3.0e-3
		$\theta=4$	7.0e-2	0
	Proposed (x= 6)	$\theta=3$	5.3e-2	3.0e-3
		$\theta=4$	6.6e-2	0
HDA2	Checking full block	$\theta=0$	6.2e-2	1.6e-2
	Proposed (x= 2)	$\theta=0$	6.1e-2	1.6e-2
	Proposed (x= 4)	$\theta=0$	5.7e-2	1.7e-2
	Proposed (x= 6)	$\theta=0$	4.5e-2	2.2e-2
Min-LLR && HDA2	Checking full block	$\theta=1$	6.8e-2	0
	Proposed (x= 4)	$\theta=1$	6.2e-2	0
	Proposed (x= 6)	$\theta=1$	5.7e-2	7.4e-4
		$\theta=3$	6.9e-2	0

Table 5-2 Average inner iteration in the proposed method and the generalized iterative method

	1st outer iteration	2nd outer iteration	3rd outer iteration
Proposed Iterative Method	1.72	2.58	3.30
Generalized Iterative Method	10	20	30

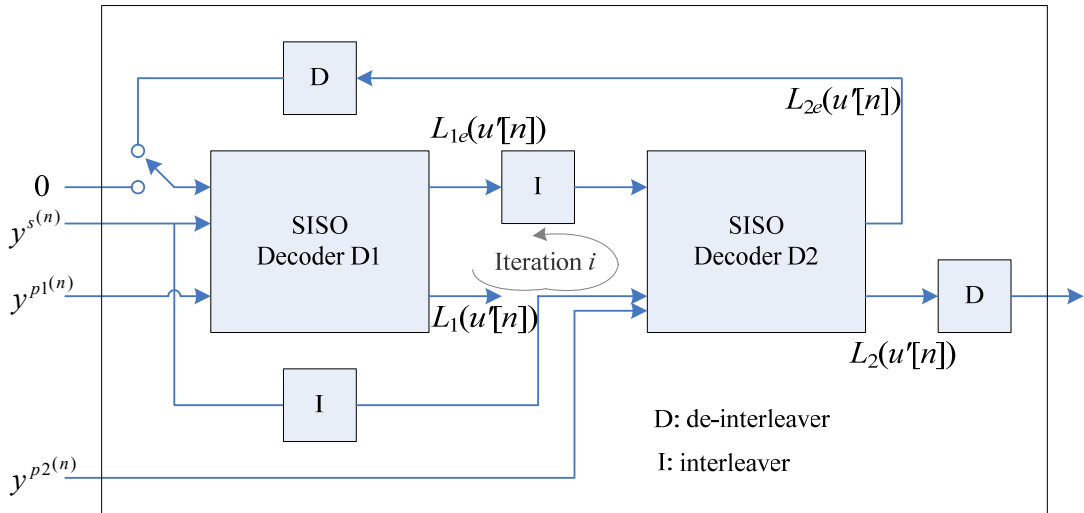


Fig. 5-1 Block diagram of turbo decoder for one user

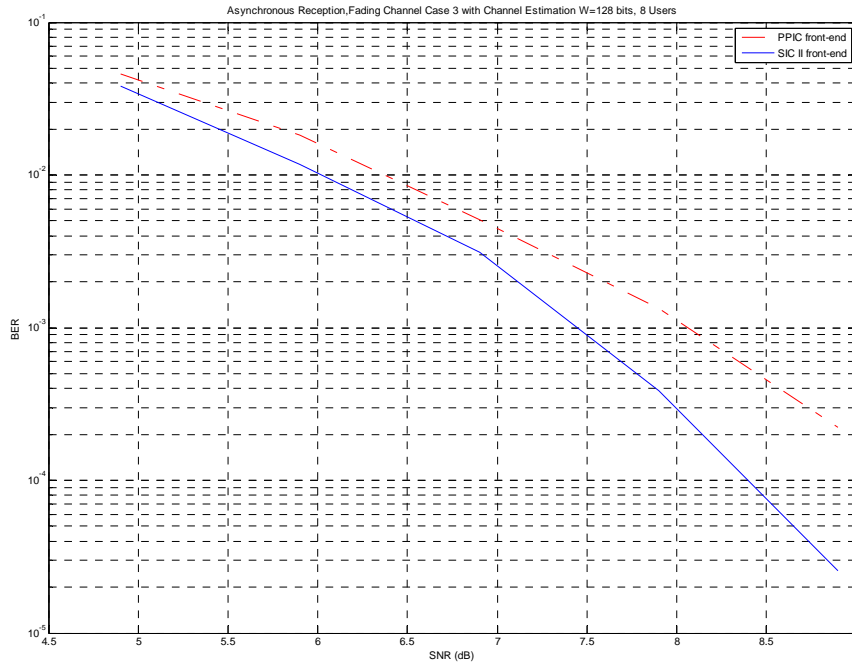


Fig. 5-2 BER comparison of turbo-coded systems with SIC II and PPIC at front-end

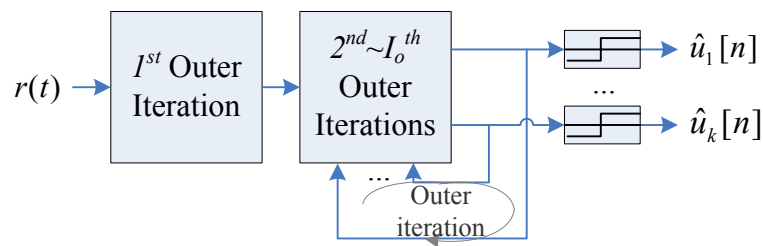


Fig. 5-3 A novel iterative IC scheme

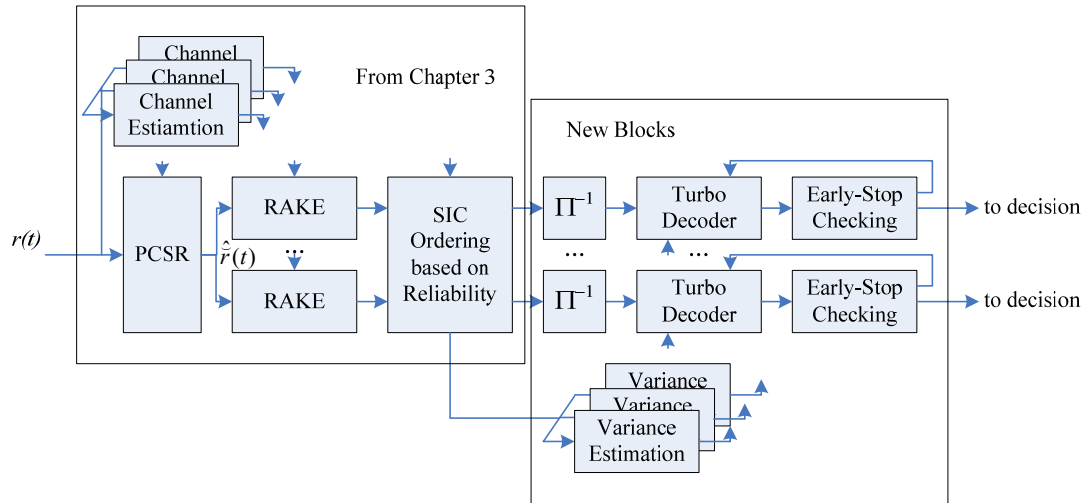


Fig. 5-4 Block diagram of SIC at front-end

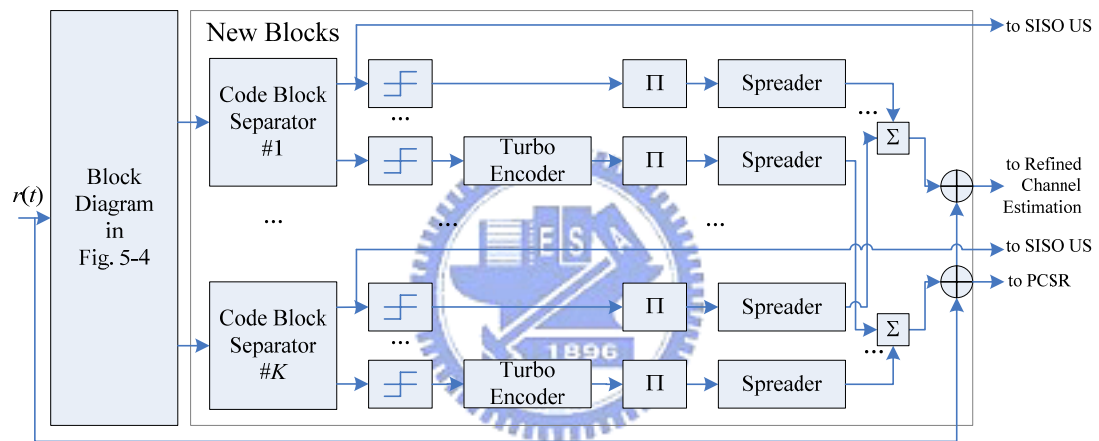


Fig. 5-5 Block diagram of the first outer iteration of the proposed iterative IC

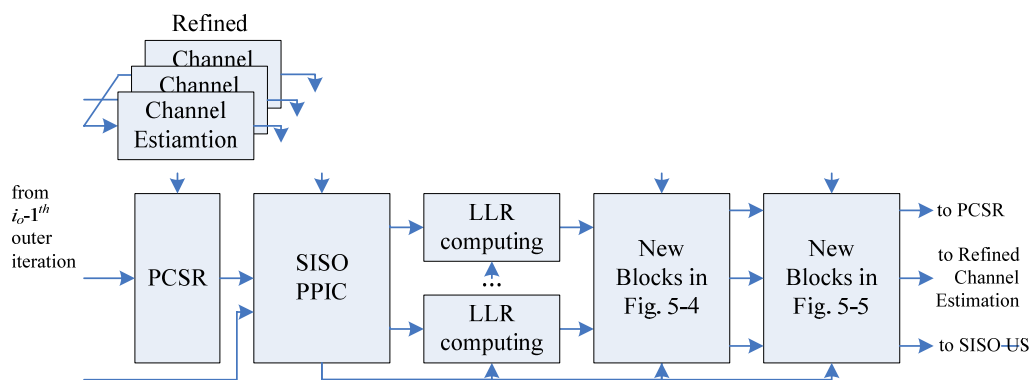


Fig. 5-6 Block diagram of the 2nd to the I_o -th outer iteration

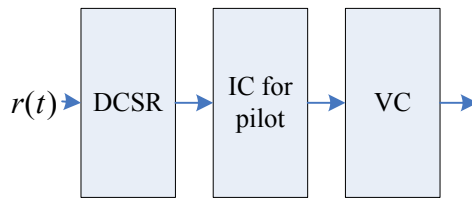


Fig. 5-7 Block diagram of variance estimation

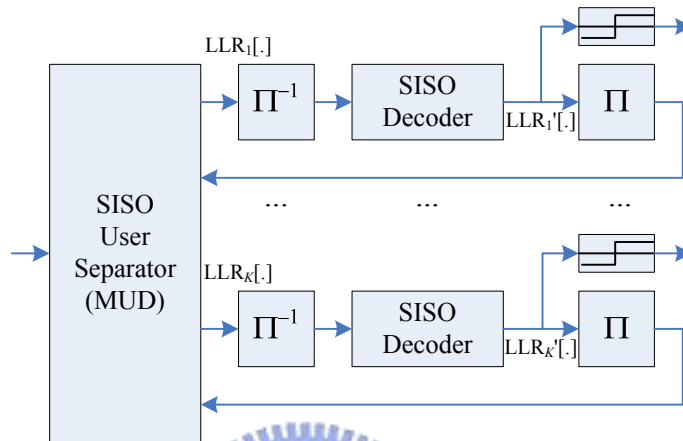


Fig. 5-8 Generalized iterative IC

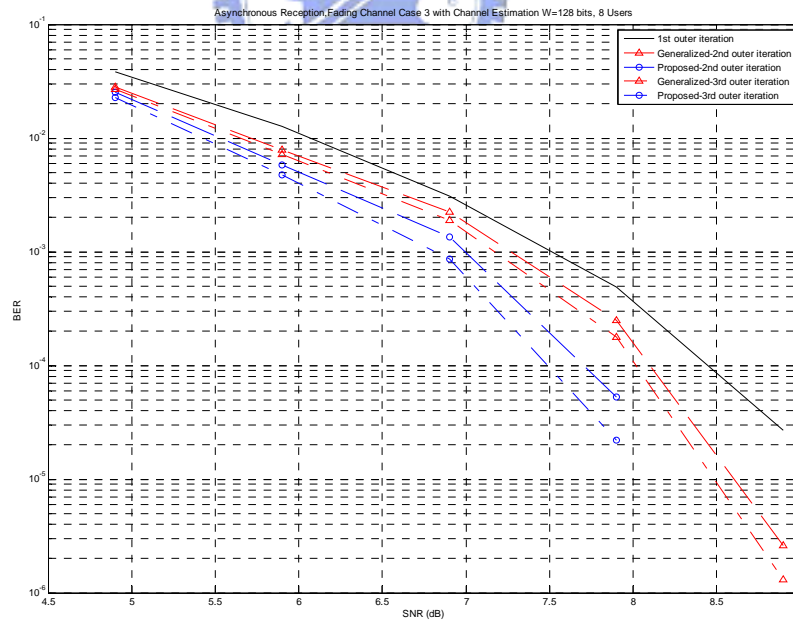


Fig. 5-9 BER comparison of our proposed iterative IC and the generalized IC without detection of correct CB

Chapter 6

Conclusions

In this thesis, we analyze the characteristics of SIC and propose techniques and architectures in the hope of making the SIC a practical technique for uplink WCDMA systems in the view of error performance and simplicity.

In Chapter 3, three ordering methods for SIC in the uplink of WCDMA systems over multipath fading channels are discussed and compared in the aspect of the implementation issues (such as reordering frequency, processing delay, latency, and computational complexity), and error performance related parameters (such as pilot-to-traffic amplitude ratio, cancellation-ordering method, grouping interval, received power distribution ratio and channel estimation as well as timing estimation errors). The scheme decides the cancellation order and performs data detection in a group manner for each user. SIC I decides the cancellation order according to average power as that in [90]. In SIC II, the G -bit summation of the RAKE output strengths in each stage are used to find the next detected user. SIC III decides the cancellation order based on the G -bit summation of the RAKE bank output strengths at the first stage.

Channel estimation performed independently with the pilot channel of each user is taken into consideration in the analyses. The interference between traffic channel signals and pilot channel signals are taken into consideration. In order to alleviate these interferences pilot-channel signal of all users are estimated and removed before data detection.

Architectures for the three SICs are presented. To minimize the complexity of the receiver, we adopt the MRC RAKE receiver with hard decision for data detection and

windowed moving average technique for channel estimation.

In addition to consider the single-rate systems, a generalized pilot-channel aided SIC scheme is presented for application in multirate communications. The SIC III is slightly modified to adapt to multirate systems. The characteristics of grouping interval shown in the single-rate systems can be also found in multirate systems.

In Chapter 4, a pilot-channel aided pipeline scheme for SIC is proposed. Generally speaking, pipelined implementation is inherent in SIC but not in channel estimation. This scheme combines channel estimation and user data detection into sequential type with low complexity and leads to pipeline implementation. Compared with conventional channel estimation using correlator output and SIC without pilot signal remover, the proposed scheme shows better quality both on channel estimation and user data detection.

We propose a pilot channel aided adaptable interference cancellation (IC) scheme which combines serial (SIC) and parallel (PIC) interference cancellation to adapt to different services under different circumstances. The processing delay and computational complexity can be adjusted based on system loading and required performance. In addition to removing interference from pilot channel to traffic channel, the interferences from traffic channel to pilot channel are also cancelled. This results in better quality both on channel parameter estimation and user data detection. Compared with SIC and PIC, the proposed scheme shows better performance with reasonable hardware cost while it needs shorter processing delay than SIC.

In Chapter 5, to extend the SIC technique to turbo-coded systems, an iterative IC with ordered SIC at front-end of having good performance and low complexity is proposed. The ordering information obtained from SIC front-end is utilized in a new stopping criterion with quite low complexity and data memory to save needless iterations in turbo decoding. From the second outer iteration, only the bits in incorrect blocks should be processed. As a

result, huge amount of computation can be saved. In addition, channel estimates from pilot-channel signal are refined from the second outer iteration with estimated traffic-channel signal removal. With the analyses in complexity and computer simulations in BER, this scheme is shown to be superior and practical in current communication systems.



Appendix A HSDPA

In Release 5, the biggest change impacting the physical layer is the addition of the high speed downlink packet access (HSDPA) to increase system throughput and deliver an improved user experience. The HSDPA is a concept to increase downlink packet data throughput by means of fast L1 retransmission and transmission combining, as well as fast link adaptation controlled by the base station (Node B).

HSDPA is fully backwards-compatible with W-CDMA, and any application developed for W-CDMA also works with HSDPA. In Release '99, individual DCH UEs have their own dedicated radio resource channels, whether they have downlink data or not. In the case of HSDPA, a wide band downlink channel can be shared among all HSDPA-capable UEs, Node B schedules to share a "fat pipe" and can simultaneously transmit high rate data to the user with good interference/channel condition in the short term sense. Two features in WCDMA Release '99, variable SF and fast power control are replaced by means of adaptive modulation and coding (AMC), extensive multicode operation up to 15 multicodes in parallel and a fast and spectrally efficient retransmission strategy, named Hybrid Automatic Repeat Request (HARQ).

The retransmission procedure for the packet data is located in the SRNC in R'99. In HSDPA, the retransmission can be controlled directly by the Node B by taking into account available memory in the terminal. Fig. 2-23 presents the difference between retransmission handling with HSDPA and Release '99. The HARQ functionality used in HSDPA can be soft combining or incremental redundancy. The former method sends the identical data as the previous transmission. The latter method transmits additional data in retransmission and has a slightly better performance with more memory required.

The Node B decides the modulation scheme and TrBk size the UE shall use or control

the transmitter power of the PhCHs of the UE for each TTI according to UE capabilities, QoS Requirements for pending data, retransmission buffer states and estimated channel quality. According to changing radio environment needs, the modulation scheme and coding rate can be quickly and flexibly modified. Both QPSK, which is used in Release '99, and modulation with higher capability, i.e. 16QAM, can be supported in HSDPA. The achievable theoretical maximum data rate of HSDPA can be 14.4 Mbps.

To implement the features such as fast L1 retransmission and transmission combining, as well as fast link adaptation controlled by the Node B, a new common TrCH - High Speed Downlink Shared Channel (HS-DSCH) shared by several UEs is added in HSDPA. The HS-DSCH is associated with one downlink DPCH, and one or several Shared Control Channels (HS-SCCH). The HS-DSCH is transmitted over the entire cell or over only part of the cell using e.g. beam-forming antennas. A new definition of frame structure named sub-frame is introduced in Release 5. The sub-frame is the basic time interval for HS-DSCH transmission and HS-DSCH-related signaling at the physical layer. The length of a sub-frame corresponds to 3 slots (7680 chips). The mapping of TrCH HS-DSCH onto PhCHs and its corresponding control channels are shown in Fig. 2-6.

A simple illustration of the general functionality of HSDPA is summarized in Fig. 2-25. The Node B estimates the channel quality of each active HSDPA users. Scheduling and link adaptation are then conducted at a fast pace. Three new PhCHs are associated with HS-DSCH. The HS-PDSCH is used to carry the user data shared by several UE in the downlink from HS-DPCH. HS-SCCH carries the necessary physical layer control information to enable decoding of the data on HS-DSCH whereas the Uplink HS-DPCCH carries the necessary control information in the uplink. Fig. 2-24 illustrates the spreading operation for the Dedicated Physical Control CHannel (HS-DPCCH). The HS-DPCCH shall be spread to the chip rate by the specified channelisation code c_{hs} [74]. After channelisation,

the real-valued spread signals are weighted by gain factor β_{hs} derived from signals from higher layers [75]. The multiplexing and coding for HS-DSCH is shown in Fig. 2-26 where the HARQ functionality after channel coding is shown in Fig. 2-27. Details of the multiplexing and coding for HS-DSCH, HS-DPCCH and HS-SCCH are described in [73].

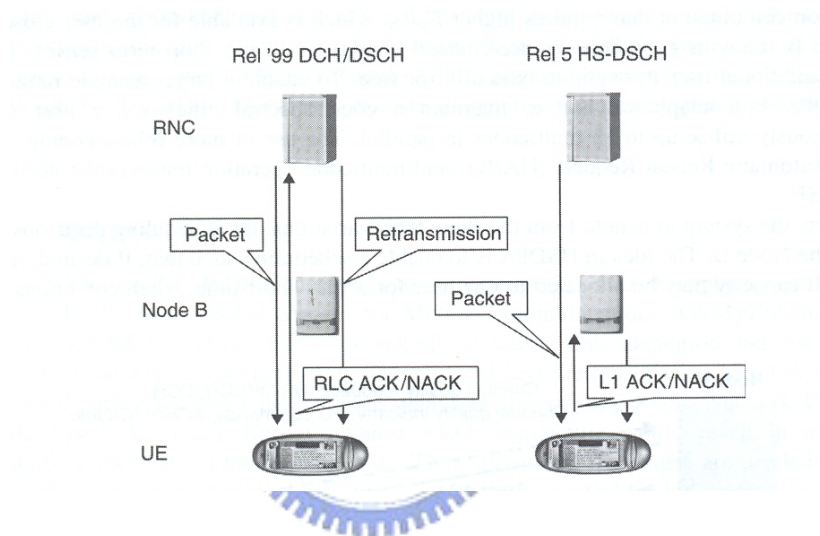


Fig. 2-23 The difference between retransmission handling with HSDPA and Release '99 [33]

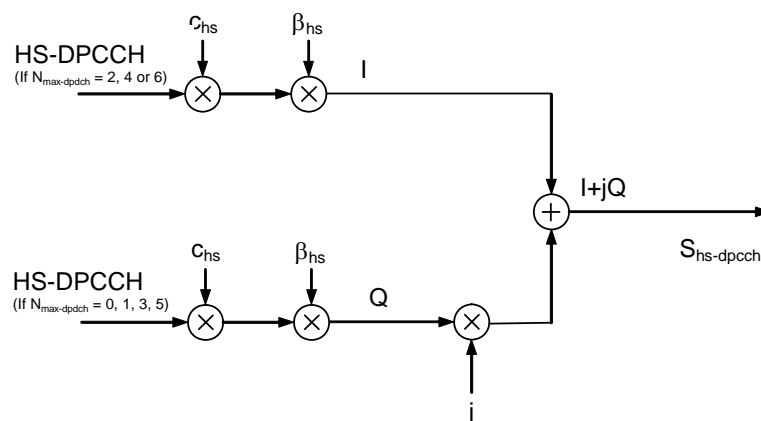


Fig. 2-24 Spreading for uplink HS-DPCCH

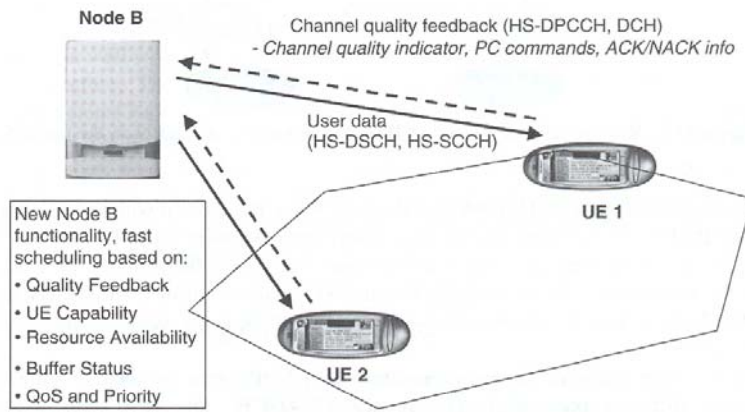


Fig. 2-25 A simple illustration of the general functionality of HSDPA [33]

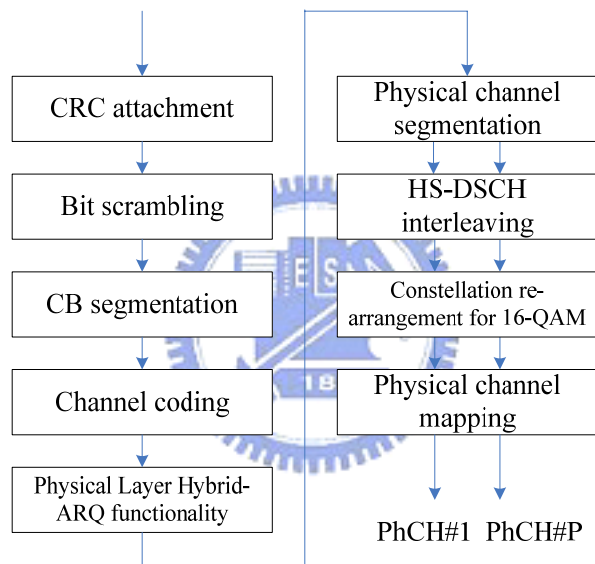


Fig. 2-26 Coding chain for HS-DSCH

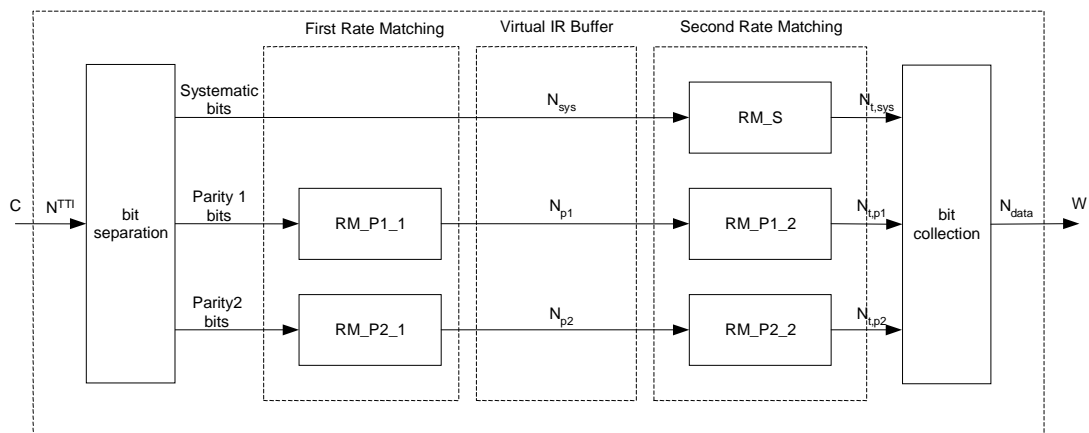


Fig. 2-27 HS-DSCH HARQ functionality

Appendix B HSUPA

After introducing HSDPA, the growth of downlink traffic load reveals the shortage of uplink capacity. Mobile communications with higher data rate and shorter latency are inevitable for interactive services such as video clips sharing between users and gaming. To meet the demand, the technique so called high speed uplink packet access (HSUPA) is introduced in 3GPP Release 6. HSUPA has four key features: *HARQ*, *fast Node B scheduling*, *soft handover* and *shorter TTI*. Theoretically, the maximum peak rate is 2Mbps in 10ms HSUPA TTI and 5.76 Mbps in 2ms HSUPA TTI.

HSUPA is expected to achieve significant improvement in overall system performance when operated together with HSDPA. HSUPA is mainly optimized for the middle or low speed (less than 60km/Hr). The uplink and downlink data transmitter have the fundamental difference in handling the total transmission power resource. In the uplink, the power amplifier capacity of a user terminal is limited, and using a higher order modulation such as 16-QAM would increase the peak to average power ratio (PAPR). Additionally, the power control cannot be abandoned in the case of continuous uplink transmission due to the near far problem. Unlike HSDPA, HSUPA use adaptive power control and also uses the same modulation method as regular WCDMA.

Scheduling is performed by Node B in order to make the Noise Rise (Signal to Noise Power) within a required level. The proper data rate is decided by Node B under the maximum rate set by RNC. When a smaller Noise Raise Margin is set, uplink capacity can be increased. UE sends control signals with rate-increasing requirement for uplink as Rate Request to Node B. Node B returns UE L1 signals as Rate Grant. Downlink control signals are Absolute Grant (AG) and Relative Grant (RG). AG means the absolute value of the power offset permitted for the power usage. Node B that controls a serving cell can send AG. RG is used as an over-load indicator to avoid larger interference and is sent from all cells in

HSUPA neighboring cells including serving cell and non-serving cells.

To maintain reasonable performance at the cell edge, soft handover is supported in HSUPA. SRNC performs soft handover between two Node Bs and provides diversity combining and re-ordering. SRNC decides the serving cell among active cells and indicates it to the Node B and the UE. UE receives ACK/NACK from both Node Bs. When UE receives any ACK from Node B, the UE quits the retransmission process.

HARQ can be classified as being synchronous or asynchronous: synchronous HARQ implies that (re)transmissions for a certain HARQ process are restricted to occur at known time instants. No explicit signaling of the HARQ process number is required as the process number can be derived from. Asynchronous HARQ implies that (re)transmission for a certain HARQ process may occur at any time. Explicit signaling of the HARQ process number is therefore required. Non-Adaptive implies that changes, if any, in the transmission attributes for the retransmissions, are known to both the transmitter and receiver at the time of the initial transmission. Hence, the associated control information need not be transmitted for the retransmission. The HSDPA uses an adaptive, asynchronous HARQ scheme, while HSUPA uses a synchronous, non-adaptive HARQ scheme. Hybrid ARQ in HSUPA is a 'Stop and Wait' between Node Bs and UE.

A new dedicated TrCH named Enhanced Dedicated CHannel (E-DCH) is introduced in HSUPA. The E-DCH is an uplink TrCH that carries user data or control information from layers above the physical layer. The E-DCH supports soft handover. Fig. 2-31 shows the processing structure for the E-DCH mapping to E-DPDCH. Data arrives to the coding unit in form of a maximum of one TrBk once every transmission time interval (TTI). The HSUPA supports 2ms and 10ms TTI. The HARQ functionality is shown in Fig. 2-32. It matches the number of bits at the output of the channel coder to the total number of bits of the E-DPDCH set. The HARQ functionality is controlled by the redundancy version (RV) parameters. The

parameters of the HARQ rate matching depend on the value Retransmission Sequence Number (RSN) set by higher layers [77]. When more than one E-DPDCH is used, PhCH segmentation divides the bits among the different PhCHs. An example of channel coding and multiplexing of E-DPDCH is given in Fig. 2-30 with parameters given in Table 2-5 [71]. Fig. 2-6 summarizes the mapping of E-DCH onto PhCHs. The multiplexing and coding for E-DPCCH and E-AGCH are described in [73].

The E-DPDCH is used to carry the TrCH E-DCH. The E-DPCCH is a PhCH used to transmit control information associated with the E-DCH. The control information includes the uplink HARQ transmission number and happy bit which indicates whether the UE could use more resources or not. Fig. 2-28 shows the E-DPDCH and E-DPCCH (sub)frame structure. Each radio frame is divided in 5 subframes, each of length 2ms. SF of the E-DPDCH ranges from 2~256. Fig. 2-29 illustrates the spreading operation for the E-DPDCHs and the E-DPCCH. The channelisation code c_{ec} and $c_{ed,k}$ for the k -th E-DPDCH are specified in [74]. The gain factor β_{ec} and $\beta_{ed,k}$ are specified in [75]. After weighting, the real-valued spread signals are mapped to the I branch or the Q branch according to the $i_{q_{ec}}$ specified in [74]. The E-DPCCH is mapped to the I branch, i.e. $i_{q_{ec}} = 1$. The spreading operation is described in 2.1.4 and shown in Fig. 2-13. The possible combinations of the maximum number of respective dedicated PhCHs which may be configured simultaneously for a UE in addition to the DPCCH are specified in Table 2-4.

The E-DCH Absolute Grant Channel (E-AGCH) is a common downlink PhCH carrying the uplink E-DCH AG which is sent from the serving E-DCH cell and allows the Node B scheduler to directly adjust the granted rate of UEs under its control. The E-DCH Relative Grant Channel (E-RGCH) is a dedicated downlink PhCH carrying the uplink E-DCH RGs.

The E-DCH Hybrid ARQ Indicator Channel (E-HICH) is a dedicated downlink PhCH carrying the uplink E-DCH HARQ ACK indicator. This control information is used in

support of the uplink HARQ functionality. In each cell, the E-RGCH and E-HICH assigned to a UE shall be configured with the same channelization code.

Table 2-4 Maximum number of simultaneously-configured uplink dedicated channels

	DPDCH	HS-DPCCH	E-DPDCH	E-DPCCH
Case 1	6	1	-	-
Case 2	1	1	2	1
Case 3	-	1	4	1

Table 2-5 E-DPDCH Fixed reference channel 5 (FRC5)

Parameter	Unit	Value
Maximum. Inf. Bit Rate	kbps	978.0
TTI	ms	10
Number of HARQ Processes	Processes	4
Information Bit Payload (N_{INF})	Bits	9780
Binary Channel Bits per TTI (N_{BIN}) ($3840 / SF \times TTI$ sum for all channels)	Bits	19200
Coding Rate (N_{INF} / N_{BIN})		0.509
PhCH Codes	SF for each PhCH	{4,4}
E-DPDCH testing: E-DPDCH/DPCCH power ratio E-DPCCH/DPCCH power ratio	dB dB dB dB	Diversity: 8.94 Non-diversity: 12.04 Diversity: -1.94 Non-diversity: 0.0 E-DPDCH /DPCCH power ratio is calculated for a single E-DPDCH.

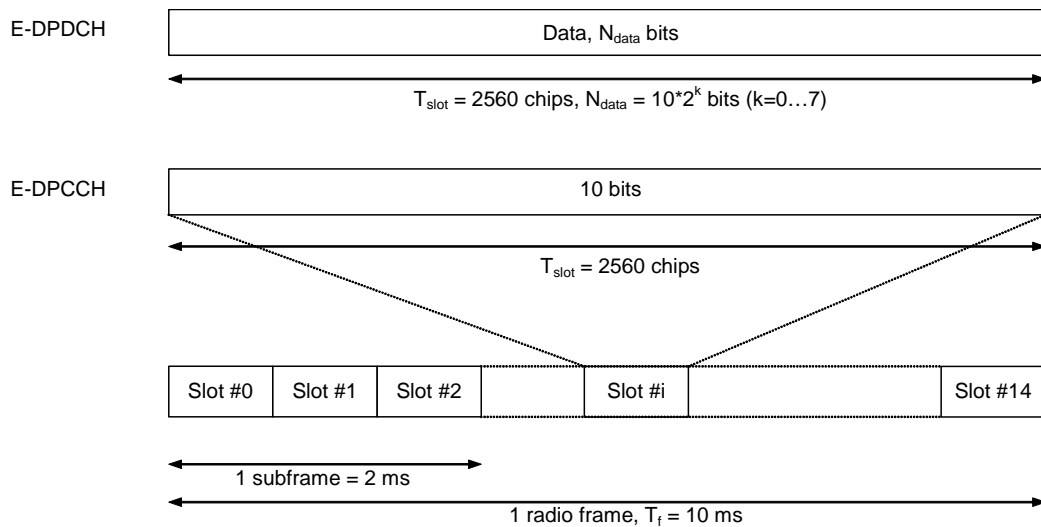


Fig. 2-28 E-DPDCH frame structure

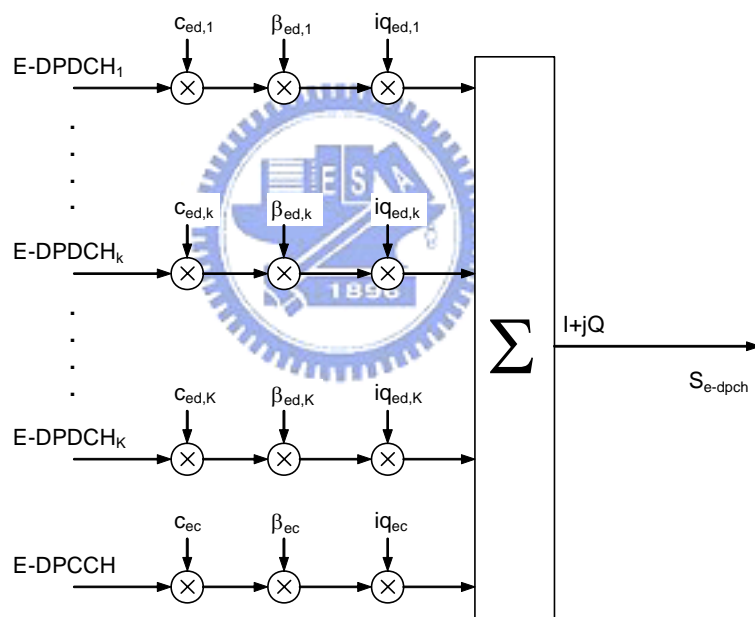


Fig. 2-29 Spreading for E-DPDCH/E-DPCCH

Information Bit Payload	$N_{INF} = 9780$	
CRC Addition	$N_{INF} = 9780$	24
Code Block Segmentation	$(9780+24)/2 = 4902$	$(9780+24)/2 = 4902$
Turbo Encoding (R=1/3)	$3 \times (N_{INF}+24)/2 = 14706$	12
RV Selection	19200	
Physical Channel Segmentation	9600	9600

Fig. 2-30 E-DPDCH Fixed reference channel 5 (FRC5)

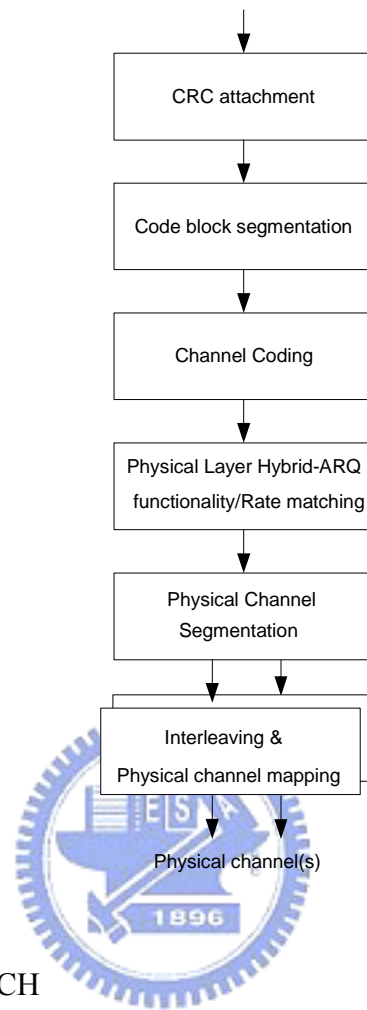


Fig. 2-31 TrCH processing for E-DCH

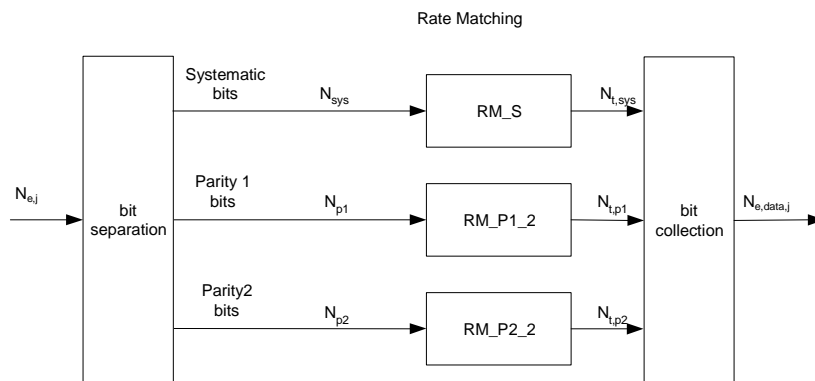


Fig. 2-32 E-DCH HARQ functionality

Appendix C Derivation of Equation (2-4)

We are to derive $MAI_{\hat{\alpha}_{J,f}}^{(n)}$ in (2-4) by first considering the following expression,

$$\frac{1}{2T_b} \int_{nT_b+\tau_J}^{(n+1)T_b+\tau_J} b_k(t-\tau_{k,p}) C_{OVSF}(t-\tau_{k,p}) C_{scramb,k}(t-\tau_{k,p}) C_{scramb,J}^*(t-\tau_{J,f}) dt. \quad (C1)$$

After taking definitions of $b_k(t)$, $C_{OVSF}(t)$ and $C_{scramb,k}(t)$ into (A1), it becomes

$$\frac{1}{2T_b} \sum_n \sum_m \sum_q b_k[n] c_{OVSF}[q] c_k[q] c_J^*[m] \int_{nSFT_c+\tau_{J,f}}^{(n+1)SFT_c+\tau_{J,f}} p(t-qT_c-\tau_{k,p}) p(t-qT_c-\tau_{k,p}) p(t-mT_c-\tau_{J,p}) dt,$$

where n, m, q are all nonzero integers. With timing delay illustration shown in Fig. 3-1,

we define $\tau_{k,p} = q'T_c + \tau'_{k,p}$, $\tau'_{k,p} < T_c$ and $\tau_{J,f} = m'T_c + \tau'_{J,f}$, $\tau'_{J,f} < T_c$ for $q' \geq 0$, $m' \geq 0$,

$\tau'_{k,p} - \tau'_{J,f} = \tau'_{k,p;J,f}$. In the following, we take $\tau = \tau_{k,p;J,f}$ and $\tau' = \tau'_{k,p;J,f}$ for notational

simplicity. If $\tau = iT_c + \tau'$ for $0 \leq \tau'_{k,p;J,f} < T_c$ where i is a nonzero integer, when $\tau \geq 0$, (C1)

becomes

$$\begin{aligned} & \frac{1}{2T_b} b_k[n] \sum_m \sum_q c_{OVSF}[q] c_k[q] c_J^*[m] \int_{nSFT_c+\tau}^{(n+1)SFT_c} p(\lambda - (q-m+i)T_c - \tau') p(\lambda) d\lambda \\ & + \frac{1}{2T_b} b_k[n-1] \sum_m \sum_q c_{OVSF}[q] c_k[q] c_J^*[m] \int_{nSFT_c}^{nSFT_c+\tau} p(\lambda - (q-m+i)T_c - \tau') p(\lambda) d\lambda \end{aligned} \quad (C2)$$

where $\lambda = t - mT_c$. We can find that $|(q-m+i)T_c + \tau'| < T_c$ such that the integral is nonzero,

i.e., $-\tau'/T_c + m - i - 1 < q < -\tau'/T_c + m - i + 1$. Thus, (C2) becomes

$$\frac{1}{2SF} \frac{T_c - \tau'}{T_c} \left\{ b_k[n] \sum_{m=nSF+i}^{(n+1)SF-1} c_{OVSF}[m-i] c_k[m-i] c_J^*[m] + b_k[n-1] \sum_{m=nSF}^{nSF+i-1} c_{OVSF}[m-i] c_k[m-i] c_J^*[m] \right\}$$

when $q = m - i$, and

$$\frac{1}{2SF} \frac{\tau'}{T_c} \left\{ b_k[n] \sum_{m=nSF+i+1}^{(n+1)SF-1} c_{OVSF}[m-i-1] c_k[m-i-1] c_J^*[m] + b_k[n-1] \sum_{m=nSF}^{nSF+i} c_{OVSF}[m-i-1] c_k[m-i-1] c_J^*[m] \right\}$$

when $q = m - i - 1$. Similarly, when $\tau < 0$, $\tau = -iT_c + \tau'$ where $0 \geq \tau' > -T_c$ and (C1)

becomes

$$\begin{aligned} & \frac{1}{2T_b} b_k[n] \sum_m \sum_q c_{OVSF}[q] c_k[q] c_j^*[m] \int_{nSF T_c}^{(n+1)SF T_c + \tau} p(\lambda - (q-m-i)T_c - \tau') p(\lambda) d\lambda \\ & + \frac{1}{2T_b} b_k[n+1] \sum_m \sum_q c_{OVSF}[q] c_k[q] c_j^*[m] \int_{(n+1)SF T_c}^{(n+1)SF T_c + \tau} p(\lambda - (q-m-i)T_c - \tau') p(\lambda) d\lambda \end{aligned} \quad (C3)$$

where $\lambda = t - mT_c$. We can find that $|(q-m-i)T_c + \tau'| < T_c$ such that the integral is nonzero,

that is, $-\tau'/T_c + m+i-1 < q < -\tau'/T_c + m+i+1$. When $q = m+i$, (C3) becomes

$$\frac{1}{2SF} \frac{T_c - \tau'}{T_c} \left\{ b_k[n] \sum_{m=nSF}^{(n+1)SF-i-1} c_{OVSF}[m+i] c_k[m+i] c_j^*[m] + b_k[n+1] \sum_{m=(n+1)SF-i}^{(n+1)SF-1} c_{OVSF}[m+i] c_k[m+i] c_j^*[m] \right\}.$$

When $q = m+i+1$, (A3) becomes

$$\frac{1}{2SF} \frac{\tau'}{T_c} \left\{ b_k[n] \sum_{m=nSF-1}^{(n+1)SF-i-2} c_{OVSF}[m+i+1] c_k[m+i+1] c_j^*[m] + b_k[n+1] \sum_{(n+1)SF-i-1}^{(n+1)SF-1} c_{OVSF}[m+i+1] c_k[m+i+1] c_j^*[m] \right\}.$$

We rearrange the above results and obtain

$$\rho_{k,p;J,f}^{(n)}(\tau) = \begin{cases} \frac{1}{2SF} \left\{ \sum_{m=nSF+i}^{(n+1)SF-1} \frac{T_c - \tau'}{T_c} c_{OVSF}[m-i] c_k[m-i] c_j^*[m] + \sum_{m=nSF+i+1}^{(n+1)SF-1} \frac{\tau'}{T_c} c_{OVSF}[m-i-1] c_k[m-i-1] c_j^*[m] \right\}, & \tau \geq 0 \\ \frac{1}{2SF} \left\{ \sum_{m=nSF}^{(n+1)SF-i-1} \frac{T_c - \tau'}{T_c} c_{OVSF}[m+i] c_k[m+i] c_j^*[m] + \sum_{m=nSF}^{(n+1)SF-i-2} \frac{\tau'}{T_c} c_{OVSF}[m+i+1] c_k[m+i+1] c_j^*[m] \right\}, & \tau < 0 \end{cases} \quad (C4)$$

and

$$\dot{\rho}_{k,p;J,f}^{(n)}(\tau) = \begin{cases} \frac{1}{2SF} \left\{ \sum_{m=nSF}^{nSF+i-1} \frac{T_c - \tau'}{T_c} c_{OVSF}[m-i] c_k[m-i] c_j^*[m] + \sum_{m=nSF}^{nSF+i} \frac{\tau'}{T_c} c_{OVSF}[m-i-1] c_k[m-i-1] c_j^*[m] \right\}, & \tau \geq 0 \\ \frac{1}{2SF} \left\{ \sum_{m=(n+1)SF-i}^{(n+1)SF-1} \frac{T_c - \tau'}{T_c} c_{OVSF}[m+i] c_k[m+i] c_j^*[m] + \sum_{m=(n+1)SF-i-1}^{(n+1)SF-1} \frac{\tau'}{T_c} c_{OVSF}[m+i+1] c_k[m+i+1] c_j^*[m] \right\}, & \tau < 0 \end{cases} \quad (C5)$$

Also,

$$\gamma_{k,p;J,f}^{(n)}(\tau) = \begin{cases} \frac{1}{2SF} \left\{ \sum_{m=nSF+i}^{(n+1)SF-1} \frac{T_c - \tau'}{T_c} c_k[m-i] c_j^*[m] + \sum_{m=nSF+i+1}^{(n+1)SF-1} \frac{\tau'}{T_c} c_k[m-i-1] c_j^*[m] \right\}, & \tau \geq 0 \\ \frac{1}{2SF} \left\{ \sum_{m=nSF}^{(n+1)SF-i-1} \frac{T_c - \tau'}{T_c} c_k[m+i] c_j^*[m] + \sum_{m=nSF}^{(n+1)SF-i-2} \frac{\tau'}{T_c} c_k[m+i+1] c_j^*[m] \right\}, & \tau < 0 \end{cases} \quad (C6)$$

$$\dot{\gamma}_{k,p;J,f}^{(n)}(\tau) = \begin{cases} \frac{1}{2SF} \left\{ \sum_{m=nSF}^{nSF+i-1} \frac{T_c - \tau'}{T_c} c_k[m-i] c_j^*[m] + \sum_{m=nSF}^{nSF+i} \frac{\tau'}{T_c} c_k[m-i-1] c_j^*[m] \right\}, & \tau \geq 0 \\ \frac{1}{2SF} \left\{ \sum_{m=(n+1)SF-i}^{(n+1)SF-1} \frac{T_c - \tau'}{T_c} c_k[m+i] c_j^*[m] + \sum_{m=(n+1)SF-i-1}^{(n+1)SF-1} \frac{\tau'}{T_c} c_k[m+i+1] c_j^*[m] \right\}, & \tau < 0 \end{cases} \quad (C7)$$

$$\rho'_{k,p,J,f}^{(n)}(\tau) = \begin{cases} \frac{1}{2SF} \left\{ \sum_{m=nSF+i}^{(n+1)SF-1} \frac{T_c - \tau'}{T_c} c_{OVSF}[m-i] c_{OVSF}[m] c_k[m-i] c_j^*[m] + \sum_{m=nSF+i+1}^{(n+1)SF-1} \frac{\tau'}{T_c} c_{OVSF}[m-i-1] c_{OVSF}[m] c_k[m-i-1] c_j^*[m] \right\}, & \tau \geq 0 \\ \frac{1}{2SF} \left\{ \sum_{m=nSF}^{(n+1)SF-i-1} \frac{T_c - \tau'}{T_c} c_{OVSF}[m+i] c_{OVSF}[m] c_k[m+i] c_j^*[m] + \sum_{m=nSF}^{(n+1)SF-i-2} \frac{\tau'}{T_c} c_{OVSF}[m+i+1] c_{OVSF}[m] c_k[m+i+1] c_j^*[m] \right\}, & \tau < 0 \end{cases}, \quad (C8)$$

$$\rho'_{k,p,J,f}^{(n)}(\tau) = \begin{cases} \frac{1}{2SF} \left\{ \sum_{m=nSF}^{nSF+i-1} \frac{T_c - \tau'}{T_c} c_{OVSF}[m-i] c_{OVSF}[m] c_k[m-i] c_j^*[m] + \sum_{m=nSF}^{nSF+i} \frac{\tau'}{T_c} c_{OVSF}[m-i-1] c_{OVSF}[m] c_k[m-i-1] c_j^*[m] \right\}, & \tau \geq 0 \\ \frac{1}{2SF} \left\{ \sum_{m=(n+1)SF-i}^{(n+1)SF-1} \frac{T_c - \tau'}{T_c} c_{OVSF}[m+i] c_{OVSF}[m] c_k[m+i] c_j^*[m] + \sum_{m=(n+1)SF-i-1}^{(n+1)SF-1} \frac{\tau'}{T_c} c_{OVSF}[m+i+1] c_{OVSF}[m] c_k[m+i+1] c_j^*[m] \right\}, & \tau < 0 \end{cases}, \quad (C9)$$

$$\gamma'_{k,p,J,f}^{(n)}(\tau) = \begin{cases} \frac{1}{2SF} \left\{ \sum_{m=nSF+i}^{(n+1)SF-1} \frac{T_c - \tau'}{T_c} c_{OVSF}[m] c_k[m-i] c_j^*[m] + \sum_{m=nSF+i+1}^{(n+1)SF-1} \frac{\tau'}{T_c} c_{OVSF}[m] c_k[m-i-1] c_j^*[m] \right\}, & \tau \geq 0 \\ \frac{1}{2SF} \left\{ \sum_{m=nSF}^{(n+1)SF-i-1} \frac{T_c - \tau'}{T_c} c_{OVSF}[m] c_k[m+i] c_j^*[m] + \sum_{m=nSF}^{(n+1)SF-i-2} \frac{\tau'}{T_c} c_{OVSF}[m] c_k[m+i+1] c_j^*[m] \right\}, & \tau < 0 \end{cases} \quad (C10)$$

and

$$\dot{\gamma}'_{k,p,J,f}^{(n)}(\tau) = \begin{cases} \frac{1}{2SF} \left\{ \sum_{m=nSF}^{nSF+i-1} \frac{T_c - \tau'}{T_c} c_{OVSF}[m] c_k[m-i] c_j^*[m] + \sum_{m=nSF}^{nSF+i} \frac{\tau'}{T_c} c_{OVSF}[m] c_k[m-i-1] c_j^*[m] \right\}, & \tau \geq 0 \\ \frac{1}{2SF} \left\{ \sum_{m=(n+1)SF-i}^{(n+1)SF-1} \frac{T_c - \tau'}{T_c} c_{OVSF}[m] c_k[m+i] c_j^*[m] + \sum_{m=(n+1)SF-i-1}^{(n+1)SF-1} \frac{\tau'}{T_c} c_{OVSF}[m] c_k[m+i+1] c_j^*[m] \right\}, & \tau < 0 \end{cases}. \quad (C11)$$



Bibliography

- [1] J. G. Proakis, *Digital Communications*, 4th edition. New York: McGraw-Hill 2000
- [2] A. Agrawal, J. G. Andrews, J. M. Cioffi, and Teresa Meng, "Iterative Power Control with Successive Interference Cancellation for DS-CDMA Systems," *IEEE Trans. Wireless Commun.*, vol. 4, no. 3, May 2005
- [3] P. Alexander, A. Grant, and M. Reed, "Iterative detection in code-division multiple-access with error control coding," *Eur. Trans. Telecommun. (Special Issue on CDMA Techniques for Wireless Communications Systems)*, vol. 9, pp. 419–426, Sep.–Oct. 1998
- [4] P. D. Alexander, M. C. Reed, J. A. Asenstorfer, and C. B. Schlegel, "Iterative multiuser interference reduction: Turbo CDMA," *IEEE Trans. Commun.*, vol. 47, no. 7, pp. 1008–1014, Jul. 1999.
- [5] J. G. Andrews and T. H. Meng, "Transmit power and other-cell interference reduction via successive interference cancellation with imperfect channel estimation," *in proc. IEEE International Conference on Communications, 2001*, vol. 6, pp. 1940 -1944, 2001
- [6] J. G. Andrews and T. H. Meng, "Optimum power control for successive interference cancellation with imperfect channel estimation," *IEEE Trans..on Wireless Communications*, vol. 2, Issue: 2, pp. 375 –383, March 2003
- [7] J. G. Andrews, A. Agrawal and T. H. Meng, "Iterative Power Control for Imperfect Successive Interference Cancellation," *IEEE Trans. on Wireless Communications*, vol. 4, Issue 3, pp.878 – 884, May 2005
- [8] A. Arkhipov, R. Raulefs, and M. Schnell, "OFDMA-CDM performance enhancement by combining H-ARQ and interference cancellation." *IEEE Journal on Selected*

Areas in Communications; vol. 24, Issue 6, pp.1199 – 1207, June 2006

- [9] L. Bahl, J. Cocke, F. Jelinek, and J. Raviv, "Optimal decoding of linear codes for minimizing symbol error rate (Corresp.)," *IEEE Transactions on Information Theory*, vol. 20, Issue: 2, pp. 284 – 287, Mar 1974
- [10] I. Barbancho, A. M. Barbancho, and L. J. Tardon, "Multirate SIC receiver for UMTS," *IEE Electronics Letters*, vol. 39, Issue: 1, pp. 134-136, Jan. 2003
- [11] C. Berrou, A. Glavieux, and P. Thitimajshima, "Near Shannon limit error-correcting coding and decoding: turbo-codes," in *Conf. Rec. Int. Conf. Commun*, pp. 1064 -1070, May 1993
- [12] C. Berrou, A. Glavieux, and P. Thitimajshima, "A low complexity soft-output Viterbi decoder architecture," in *proc. Int. Conf. Commun*, pp. 737 - 740, May 1993
- [13] C. Berrou and A. Glavieux, "Near optimum error correcting and decoding: Turbo-codes," *IEEE Trans. Commun.*, vol. 44, no. 10, pp. 1261 -1271, 1996
- [14] J. Boutros and G. Caire, "Iterative multiuser joint decoding: Unified framework and asymptotic analysis," *IEEE Trans. Inf. Theory*, vol. 48, no. 7, pp. 1772–1793, Jul. 2002
- [15] R. M. Buehrer, S. P. Nicoloso, and S. Gollamudi, "Linear versus Non-linear Interference Cancellation," *Journal of Communications and Networks*, vol. 1, no. 2, pp. 118 –133, June 1999
- [16] R. M. Buehrer, "Equal BER performance in linear successive interference cancellation for CDMA systems," *IEEE Transactions on Communications*, vol. 49, Issue: 7, pp. 1250 –1258, July 2001
- [17] R. M. Buehrer and R. Mahajan, "On the usefulness of outer-loop power control with successive interference cancellation" *IEEE Trans. on Communications*, vol. 51, Issue: 12, pp. 2091 – 2102, Dec. 2003

- [18] R. M. Buehrer, S. P. Nicoloso, and S. Gollamudi, "Linear Versus Non-linear Interference Cancellation," *IEEE/IEICE Journal on Communications Networks*, vol. 1, no. 2, pp. 118-133, June 1999.
- [19] C. C. Chan and S. V. Hanly, "The capacity improvement of an integrated successive decoding and power control scheme," *in proc. IEEE 6th International Conference on Universal Personal Communications, 1997*, vol. 2, pp. 800 -804, Oct. 1997
- [20] N. S. Correal, R. M. Buehrer, and B. D. Woerner, "A DSP-based DS-CDMA multiuser receiver employing partial parallel interference cancellation," *IEEE Journal on Selective Areas in Communications*, vol. 17, pp. 613-630, Apr, 1999
- [21] H. A. David, *Order Statistics*. New York: Wiley 1981
- [22] D. Divsalar, M. K. Simon, and D. Raphaeli, "Improved parallel interference cancellation for CDMA," *IEEE Transactions on Communications*, vol. 46 2 , pp. 258 -268, Feb. 1998
- [23] A. Duel-Hallen, J. Holtzman, and Z. Zvonar, "Multiuser detection for CDMA systems," *IEEE Personal Communications Magazine*, vol. 2 2, pp. 46 -58, Apr. 1995
- [24] W. J. Ebel Y. Wu, B. D. Woerner, "A simple stopping criterion for turbo decoding," *IEEE Comm. Letters*, vol. 4, no. 8, pp. 258 – 260, Aug. 2000
- [25] J. Erfanian, S. Pasupathy, and G. Gulak, "Reduced complexity symbol detectors with parallel structure for ISI channels," *IEEE Transactions on Communications*, vol. 42, Issue 234, Part 3, pp. 1661 – 1671, Feb./March/April 1994
- [26] M. Ewerbring, B. Gudmundson, P. Teder, and P. Willars, "CDMA-IC: A proposal for future high capacity digital cellular systems," *in proc. 1993 IEEE VTC'93, 43rd*, pp. 440 –443, 18-20 May 1993
- [27] R. Fantacci and A. Galligani, "An efficient RAKE receiver architecture with pilot signal cancellation for downlink communications in DS-CDMA indoor wireless

- networks,” *IEEE Transactions on Communications*, vol. 47, pp. 823 – 827, June 1999
- [28] H. Gamal and E. Geraniotis, “Iterative multiuser detection for coded CDMA signals in AWGN and fading channels,” *IEEE J. Sel. Areas Commun.*, vol. 18, no. 1, pp. 30–41, Jan. 2000
- [29] F. Gilbert, F. Kienle, and N. Wehn, “Low complexity stopping criteria for umts turbo-decoders,” in *Proc. IEEE VTC 2003-Spring*, vol. 4, pp. 2376 – 2380, April 2003
- [30] J. Hagenauer, E. Offer, and L. Papke, “Iterative decoding of binary block and convolutional codes,” *IEEE Trans. Inform. Theory*, vol. 42, no. 2, pp. 429 – 445, March 1996
- [31] P. Hatrack and J. M. Holtzman, ”Reduction of other-cell interference with integrated interference cancellation /power control,” in *proc. IEEE 47th Vehicular Technology Conference*, vol. 3, pp. 1842 -1846, May 1997
- [32] P. A. Hoeher I. Land, “Using the mean reliability as a design and stopping criterion for Turbo codes,” in *Proc. IEEE Inform. Theory Workshop (ITW)*, pp. 27 – 29, Sept. 2001.
- [33] H. Holma and A. Toskala, *WCDMA for UMTS*, 3rd edition. England: John Wiley 2004
- [34] H. Holma, A. Harri, Toskala, and Antti, *HSDPA/HSUPA for UMTS :high speed radio access for mobile communications*, Chichester, England, John Wiley, 2006
- [35] D.-K. Hong, Y.-H. You, S.-S. Jeong and Chang-Eon Kang, “Pipelined successive interference cancellation scheme for a DS/CDMA system,” in *proc. IEEE Wireless Communications and Networking Conference, 1999*, vol. 3, pp. 1489 –1492, 1999
- [36] D.-K. Hong, T.-Y. Kim, D. Hong, and C.-E. Kan, “Pilot to data channel power allocation for PCA-DS/CDMA with interference canceler,” *IEEE Communications Letters*, vol 5, pp. 331 - 333, Aug. 2001
- [37] J. Hou, J. E. Smee, H. D. Pfister, and S. Tomasin, “Implementing Interference

- Cancellation to Increase the EV-DO Rev A Reverse Link Capacity”, *IEEE Communication Magazine*, vol. 44, Issue 2, pp. 96-102, Feb 2006
- [38] W. C. Jakes, *Microwave Mobile Communications*, New York: IEEE Press, 1974
- [39] S. Jalali and B.K.Khalaj, “Power management for multirate DS-CDMA systems with imperfect successive interference cancellation,” *IEEE ICC 2004*, vol 6, pp. 3256 – 3260, 20-24 June 2004
- [40] M. Juntti, “Multiuser Detector Performance Comparisons in Multirate CDMA Systems,” *in proc. IEEE Conf. on Vehicular Technology, 1998* , pp. 36-40, Ottawa, Canada, May 1998
- [41] S. Kaiser and J. Hagenauer, “Multi-carrier CDMA with iterative decoding and soft-interference cancellation.” *IEEE GLOBECOM '97*, vol.1, pp.6 – 10, Nov. 1997
- [42] J. H. Kim and S. W. Kim, “Combined power control and successive interference cancellation in DS/CDMA communications,” *in proc. The 5th International Symposium on Wireless Personal Multimedia Communications, 2002*, vol.: 3, pp. 931 –935, 2002
- [43] W. Koch and A. Baier, “Optimum and sub-optimum detection of coded data disturbed by time-varying intersymbol interference [applicable to digital mobile radio receivers],” *in proc. IEEE Global Telecommunications Conference, 1990*, vol.3, pp. 1679 – 1684, Dec. 1990
- [44] W. Lee, S. Lin, C. Tsai, T. Lee, and Y. Hwang, “A new low power turbo decoder using hda-dhdd stopping iteration,” *in Proc. of IEEE ISCAS*, pp. 1040 – 1043, May 2005
- [45] Qinghua Li, Xiaodong Wang and Georghades, C.N, “Turbo multiuser detection for turbo-coded CDMA in multipath fading channels.” *IEEE Transactions on Vehicular Technology*, vol 51, Issue 5, pp. 1096 – 1108, Sept. 2002

- [46] Zhanli Liu, Jing Wang, Chunming Zhao, Jiaheng Wang and Ming jiang. "A Novel Turbo Equalization for MIMO Frequency Selective Fading Channels." *IEEE International Conference on Communications, Circuits and Systems Proceedings, 2006* vol 2, pp. 1063 – 1067 June 2006
- [47] A. Matache, S. Dolinar, and F. Pollara, "Stopping rules for turbo decoders," Tech. Rep., Jet Propulsion Laboratory, Pasadena, California, Aug. 2000
- [48] R. Lupas and S. Vedu, "Linear multiuser detectors for asynchronous code division multiple access channels," *IEEE Trans. on Inform Theory*, vol. 35, pp.123-136, Jan 1989
- [49] U. Meadow and M. Honig, "MMSE interference suppression for direct-sequence spread-spectrum CDMA," *IEEE Trans. on Communications.*, vol.42, pp.3178-3188, Dec. 1994
- [50] M. Moher, "An iterative multiuser decoder for near-capacity communications," *IEEE Trans. Commun.*, vol. 47, no. 7, pp. 870–880, Jul. 1998
- [51] Z. Qin, K. Teh, and E. Gunawan, "Iterative multiuser detection for asynchronous CDMA with concatenated convolutional coding," *IEEE J. Sel. Areas Commun.*, vol. 19, no. 9, pp. 1784–1792, Sep. 2001
- [52] P. R. Patel and J. M Holtzman, "Analysis of a DS/CDMA successive interference cancellation scheme using correlations," *in proc. IEEE GLOBECOM'93*, vol. 1, pp. 76 -80, 1993
- [53] P. R. Patel and J. M. Holtzman, "Performance comparison of a DS/CDMA system using a successive interference cancellation (IC) scheme and a parallel IC scheme under fading," *in proc. IEEE International Conference on Communications 1994*, vol. 1, pp. 510 -514
- [54] P. Patel, and J. Holtzman, "Analysis of a simple successive interference cancellation

- scheme in a DS/CDMA system,” *IEEE Journal on Selected Areas in Communications*, vol. 12, Issue: 5, pp. 796 -807, June 1994
- [55] K. I. Pedersen, T. E. Kolding; I. Seskar, and J. M. Holtzman, “Practical implementation of successive interference cancellation in DS/CDMA systems,” *Proc. IEEE Int. Conf. on Universal Personal Communications*, vol. 1 , pp. 321 –325, Sep. 1996
- [56] R. Peterson, R. Ziemer, and D. Borth, *Introduction to Spread-Spectrum Communications*, New Jersey: Prentice Hall PTR, 1995
- [57] H.V Poor, “Iterative multiuser detection.” *IEEE Signal Processing Magazine*, vol 21, Issue 1, pp.81 – 88, Jan. 2004
- [58] K. Puttegowda, G. Verma, S. Bali, and R. M. Buehrer, “On the effect of cancellation order in successive interference cancellation for CDMA systems,” *in proc. IEEE VTC, 2003-Fall 57th*, vol. 2, pp. 1035 – 1039, Oct. 2003
- [59] L. K. Rasmussen, Sun Sumei, T. J. Lim, and H. Sugimoto,”Impact of estimation errors on multiuser detection in CDMA” *in proc. IEEE VTC’98. 48th*, vol 3, pp.1844 – 1848, May 1998
- [60] P. Robertson, E. Villebrun, and P. Hoeher, “A comparison of optimal and sub-optimal MAP decoding algorithms operating in the log domain.” *in proc. IEEE ICC 95*, vol. 2, pp. 1009 – 1013, June 1995
- [61] William E. Ryan, “A Turbo code tutorial.” <http://www.ece.arizona.edu/~ryan/publications/turbo2c.pdf>
- [62] R. Y. Shao, S. Lin, and M.P.C.Fossorier, “Two simple stopping criteria for turbo decoding,” *IEEE Trans. Comm.*, vol. 47, no. 8, pp. 1117 – 1120, Aug. 1999
- [63] A. Shibutani, H. Suda, and Y. Yamao, “Performance of W-CDMA mobile radio with Turbo codes using prime interleaver,” *in Proc. IEEE VTC 2000*, vol. 2, pp. 946-950,

2000.

- [64] Z. Shi and C. Schlegel, "Joint iterative decoding of serially concatenated error control coded CDMA," *IEEE J. Sel. Areas Commun.*, vol. 19, no. 8, pp. 1646–1653, Aug. 2001
- [65] S.-M Shum and Roger S. Cheng, "Power Control for Multirate CDMA System with Interference Cancellation," *IEEE Globalcom 2000*, vol. 2, pp 895-900, 2000
- [66] A. C. K. Soong and W. A. Krzymien, "A novel CDMA multiuser interference cancellation receiver with reference symbol aided estimation of channel parameters," *IEEE Journal on Selected Areas in Communications*, vol. 14, no. 8, pp. 1536 –1547, Oct. 1996
- [67] C.-H. Tang, W.-Y. Chang, and C.-H. Wei, "Pilot channel aided adaptable interference cancellation scheme for uplink DS/CDMA mobile radio systems," in *proc. IEEE GLOBECOM 2001*, vol. 5, pp. 3163 –3167, 25-29 Nov 2001
- [68] C.-H. Tang and C.-H. Wei, "Pilot-Channel Aided Pipeline Scheme for Interference Cancellation in Uplink DS/CDMA System," in *proc. IEEE Conf. on Vehicular Technology, 2002-Fall 56th*, Vancouver, Canada, vol. 4, pp. 2361 -2365, 2002
- [69] C.-H. Tang and C.-H. Wei, "Pilot-Channel Aided Successive Interference Cancellation for Uplink WCDMA Systems Over Multipath Fading Channels," in *proc. IEEE International Symposium on Communications and Information Technologies 2004*, pp. 149- 153, Oct. 2004
- [70] C.-H. Tang and C.-H. Wei, "Pilot-Channel Aided SIC Scheme for Multirate WCDMA Systems In Multipath Fading Channels," in *proc. IEEE VTC 2005-Fall, 62nd*, vol. 3, pp.1980 – 1983, Sep. 2005
- [71] *Third Generation Partnership Project 3G TS 25.104 V6.7.0*, <http://www.3gpp.org>
- [72] *Third Generation Partnership Project 3G TS 25.211*, <http://www.3gpp.org>

- [73] *Third Generation Partnership Project 3G TS 25.212*, <http://www.3gpp.org>
- [74] *Third Generation Partnership Project 3G TS 25.213*, <http://www.3gpp.org>
- [75] *Third Generation Partnership Project 3G TS 25.214*, <http://www.3gpp.org>
- [76] *Third Generation Partnership Project 3G TS 25.215*, <http://www.3gpp.org>
- [77] *Third Generation Partnership Project 3G TS 25.321*, "Medium Access Control (MAC) protocol specification
- [78] M. K. Varanasi and B. Aazhang, "Multistage detection in asynchronous code-division multiple-access communications," *IEEE Tran. on Communications*, vol. 38, pp. 509-519, Apr. 1990
- [79] S. Verdú, *Multiuser Detection* Cambridge, U.K.: Cambridge Univ. Press, 1998.
- [80] S. Verdú, "Minimum probability of error for asynchronous Gaussian multiple-access channels," *IEEE Trans. Inform. Theory*, vol. IT-32, pp. 85-96, June 1986
- [81] A. J. Viterbi, "Very low rate convolution codes for maximum theoretical performance of spread-spectrum multiple-access channels," *IEEE Journal on Selected Areas in Communications*, vol, 8 4, pp. 641 -649, May 1990
- [82] Branka Vucetic and Jinhong Yuan, *Turbo codes: Principle and Application*. Boston: Kluwer Academic, 2000
- [83] Hongfeng Wang, Yuping Zhang, and K. K. Parhi, "Study of Early Stopping Criteria for Turbo Decoding and Their Applications in WCDMA Systems," in *Proc IEEE ICASSP 2006*, vol 3, pp. III-1016 - III-1019, May 2006
- [84] X. Wang and H. V. Poor, "Iterative (turbo) soft interference cancellation and decoding for coded CDMA," *IEEE Trans. Commun.*, vol. 47, no. 7, pp. 1046–1061, Jul. 1999
- [85] Z. Wang, H. Suzuki, and K. K. Parhi, "Vlsi implementation issues of turbo decoder design for wireless applications," in *Proc. of 1999 IEEE Workshop on Signal*

Processing Systems (SIPS'99), pp. 503–512, Oct. 1999

- [86] Z. Wang and K. K. Parhi, “Decoding metrics and their applications in vlsi turbo decoders,” in *Proc. ICASSP*, pp. 3370– 3373, 2000
- [87] D. Warriar and U. Madhow, “ On the capacity of cellular CDMA with successive decoding and controlled power disparities,” in *proc. IEEE 48th Vehicular Technology Conference, 1998*, vol.3, pp. 1873 -1877 May 1998
- [88] J. Weng, G. Xue, T. Le-Ngoc, and S. Tahar, ”Multistage interference cancellation with diversity reception for asynchronous QPSK DS/CDMA systems over multipath fading channels,” *IEEE Journal on Selected Areas in Communications*, vol. 17, Issue: 12, pp. 2162 -2180, Dec. 1999
- [89] C. S. Wijting, T. Ojanper M. J. Juntti, K. Kansanen & R. Prasad, “Groupwise multiuser detectors for multirate DS-CDMA,” *Proceedings of IEEE Vehicular Technology Conference (VTC'99)*, Houston, USA, pp. 836-840, May 16-20, 1999
- [90] G. Xue, J. Weng, T. Le-Ngoc, and S. Tahar, “Multistage Interference Cancellation with Diversity Reception for Asynchronous QPSK DS/CDMA Systems over Multipath Fading Channels,” *IEEE Journal on Selective Areas in Communications*, vol. 17, no, 12, pp. 2162-2180, Dec, 1999
- [91] Kuo-Ming Wu and Chin-Liang Wang, ”Soft-input soft-output partial parallel interference cancellation for DS-CDMA systems,” in *proc. IEEE ICC 2001*, vol. 4, pp. 1172 – 1176 June 2001
- [92] Y. C Yoon, R. Kohno, and H. Imai, “A spread-spectrum multiaccess system with cochannel interference cancellation for multipath fading channels,” *IEEE Journal on Selected Areas in Communications*, vol. 11, Issue: 7, pp. 1067- 1075, Sept. 1993
- [93] N. Y. Yu, M. G. Kim, Y. S. Kim, and S. U. Chung, “Efficient stopping criterion for iterative decoding of Turbo codes,” *Electronics Letters*, vol. 39, no. 1, pp. 73–75, Jan.

2003

- [94] F. Zhai and I. J. Fair, “New error detection techniques and stopping criteria for turbo decoding,” in *Proc. 2000 IEEE Canadian Conference on Electrical and Computer Engineering*, pp. 58–62, March 2000

